



National Library
of Canada

Bibliothèque nationale
du Canada

Canadian Theses Service

Services des thèses canadiennes

Ottawa, Canada
K1A 0N4

CANADIAN THESES

THÈSES CANADIENNES

NOTICE

The quality of this microfiche is heavily dependent upon the quality of the original thesis submitted for microfilming. Every effort has been made to ensure the highest quality of reproduction possible.

If pages are missing, contact the university which granted the degree.

Some pages may have indistinct print especially if the original pages were typed with a poor typewriter ribbon or if the university sent us an inferior photocopy.

Previously copyrighted materials (journal articles, published tests, etc.) are not filmed.

Reproduction in full or in part of this film is governed by the Canadian Copyright Act, R.S.C. 1970, c. C-30.

**THIS DISSERTATION
HAS BEEN MICROFILMED
EXACTLY AS RECEIVED**

AVIS

La qualité de cette microfiche dépend grandement de la qualité de la thèse soumise au microfilmage. Nous avons tout fait pour assurer une qualité supérieure de reproduction.

S'il manque des pages, veuillez communiquer avec l'université qui a conféré le grade.

La qualité d'impression de certaines pages peut laisser à désirer, surtout si les pages originales ont été dactylographiées à l'aide d'un ruban usé ou si l'université nous a fait parvenir une photocopie de qualité inférieure.

Les documents qui font déjà l'objet d'un droit d'auteur (articles de revue, examens publiés, etc.) ne sont pas microfilmés.

La reproduction, même partielle, de ce microfilm est soumise à la Loi canadienne sur le droit d'auteur, SRC.1970, c. C-30.

**LA THÈSE A ÉTÉ
MICROFILMÉE TELLE QUE
NOUS L'AVONS REÇUE**

THE UNIVERSITY OF ALBERTA

DIAGENESIS OF CLASTIC ROCKS FROM THE BIRD FIORD, WEATHERALL AND
BASAL HECLA BAY FORMATIONS, MIDDLE-UPPER DEVONIAN, BATHURST AND
MELVILLE ISLANDS, CANADIAN ARCTIC ARCHIPELAGO

by

(C)
DESMOND N.H. LEE

A THESIS

SUBMITTED TO THE FACULTY OF GRADUATE STUDIES AND RESEARCH
IN PARTIAL FULFILMENT OF THE REQUIREMENTS FOR THE DEGREE
OF MASTER OF SCIENCE

DEPARTMENT OF GEOLOGY

EDMONTON, ALBERTA

SPRING 1986

Permission has been granted to the National Library of Canada to microfilm this thesis and to lend or sell copies of the film.

The author (copyright owner) has reserved other publication rights, and neither the thesis nor extensive extracts from it may be printed or otherwise reproduced without his/her written permission.

2
L'autorisation a été accordée à la Bibliothèque nationale du Canada de microfilmer cette thèse et de prêter ou de vendre des exemplaires du film.

L'auteur (titulaire du droit d'auteur) se réserve les autres droits de publication; ni la thèse ni de longs extraits de celle-ci ne doivent être imprimés ou autrement reproduits sans son autorisation écrite.

ISBN 0-315-30273-9

THE UNIVERSITY OF ALBERTA

RELEASE FORM

NAME OF AUTHOR DESMOND N.H. LEE

TITLE OF THESIS DIAGENESIS OF CLASTIC ROCKS FROM THE BIRD FIORD,
WEATHERALL AND BASAL HECLA BAY FORMATIONS,
MIDDLE-UPPER DEVONIAN, BATHURST AND MELVILLE
ISLANDS, CANADIAN ARCTIC ARCHIPELAGO

DEGREE FOR WHICH THESIS WAS PRESENTED MASTER OF SCIENCE

YEAR THIS DEGREE GRANTED SPRING 1986

Permission is hereby granted to THE UNIVERSITY OF ALBERTA LIBRARY to reproduce single copies of this thesis and to lend or sell such copies for private, scholarly or scientific research purposes only.

The author reserves other publication rights, and neither the thesis nor extensive extracts from it may be printed or otherwise reproduced without the author's written permission.

(SIGNED)

PERMANENT ADDRESS:

784 KENYALANG PARK

KUCHING, SARAWAK

MALAYSIA

DATED 20th Dec 1985

THE UNIVERSITY OF ALBERTA
FACULTY OF GRADUATE STUDIES AND RESEARCH

The undersigned certify that they have read, and recommend to the Faculty of Graduate Studies and Research, for acceptance, a thesis entitled DIAGENESIS OF CLASTIC ROCKS FROM THE BIRD FIORD, WEATHERALL AND BASAL HECLA BAY FORMATIONS, MIDDLE-UPPER DEVONIAN, BATHURST AND MELVILLE ISLANDS, CANADIAN ARCTIC ARCHIPELAGO submitted by DESMOND N.H. LEE in partial fulfilment of the requirements for the degree of MASTER OF SCIENCE.

F. J. Craystappe

Supervisor

J. L. ...

Date... *Dec 20, 1985*

DEDICATION

This thesis is dedicated to my family and fiancée.

ABSTRACT

X-ray diffraction, petrographic, scanning electron microscope and stable isotope studies were performed on clastic rocks from the Bird Fiord, Weatherall and basal Hecla Bay Formations to determine the physiochemical controls upon their diagenesis. These units are part of the Middle-Upper Devonian clastic wedge of the Franklinian Geosyncline. The diagenetic history of these sandstones has been controlled by their burial history which has, in turn, influenced the evolution of subsurface pore-fluids.

Surface and near-surface diagenesis is characterized by grain-coating, Fe-rich chlorite and early calcite cement which were probably precipitated from original connate water.

Intermediate to deep subsurface diagenesis is characterized by quartz cementation, an initial stage of dissolution and/or alteration, carbonate cementation, and hydrocarbon generation. Meteoric waters probably supplied most of the silica for quartz cementation at intermediate burial depths (500-1,800m). Following quartz cementation, influx of acidic fluids resulted in the first stage of dissolution and/or alteration of feldspar, rock and shell fragments, quartz, micas and early calcite. The acidic fluids were probably derived by mixing of surface-derived, meteoric waters, and lesser amounts of acidic fluids released from interbedded and underlying shales during hydrocarbon maturation. The first, minor uplift in Late Frasnian time probably enhanced the influx of meteoric waters into the system. As burial resumed in Latest Frasnian time, carbonate cements were formed. The $\delta^{18}\text{O}$ values of the diagenetic calcite (+18.1 to +20.0, SMOW), dolomite (+20.0) and ankerite (+19.8) are best explained by crystallization at temperatures of 100-115°C (burial depth of about 2,500-3,000m) from formation waters with $\delta^{18}\text{O}$ of about +1 to +2 permill. The $\delta^{13}\text{C}$ values (-4.5 to -0.1, PDB) of the carbonate cements probably reflect the mixing of carbon derived from marine carbonate and shell fragments, and lesser amounts of ^{13}C -depleted organic carbon from the maturation of organic matter. Maximum hydrocarbon generation in interbedded and surrounding shales probably occurred at or near maximum burial (at $>110^\circ\text{C}$).

Diagenesis during and following major uplift (Ellesmerian Orogeny) is characterized by a second stage of dissolution and/or alteration, hydrocarbon migration and emplacement, crystallization of late diagenetic clays, and tertiary migration of hydrocarbons. The beginning of the second stage of dissolution was probably contemporaneous with peak hydrocarbon maturation in interbedded and underlying shales; at least some of the acidic fluids necessary for

silicate and carbonate dissolution were probably released during peak hydrocarbon maturation. The orogeny also resulted in renewed mixing of surface-derived, meteoric waters with formation fluids; some of the fluids necessary for dissolution during the uplift were probably derived from this source as well. Hydrocarbon migration was probably contemporaneous with this stage of dissolution, and filled secondary porosity. The $\delta^{18}\text{O}$ values of the late diagenetic kaolinite (+14.4) and illite (+13.1), which were precipitated following hydrocarbon emplacement, are compatible with low temperature (<75°C) crystallization from fluids containing a sizeable fraction of meteoric water. After the crystallization of late diagenetic clays, tertiary migration of hydrocarbons occurred, filling fractures and fissures which were formed and/or reopened by tectonic activity in the overlying Sverdrup Basin.

ACKNOWLEDGEMENTS

I wish to thank Dr. B. Jones and Dr. Q.H. Goodbody for providing all the samples and some of the thin sections used in this study, and invaluable stratigraphic information. Dr. B. Jones also provided unlimited access to the facilities in his Paleontological Laboratory.

Special thanks go to Dr. F.J. Longstaffe, my supervisor, for providing financial support for this research, and invaluable advices on earlier drafts of this manuscript. C. Connolly, S. Burtch and Dr. A. Ayalon also provided helpful comments on the earlier drafts. The Department of Geology also provided Graduate Teaching Assistantships to make this research possible.

Some of the X-ray diffraction and oxygen-isotope analyses were previously done by Dr. F.J. Longstaffe. D. Caird analysed the oxygen- and carbon-isotope samples. I also thank all my friends who had helped in the production of this thesis.

Last, but not least, I would like to thank my fiancée, Jenny, for typing the earlier drafts, and for her constant support and patience.

Table of Contents

Chapter	Page
I. INTRODUCTION	1
A. GEOLOGICAL BACKGROUND AND PREVIOUS WORK	5
Regional Tectonic Setting	5
Stratigraphy	5
Source Areas	12
Geologic History and Paleogeography	14
Mineralogy	17
II. RESULTS	18
A. MINERALOGY OF SHALES AND ARGILLACEOUS LIMESTONES	18
Nature of Illite/Smectite	29
B. DETRITAL MINERALOGY OF SANDSTONES	29
C. DIAGENETIC MINERALOGY OF SANDSTONES	37
Chlorite	37
Quartz Overgrowths and Pressure Solution	44
Dissolution and Alteration of Detrital Grains	47
Calcite	47
Dolomite and Ankerite	52
Dissolution of Carbonate Cements and Detrital Grains	52
Hydrocarbon Emplacement	57
Illite	57
Illite/Smectite	62
Smectite	62
Kaolinite	65
Fracturing, Dissolution and Tertiary Hydrocarbon Migration	65
D. PARAGENETIC SEQUENCE - SUMMARY	68
E. STABLE ISOTOPE GEOCHEMISTRY	68
Clay Minerals	68
Carbonate Minerals	71
III. INTERPRETATION OF DIAGENETIC HISTORY	73

A. INTRODUCTION	73
Burial History - Summary	73
Maximum Burial Depth	73
Oxygen-Isotope Geochemistry	76
B. PARAGENETIC SEQUENCE	77
Surface and Near-Surface Diagenesis	79
Intermediate to Deep Subsurface Diagenesis	81
Diagenesis During and Following Major Uplift (Ellesmerian Orogeny)	89
IV. CONCLUSIONS	95
BIBLIOGRAPHY	97
APPENDIX 1	103
A. ANALYTICAL METHODS	103
Thin Section Petrography	103
X-Ray Diffraction Analysis	103
Scanning Electron Microscope	106
Stable Isotope Analysis	107

LIST OF TABLES

Table	Description ⁴	Page
Table 1.1	Summary of the distribution, average thickness, age and facies of the formations in the Middle-Upper Devonian clastic wedge, Canadian Arctic Archipelago	11
Table 1.2	Section 80X: Stratigraphic divisions, environment of deposition and lithologies	13
Table 2.1	Section 80X: Samples studied	19
Table 2.2	Section 81I: Samples studied	21
Table 2.3	Clay mineralogy of <2 μ m size-fraction of shales, argillaceous limestones, siltstones and sandstones, section 80X	23
Table 2.4	Clay mineralogy of <2 μ m size-fraction of shales, argillaceous limestones, siltstones and sandstones, section 81I	24
Table 2.5	Mineralogy of sandstones: Thin-section analysis, section 80X	30
Table 2.6	Types of authigenic and detrital carbonates, section 80X	38
Table 2.7	$\delta^{18}\text{O}$ and $\delta^{13}\text{C}$ for clay and carbonate minerals, section 80X	70

x

LIST OF FIGURES

Figure	Description	Page
Figure 1.1	Distribution of the Bird Fiord and Weatherall Formations and location map	2
Figure 1.2	Location map of sections 80X and 81I	3
Figure 1.3	Tectonic provinces	6
Figure 1.4	Time correlation chart	7
Figure 1.5	Distribution of the Middle-Upper Devonian clastic wedge and location map	8
Figure 1.6	Stratigraphic cross-section from Ellesmere to Banks Islands	9
Figure 1.7	Stratigraphic cross-section showing the relationship of sections 80X and 81I	10
Figure 1.8	Source areas	10
Figure 1.9	Source areas and paleogeography, Middle Eifelian	15
Figure 1.10	Late Eifelian paleogeography	16
Figure 2.1	X-ray diffractograms for representative shale and limestone samples (<2 μ m size-fraction), section 80X	25
Figure 2.2	X-ray diffractograms for representative shale and limestone samples (<0.2 μ m size-fraction), section 80X	26
Figure 2.3	X-ray diffractograms for representative shale and limestone samples (<2 μ m size-fraction), section 81I	27
Figure 2.4	Classification of sandstones in section 80X	31
Figure 2.5	Nature of clay minerals in sandstones, section 80X	43
Figure 2.6	Nature of clay minerals in sandstones, section 81I	60
Figure 2.7	Paragenetic sequence	69
Figure 2.8	$\delta^{18}\text{O}$ versus percent kaolinite in the <2 μ m size-fraction	72
Figure 3.1	Burial history of the Bird Fiord and Weatherall Formations	74
Figure 3.2	$\delta^{18}\text{O}$ of water versus temperature for authigenic carbonate and clay minerals from the Bird Fiord sandstone	78
Figure 3.3	Burial history and inferred diagenetic history	80
Figure 3.4	Model for flow of meteoric water	83

LIST OF PLATES

Plate	Description	Page
Plate 2.1	Thin section photomicrographs showing detrital mineralogy of sandstones	33
Plate 2.2	Thin section photomicrographs showing detrital mineralogy of sandstones	35
Plate 2.3	Thin section photomicrographs showing detrital mineralogy, diagenetic chlorite and quartz, and feldspar dissolution	39
Plate 2.4	SEM photomicrographs showing diagenetic chlorite and quartz	41
Plate 2.5	Thin section photomicrographs showing pressure solution, feldspar dissolution and calcite cement	45
Plate 2.6	SEM photomicrographs showing feldspar dissolution and/or alteration, and calcite	48
Plate 2.7	SEM photomicrographs showing diagenetic ankerite, illite and illite/smectite	50
Plate 2.8	Thin section photomicrographs showing diagenetic carbonates, dissolution of detrital and diagenetic minerals, and hydrocarbon residues	53
Plate 2.9	Thin section photomicrographs showing dissolution of detrital grains, and pore-filling hydrocarbons	55
Plate 2.10	Thin section photomicrographs showing hydrocarbon residues in secondary porosity, and diagenetic kaolinite	58
Plate 2.11	SEM photomicrographs showing diagenetic smectite and kaolinite	63
Plate 2.12	Thin section photomicrographs showing diagenetic kaolinite in secondary porosity, and hydrocarbons in fractures and fissures	66

I. INTRODUCTION

The main purpose of this study is to investigate the physiochemical controls upon clastic diagenesis in the Bird Fiord, Weatherall and basal Hecla Bay Formations in the Canadian Arctic Archipelago (Fig. 1.1). Two sections from the Middle-Upper Devonian clastic wedge of the Franklinian Geosyncline in central Bathurst and central Melville Islands (sections 80X and 81I, respectively; measured by Goodbody, 1985) have been studied (Figs. 1.1, 1.2). This clastic wedge is of special interest because of its high petroleum potential (Embry and Klován, 1976; Powell, 1978; Meyerhoff, 1982). A diagenetic study of the clastic rocks in this area is also useful in predicting their reservoir quality because clastic diagenesis directly affects the porosity and permeability of a sandstone reservoir.

This study involves:

1. detailed X-ray diffraction studies of sandstones and shales to determine their clay mineralogy;
2. detailed petrographic studies and scanning electron microscopy in order to determine the paragenetic sequence of diagenetic events in the sandstones, and
3. oxygen- and carbon-isotope studies of diagenetic minerals to (a) estimate the temperature(s) at which their formation has occurred, and (b) determine the roles of different fluids in the diagenesis of the sandstones.

One of the most important controls on clastic diagenesis is the hydrogeologic history of the sedimentary basin. The flow dynamics and fluid chemistries of subsurface fluid flow systems evolve throughout the burial history of clastic rocks (Galloway, 1984). The hydrogeologic history of the Franklinian Geosyncline was complicated by its complex burial history which included two episodes of uplifting, deformation and erosion. Therefore, interpretation of the diagenetic history of the clastic rocks from Bird Fiord, Weatherall and basal Hecla Bay Formations will be difficult, unless the burial history is understood in some detail.

Two possible fluid flow regimes that can influence clastic diagenesis are downward moving meteoric ground waters, and upward and outward moving waters expelled from shales. Meteoric ground waters moving downward into subsurface sandstones can be structurally and topographically controlled by uplift, deformation and erosion of the basin. Waters expelled from shales can result from compaction, dehydration reactions of clay minerals and/or

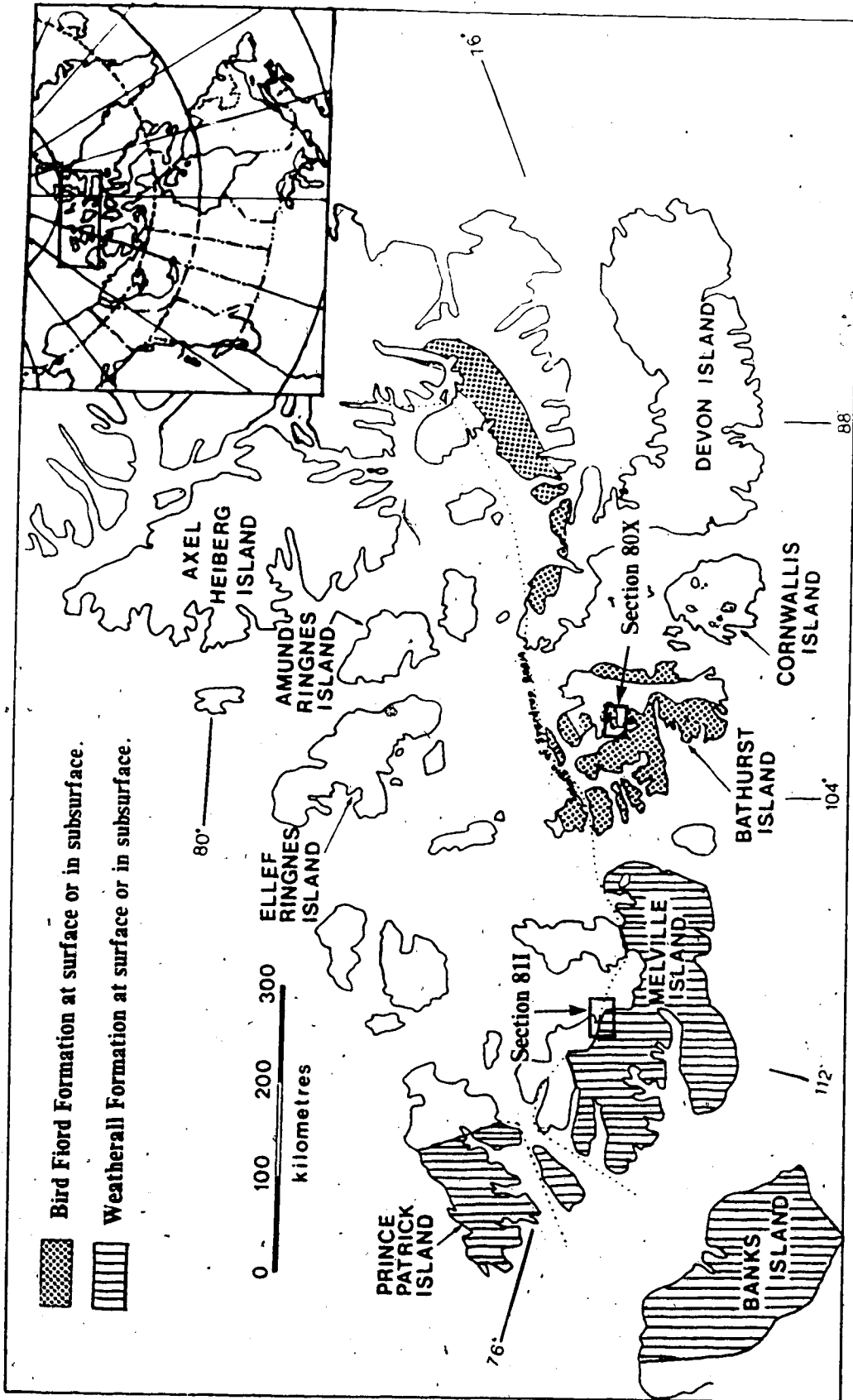
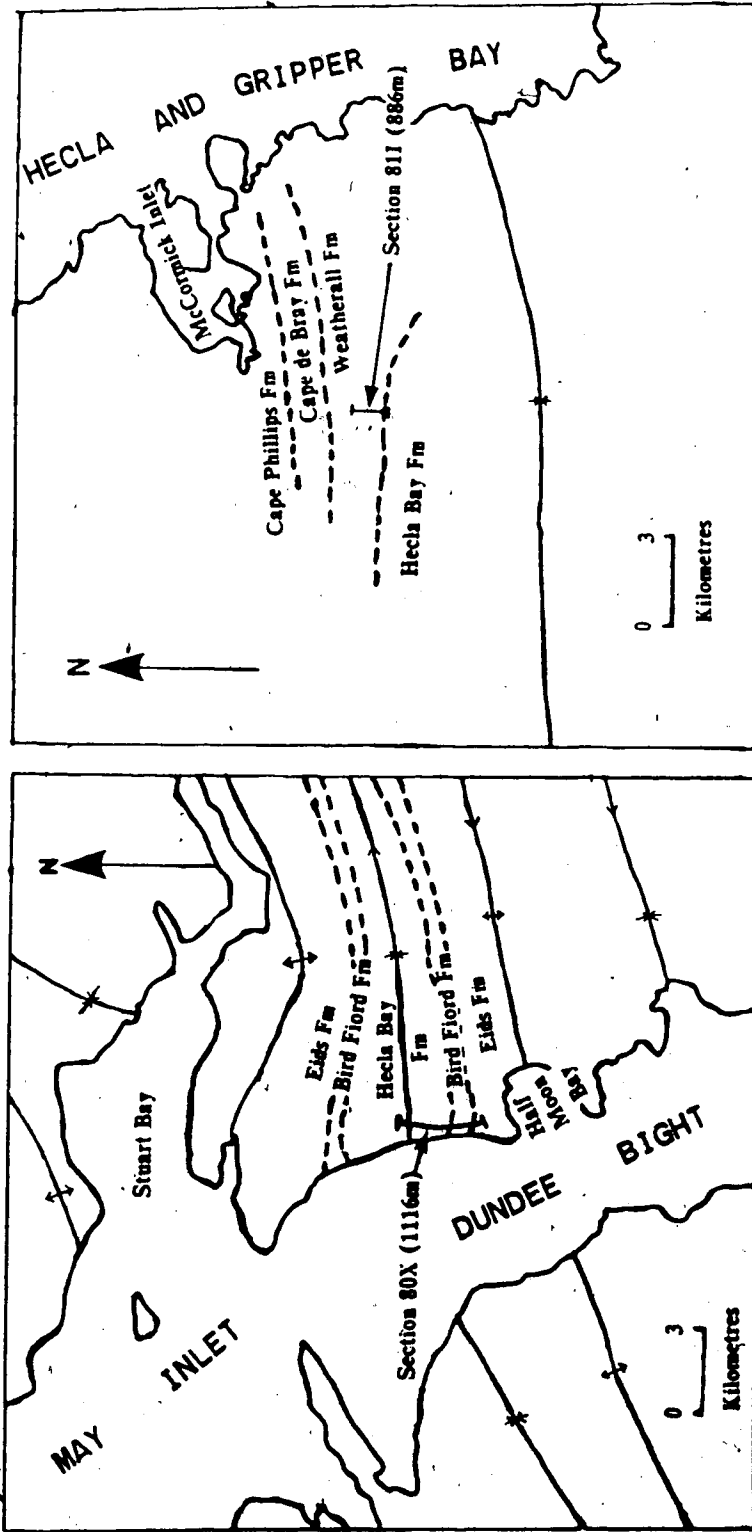


Fig. 1.1 Distribution of the Bird Fiord and Weatherall Formations and the locations of sections 80X and 811 in the Canadian Arctic Archipelago (after Embry and Klovan, 1976; Goodbody, 1985).



B SECTION 811

A SECTION 80X

Fig. 1.2 Generalized geological sketch maps showing locations of (A) Section 80X, Dundee Bight, May Inlet, central Bathurst Island (after Goodbody, 1985); (B) Section 811, South McCormick Iflet, central Melville Island (after Embry and Klovan, 1976).

hydrocarbon generation in the basin (Galloway, 1984).

The two fluid regimes control the supply of acid which is necessary for the dissolution of carbonate and silicate minerals. Some authors favoured carboxylic and carbonic acids associated with the thermal maturation of organic matter in the shales (e.g., Schmidt and McDonald, 1979; Franks, 1984; Porter and Weimer, 1982; Surdam et al., 1984; Land, 1984). The transformation of smectite to illite in the shales can also affect the diagenesis of the associated sandstones by contributing dissolved ions to the expelled acidic pore-fluids (e.g., Land and Dutton, 1978; Boles and Franks, 1979; Milliken et al., 1981; Perry and Hower, 1970; Hower et al., 1976). However, the above sources of acidic fluids appear to be limited to deep burial depths.

Shallower sandstones can be influenced by meteoric waters circulating down from the surface. The opportunity for penetration of meteoric waters into the subsurface will be enhanced if the basin is uplifted, deformed and eroded sometime during its burial history. In recent literature, many authors indicated that meteoric waters can play an important role in the diagenesis of sandstones (e.g., Longstaffe, 1983, 1984, in press; Dutton and Land, 1985; Land and Dutton, 1978). The evolving acidic meteoric waters, as a result of mixing with the original formation waters and reactions with the sediments, can cause dissolution and/or precipitation of detrital and/or diagenetic minerals. The roles of such acidic fluids in the diagenesis of the sandstones will be examined in this study.

The oxygen-isotope ratios ($^{18}\text{O}/^{16}\text{O}$) of authigenic minerals in a clastic rock sequence are a function of the oxygen-isotope composition and temperature of formation water present during mineral formation. Therefore, variations in oxygen-isotope compositions of successive authigenic cements can provide information about pore fluids evolution and thermal history during the diagenesis of sandstones. Authigenic minerals formed in equilibrium with low- ^{18}O meteoric water should have $\delta^{18}\text{O}$ values predictably lower than such minerals of detrital origin, or minerals formed from more ^{18}O -rich formation fluids (Longstaffe, 1983, 1984, in press). Authigenic minerals formed at low temperatures should have higher $\delta^{18}\text{O}$ values than the same authigenic minerals formed at higher temperatures, other conditions being constant. In addition, the carbon-isotope ratios ($^{13}\text{C}/^{12}\text{C}$) of carbonate cements can help to determine the carbon reservoirs involved in their formation. In some cases, the relationship between specific episodes of carbonate authigenesis and hydrocarbon generation can be identified.

A. GEOLOGICAL BACKGROUND AND PREVIOUS WORK

Regional Tectonic Setting

The Middle-Upper Devonian Bird Fiord, Weatherall and basal Hecla Bay Formations (Figs. 1.1, 1.2) are located in the Parry Islands and Central Ellesmere Fold Belts of the Franklinian Geosyncline (Fig. 1.3; Thorsteinsson and Tozer, 1960, 1970). These two fold belts were produced by the Ellesmerian Orogeny, which took place during Fammenian to Visean time (Thorsteinsson and Tozer, 1960, 1970). The Early-Middle Paleozoic strata of the Franklinian Geosyncline are overlain unconformably to the northwest by the Middle Pennsylvanian to Early Tertiary strata of the Sverdrup Basin (Fig. 1.3). The Sverdrup Basin was deformed during the Late Cretaceous and Tertiary. The Canadian Precambrian Shield is exposed to the south and east of the region, and is overlain to the northwest by the Early-Middle Paleozoic strata of the Arctic Platform (Fig. 1.3).

Stratigraphy

The stratigraphic ranges of the two sections (sections 80X and 811; Figs. 1.1, 1.2) chosen for this study are shown on the time-correlation chart for the Middle-Upper Devonian clastic formations in the Canadian Arctic Archipelago (Fig. 1.4; Embry and Klovan, 1976). The stratigraphy of sections 80X and 811 (same as the May Inlet and South McCormick Inlet sections, respectively, which were measured by Embry and Klovan, 1976; Fig. 1.5) can be related to the Middle-Upper Devonian clastic wedge (Fig. 1.6 and 1.7). Embry and Klovan (1976) gave the formations comprising the clastic wedge and their distribution, average thickness, maximum age range and facies content (Table 1.1). Underlying the clastic wedge are thick sequences of black, siliceous shales (Eids, Cape Phillips, Kitson, Ibbett Bay, Nanuk and Orkut Formations) and some carbonates (Blue Fiord Formations) (Figs. 1.4, 1.6, 1.7; Embry and Klovan, 1976; Goodbody, 1985).

The Bird Fiord Formation has been studied by Goodbody (1985), Embry and Klovan (1976) and McLaren (1963). This formation consists of interbedded limestone, shale, siltstone and fine-grained sandstone. The Bird Fiord Formation in central Bathurst Island is shaly and fossiliferous near its base, but it grades upwards into less shaly and less fossiliferous massive sandstones.

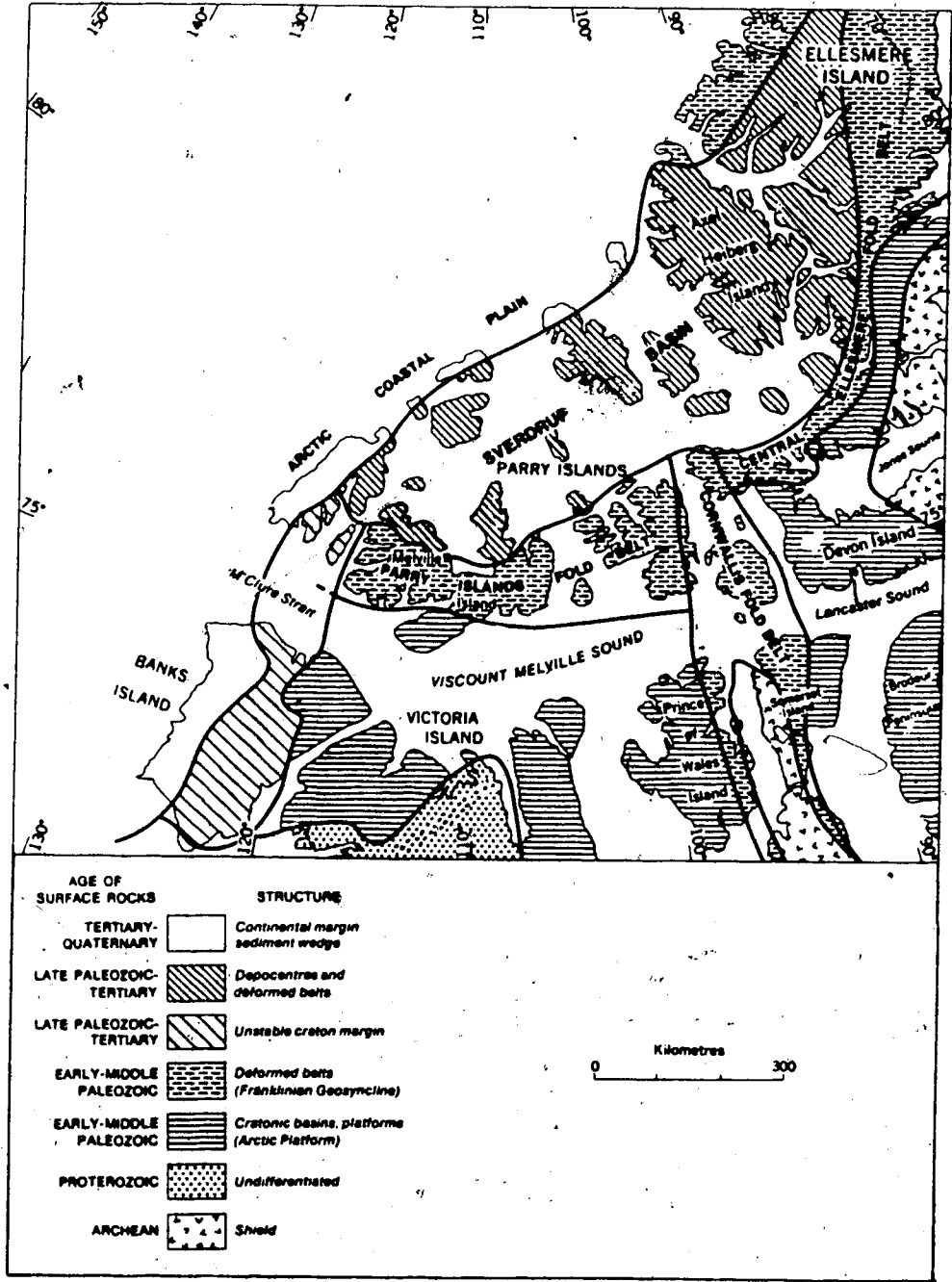


Fig. 1.3 Tectonic provinces of the Canadian Arctic Archipelago (after Thorsteinsson and Tozer, 1970).

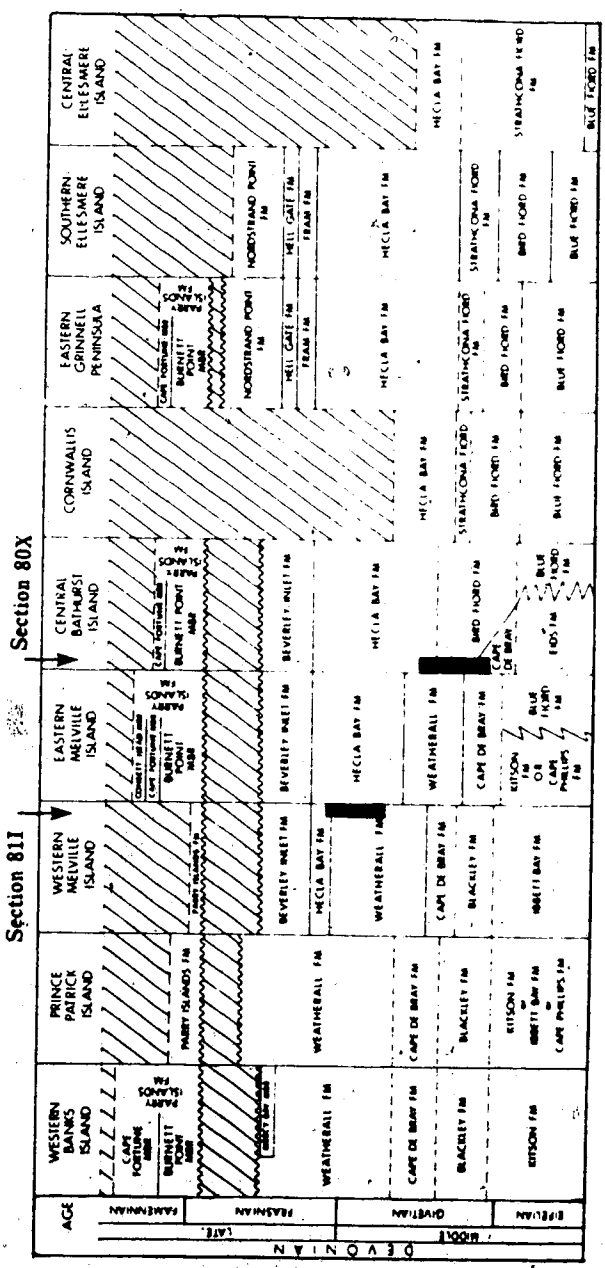


Fig. 1.4 Time-correlation chart showing the stratigraphic ranges of sections 80X and 811 in Middle-Upper Devonian strata, Canadian Arctic Islands (after Embry & Klovan, 1976).

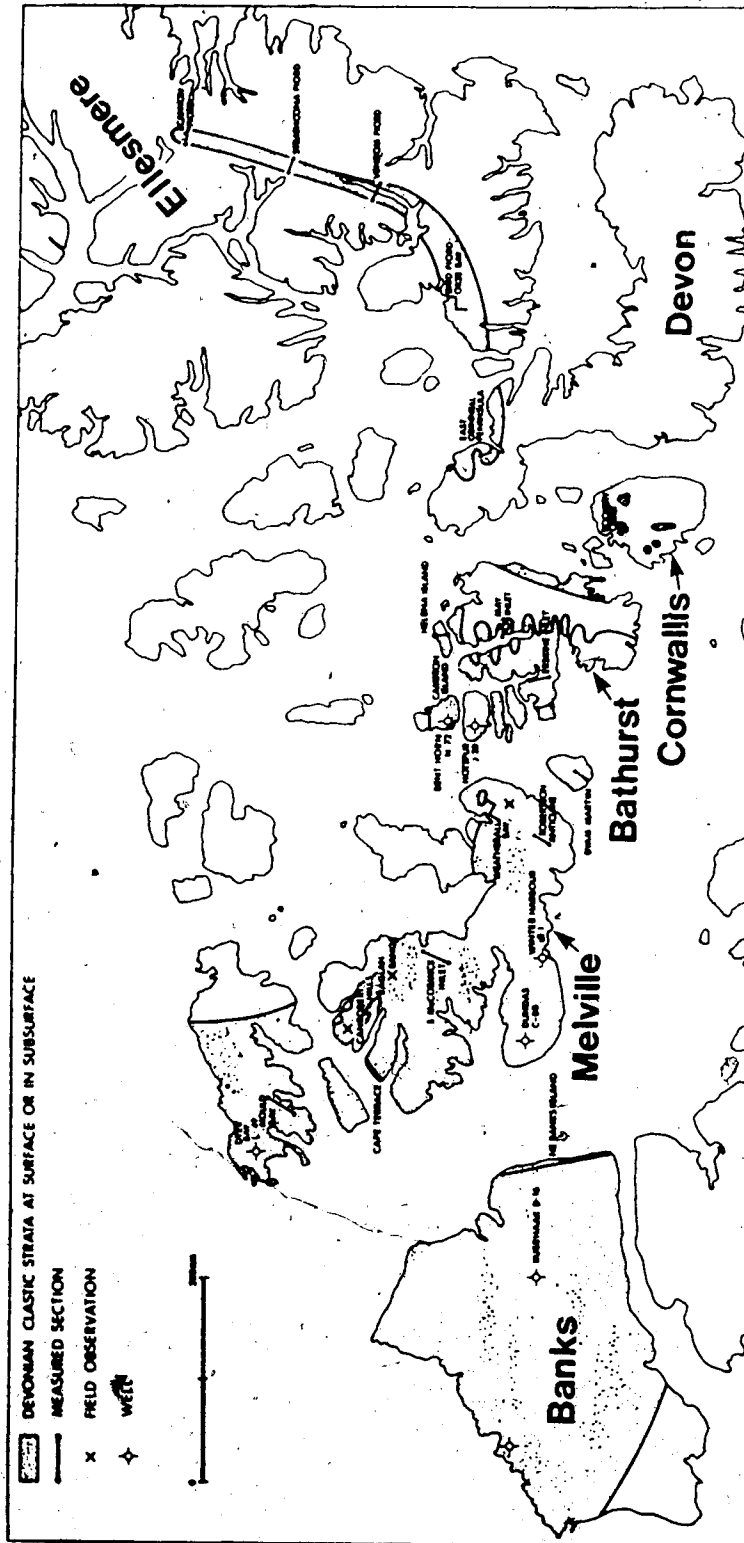


Fig. 1.5 Distribution of the Middle-Upper Devonian clastic wedge in the Canadian Arctic Archipelago and the locations of measured sections, wells and field observation points used in cross-sections A-A' and B-B' in Figures 1.6 & 1.7 respectively (after Embry and Klovan, 1976).

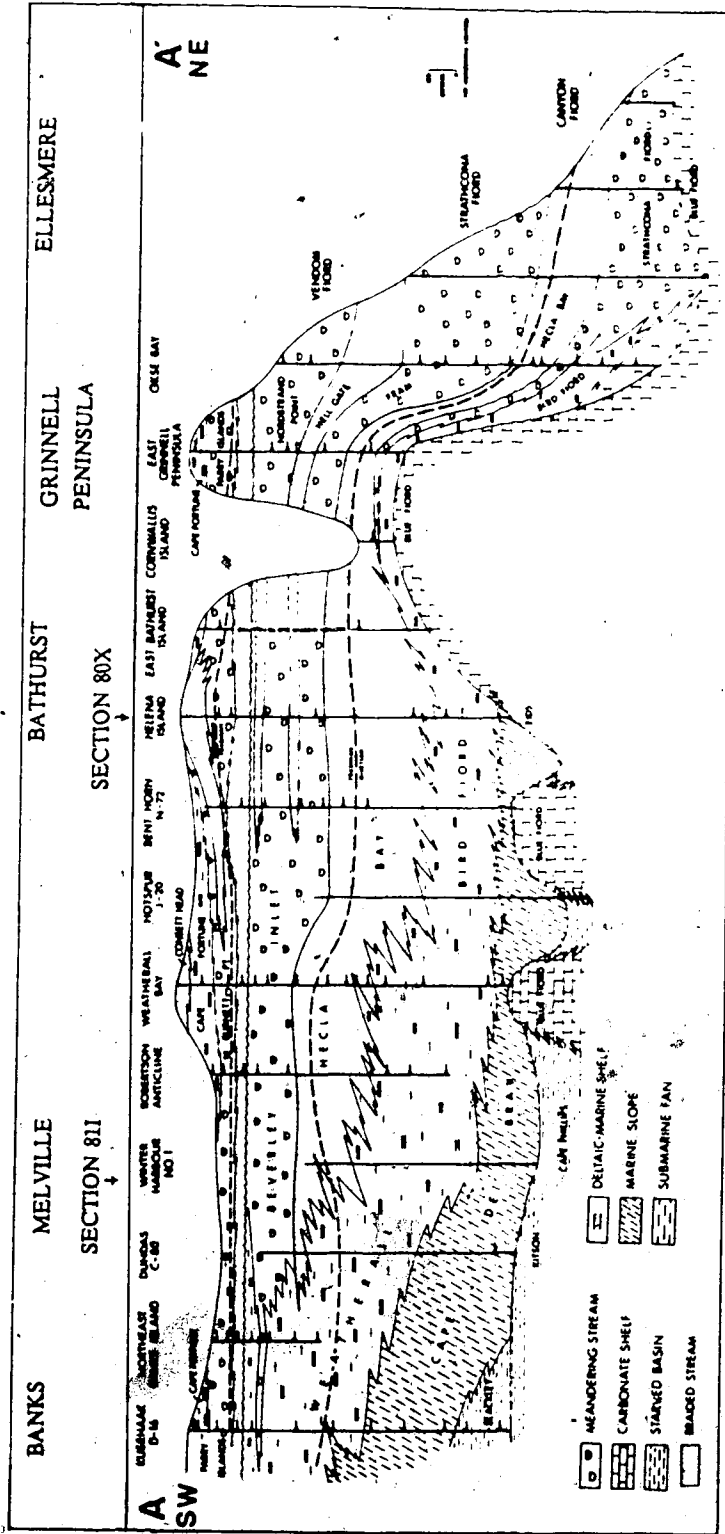


Fig. 1.6 Stratigraphic cross-section showing the regional stratigraphic relationships within the clastic wedge from Ellesmere to Banks Islands (after Embry and Klovan, 1976).

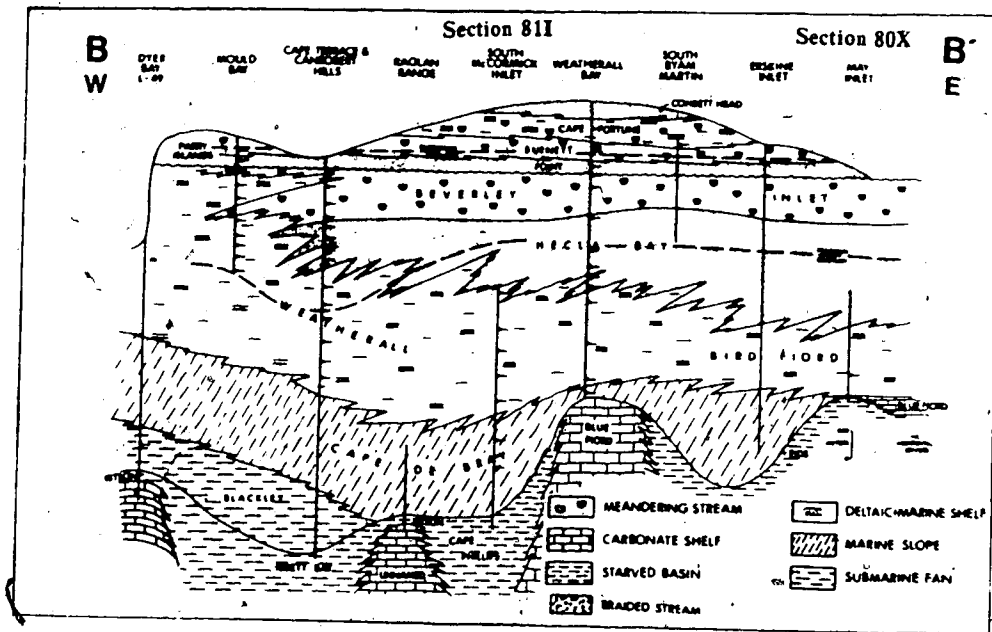


Fig. 1.7 Stratigraphic cross-section showing the relationship of the May Inlet section (80X) and South McCormick Inlet section (811) within the Middle-Upper Devonian clastic wedge (after Embry and Klovan, 1976).

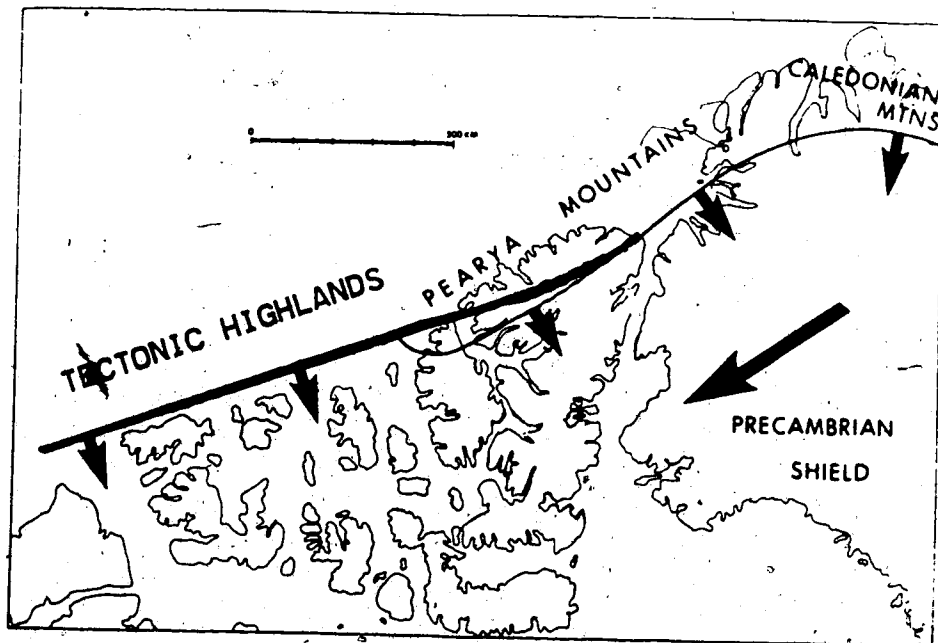


Fig. 1.8 Source areas: (i) Tectonic highlands (after Tozer and Thorsteinsson, 1964); (ii) Pearya and Caledonian Mountains and Greenland Precambrian Shield (after Embry and Klovan, 1976).

Table 1.1 Summary of the distribution, average thickness, age and facies of the formations in the Middle-Upper Devonian clastic wedge, Canadian Arctic Archipelago (after Embry and Klovan, 1976).

FORMATION	DISTRIBUTION	Avg. THICKNESS	AGE	FACIES
Parry Islands				
3 Members Consett Head	Melville	150m	Middle Famennian	Braided stream
Cape Fortune	Grinnell, Bathurst, Melville, Banks	245m	Early-Middle Famennian	Deltaic-marine, Meandering stream
Burnett Point	Grinnell, Bathurst, Melville, Banks, Prince Patrick	300m	Late Frasnian, Early Famennian	Braided stream Meandering stream
Beverley Inlet	Bathurst, Melville	450m	Early-Middle Frasnian	Meandering stream
Nordstrand Point	Ellesmere, Grinnell	600m	Middle-Late Frasnian	Meandering stream
Hell Gate	Ellesmere, Grinnell	600m	Middle Frasnian	Braided stream
Fram	Ellesmere, Grinnell	900m	Early-Middle Frasnian	Meandering stream
Hecla Bay	Ellesmere, Grinnell, Cornwallis, Bathurst, Melville	750m	Early Givetian- Early Frasnian	Braided stream Deltaic-marine
Strathcona Fjord	Ellesmere, Grinnell, Cornwallis	300m	Early Eifelian- Early Givetian	Meandering stream
Bird Fjord	Ellesmere, Grinnell, Cornwallis, Bathurst	750m	Middle Eifelian- Early Givetian	Deltaic-marine
Weatherall	Melville, Banks, Prince Patrick	1200m	Early Givetian- Middle Frasnian	Deltaic-marine
Cape de Bray	Bathurst, Melville, Banks, Prince Patrick	900m	Late Eifelian- Late Givetian	Marine slope
Blackley	Melville, Banks, Prince Patrick	600m	Late Eifelian- Early Givetian	Submarine fan

Section 80X can be divided into stratigraphic divisions with different lithologies and environment of deposition (Table 1.2). A thin carbonate unit separates the Bird Fiord Formation from the underlying siltstones and shales of the Cape de Bray Formation (Table 1.2). Overlying the Bird Fiord Formation is the Hecla Bay Formation (Table 1.2; Figs. 1.6, 1.7) which consists of interbedded fine-grained sandstone, siltstone and shale (Tozer and Thorsteinsson, 1964; Goodbody, 1985; Embry and Klovan, 1976).

The Weatherall Formation in the Canadian Arctic Archipelago consists of interbedded very fine-grained sandstones, siltstones and shales (Tozer and Thorsteinsson, 1964). In section 81I in central Melville Island, the upper 38m can be assigned to the Hecla Bay Formation; the remainder of the section (848m) belongs to the Weatherall Formation (Fig. 1.2; Goodbody, pers. comm.).

The Weatherall Formation in Melville Island is similar to the Bird Fiord Formation in Bathurst Island, and occupies the same stratigraphic position (Figs. 1.6, 1.7; Tozer and Thorsteinsson, 1964; Embry and Klovan, 1976). The two formations are separated arbitrarily by a boundary drawn down the Byam Martin Channel between Bathurst and Melville Islands.

The Hecla Bay Formation is overlain by the fluvial Beverley Inlet and Parry Islands Formations (Figs. 1.4, 1.6, 1.7; Table 1.1). These two formations are not present in sections 80X and 81I.

Source Areas

Tozer and Thorsteinsson (1964) portrayed the source area of the clastic wedge as a tectonic highland extending along the entire northwestern margin of the Canadian Arctic Archipelago (Fig. 1.8). However, Dineley (1975) suggested the eastern slope of the Caledonian Mountains chain of eastern Greenland as the source area for the clastic wedge (Fig. 1.8). Embry and Klovan (1976) demonstrated that mineralogy, facies distribution, paleocurrent patterns and regional geology all indicate that the source areas of the clastic strata lay to the north and east, and include the Caledonian and Pearya Mountain systems and Precambrian Shield of Greenland (Fig. 1.8). Chert and rock fragments characterize the detritus from the Pearya Mountains whereas detritus from the Caledonian Mountains and Precambrian Shield is characterized by a high percentage of monocrystalline quartz. The very quartzose nature of the sandstones from the Bird Fiord, Weatherall and Hecla Bay Formations on Bathurst and Melville

Table 1.2 Section 80X: Stratigraphic divisions, environment of deposition and lithologies (terminology after Goodbody, 1985).

STRATIGRAPHIC DIVISIONS	METRES ABOVE BASE	ENVIRONMENT OF DEPOSITION	LITHOLOGY
Hecla Bay Fm	919-1116	Delta plain, braided streams and deltaic marine	Non-calcareous fine grained sandstones, siltstone, shale and very fine grained sandstone
Bird Fiord Fm Member D unit 2	806-919	Delta margin distributary channels and inter-distributary bays	Non-calcareous channel fill sandstone; calcareous sandstone, siltstone and shale
Bird Fiord Fm Member D unit 1	713-806	Nearshore shelf, barrier island, nearshore bar complexes	Non-calcareous sandstone, calcareous sandstone, siltstone and shale
Bird Fiord Fm Member C unit 2	328-713	Proximal shelf, bar, interbar (storm affected)	Calcareous sandstone, siltstone and shale with minor silty limestone
Bird Fiord Fm Member C unit 1	128-328	Distal shelf, bar, interbar (storm affected)	Shale and silty shale calcareous siltstone and sandstone, and silty limestone
Bird Fiord Fm carbonate equivalent	98-128	Distal shelf or slope	Rubbly impure limestones and calcareous siltstones
Cape de Bray Fm	0-98	Marine shelf	Siltstone and shale

Islands favours the Caledonian Mountains and Precambrian Shield of Greenland as the major source areas during the deposition of these units (Embry and Klovan, 1976).

A southerly clastic source (the Canadian Precambrian Shield and Arctic Platform, Fig. 1.9) was suggested for the Bird Fiord Formation by Goodbody (1985) based on paleocurrent directions preserved in mouth bar and delta front sandstones, and direction of pinchout of sheet sandstones of the Bird Fiord Formation (Fig. 1.9). Easterly and northeasterly source areas (Fig. 1.9) are also possible according to him.

Geologic History and Paleogeography

In order to study diagenesis, the depositional and burial histories of the clastic rocks must be considered. According to Embry and Klovan (1976), the Franklinian Miogeosyncline was occupied by carbonate shelves (e.g., Blue Fiord Formation) and starved basins (e.g., Cape Phillips, Kitson and Ibbett Bay Formations) before the deposition of the Middle-Upper Devonian clastic wedge. Deposition of the clastic wedge commenced in the extreme northeast in Eifelian time, as a coastal plain gradually prograded south and west (Fig. 1.10). Climatic changes affected the paleogeography throughout the progradation, but the coastal plain continued to advance until it covered almost the entire Arctic Islands area by Middle Frasnian time. In the Late Frasnian, the entire area was uplifted and eroded. At least 300m of strata were removed in some places, forming an unconformity on the Beverley Inlet Formation on Melville and Bathurst Islands (Figs. 1.4, 1.6, 1.7). The area was transgressed gradually in the latest Frasnian; a marine shelf was widespread by Early Famennian time. Subsequent depositional events are not known due to the sparse preservation of strata younger than Early Famennian. During latest Famennian to Viséan, the Ellesmerian Orogeny uplifted and deformed the clastic wedge into a foothills belt bordering the Pearya Mountains.

Goodbody (1985) gave a slightly different and more detailed paleogeographic reconstruction of the eastern Arctic Islands during Eifelian time (Fig. 1.9). According to him, the sequence of section 80X (Table 1.2) represents a regressive change from marine slope through distal and proximal shelf to shoreline, delta margin and delta plain environments as a result of a westerly advance of a delta (Fig. 1.9).

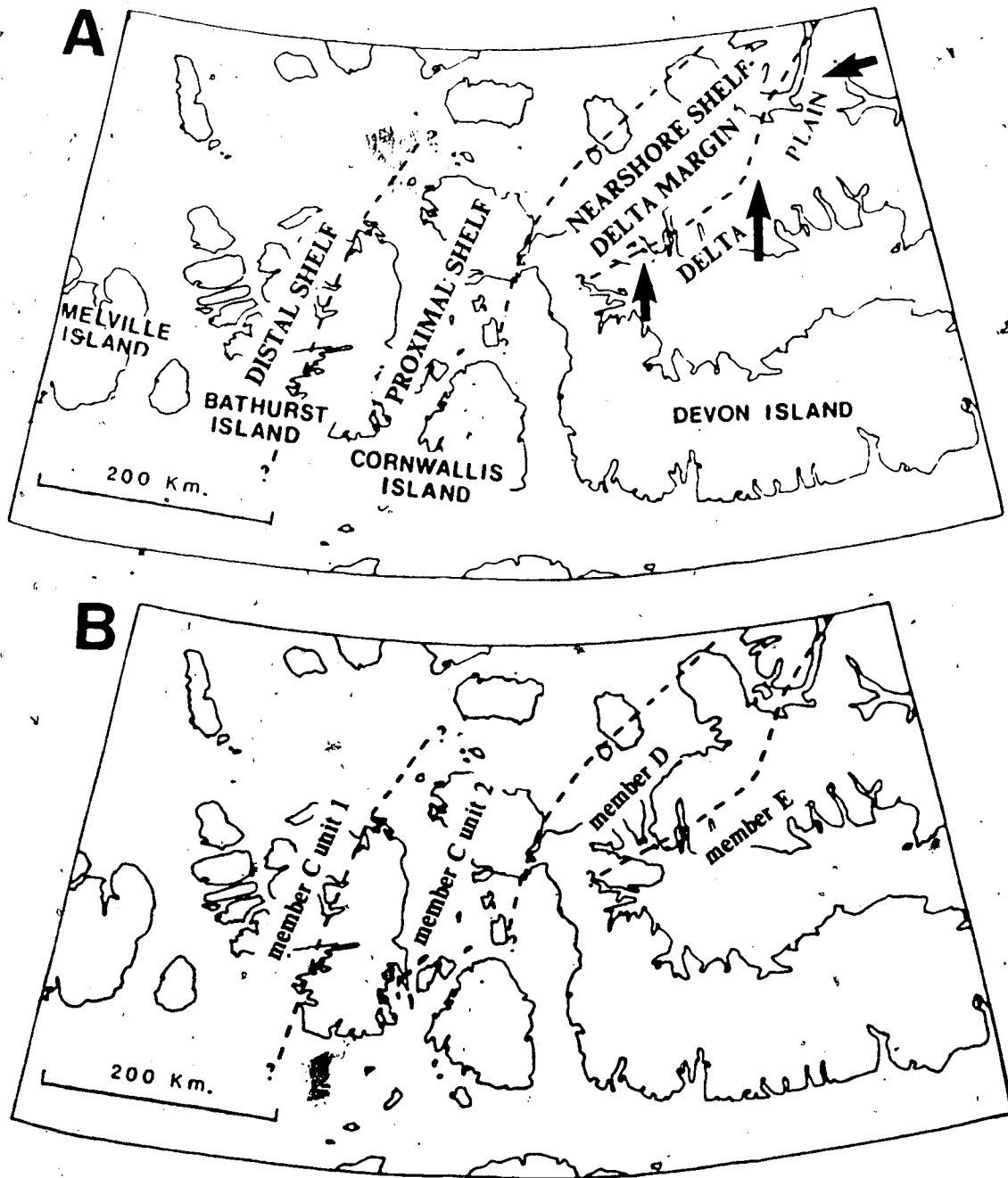


Fig. 1.9 Source areas (arrows) and paleogeography, Middle Eifelian. (A) Facies distribution (B) Rock units (after Goodbody, 1985).

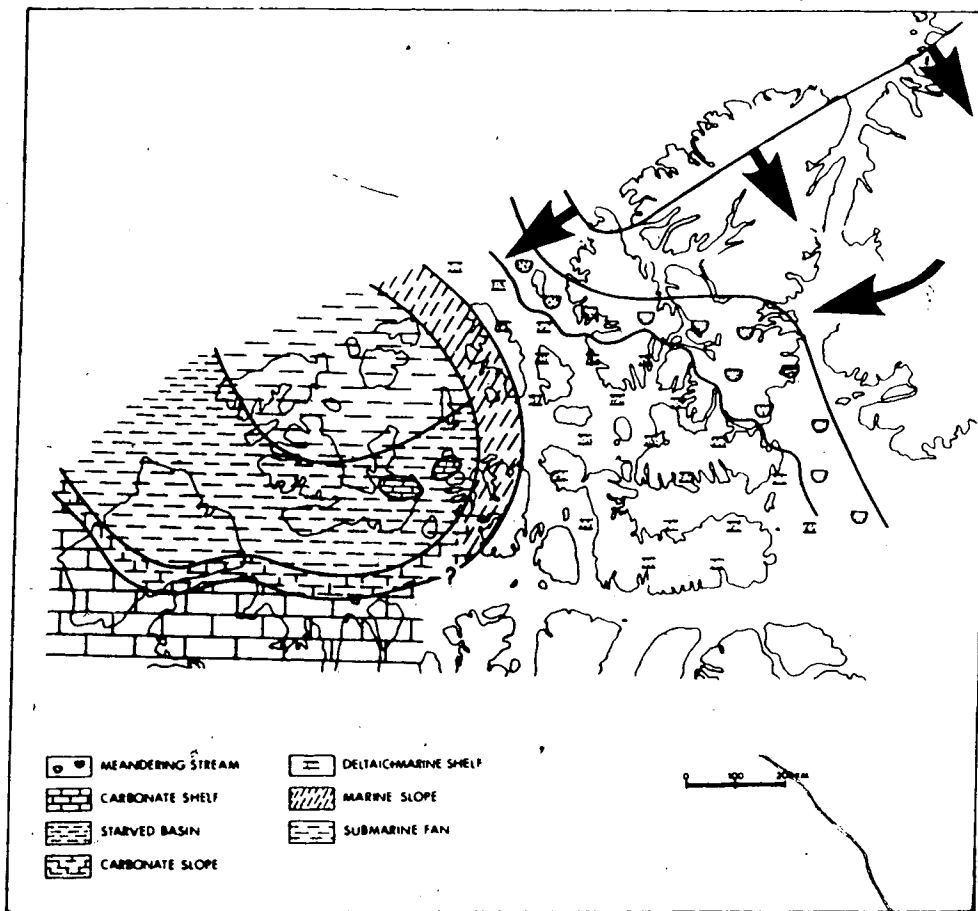


Fig. 1.10 Late Eifelian paleogeography (after Embry and Klovan, 1976).

Mineralogy

Embry and Klovan (1976) reported on the mineralogy of the clastic rocks from the Bird fiord, Weatherall and Hecla Bay Formations of the Bathurst and Melville Islands. They concluded that:

1. most of the white (kaolinitic) sandstone are quartzarenites;
2. feldspars include plagioclase and orthoclase, and rock fragments are mostly shale with minor chert;
3. authigenic kaolinite and quartz overgrowths are abundant in the sandstones;
4. calcite cement is more abundant in sandstones from the Bird Fiord Formation than from the Weatherall Formation, but is usually absent in sandstones from the Hecla Bay Formation, and
5. sandstones from the Hecla Bay Formation have the highest porosity followed by the Weatherall and Bird Fiord Formations in decreasing order.

According to Embry and Klovan (1976), clay minerals in bulk shale samples from the Bird Fiord and Weatherall Formations include kaolinite, illite, chlorite and smectite. Shales from the Bird Fiord Formation have a higher calcite content than the Weatherall shales. Cauffman (1974) determined the polytypes of clay minerals in the Middle-Upper Devonian shales on Melville Island to be 1Md kaolinite, 1Md illite and trioctahedral chlorite.

II. RESULTS

All samples examined in this study (Tables 2.1, 2.2) were from sections 80X (Dundee Bight, Bathurst Island Fig. 1.2) and section 81I (South McCormick Inlet, Melville Island; Fig. 1.2) which were collected by Goodbody (1985, pers. comm.). A detailed lithological log of section 80X is found in Goodbody (1985). Samples analysed included argillaceous limestone, shale, siltstone and sandstone.

Analytical methods used to examine the samples included thin section petrography, scanning electron microscopy-energy dispersive analysis (SEM-EDA), X-ray diffraction analysis (XRD) and stable isotope measurements of carbon and/or oxygen from diagenetic minerals. Details of analytical techniques are given in Appendix I.

A. MINERALOGY OF SHALES AND ARGILLACEOUS LIMESTONES

The clay mineralogy of the $<2\mu\text{m}$ size-fraction of shales and argillaceous limestones in sections 80X and 81I is given in Tables 2.3 and 2.4, respectively. X-ray diffractograms for the <2 and $<0.2\mu\text{m}$ size-fractions from representative shale and limestone samples are shown in Figures 2.1, 2.2 and 2.3.

Clay minerals are the most abundant phase in all the $<2\mu\text{m}$ size-fractions from the shales. Other minerals present are minor amounts of quartz and traces of K-feldspar and plagioclase (Fig. 2.1 and 2.3). Illite¹ is the most abundant clay mineral in section 80X (57-74%, Table 2.3) and section 81I (35-46%, Table 2.4). Other clay minerals present in section 80X are kaolinite² (8-20%), chlorite (10-19%) and illite/smectite (4-8%) (Fig. 2.1A,B,D); smectite (2%) is present in only one shale sample (Fig. 2.1A). In section 81I other clay minerals present are kaolinite (24-36%), chlorite (15-23%) and illite/smectite (6-12%) (Fig. 2.3A,B,C).

The $<0.2\mu\text{m}$ size-fraction of the shales in section 80X is comprised of clay minerals only - illite, kaolinite, chlorite, illite/smectite and smectite (Fig. 2.2A,B,D).

The average composition of bulk shale samples from the Bird Fiord and Weatherall Formations was given by Embry and Klovan (1976). They noted that shales of the Bird Fiord Formation have more calcite ($10\pm 4\%$) than shales of the Weatherall Formation ($1\pm 1\%$). This difference in calcite content is also observed here (compare Figures 2.1D and 2.3A,B,C).

¹Illite is used here as a general term for the clay mineral belonging to the mica group.

²Kaolinite is used here to refer to all kaolinite group minerals.

Table 2.1 Section 80X: Samples studied. The samples are from the Hecla Bay Formation (935-1070m), Bird Fiord Formation (129-891m), Bird Fiord Formation carbonate equivalent (99-119m) and Cape de Bray Formation (81m).

METRES ABOVE BASE	ROCK TYPE	THIN SECTION	X-RAY DIFFRACTION			SEM ¹
			B-P ¹	<2 μ m	<0.2 μ m	
1070	Sublitharenite	X	X	X		X
1060	Sublitharenite	X	X	X	X	X
1030	Sublitharenite	X	X	X		X
935	Sublitharenite	X	X	X		X
891	Quartzarenite	X	X	X		X
886	Sublitharenite	X	X	X		X
881	Sublitharenite	X	X			
866	Subarkose	X	X			
863.5	Subarkose	X	X	X		
844	Sublitharenite	X	X			
842	Sublitharenite	X	X			
839	Sublitharenite	X	X	X		X
805	Sublitharenite	X	X			X
799	Sublitharenite	X	X			
797	Sublitharenite	X	X	X		
767	Sublitharenite	X	X			
766	Quartzarenite	X	X			
750	Sublitharenite	X	X			
742	Quartzarenite	X	X			X
734	Subarkose	X	X	X		
725	Quartzarenite	X	X			X
720	Subarkose	X	X			
713	Shale	X	X	X	X	
704	Quartzarenite	X	X			
683	Sublitharenite	X	X	X		X
668	Sublitharenite	X	X	X		X
640	Argillaceous silty limestone	X		X		
637	Siltstone	X		X	X	
600	Sublitharenite	X	X			X
598	Sublitharenite	X	X	X		
592	Argillaceous silty limestone	X				
501	Sublitharenite	X	X	X		X
488.5	Siltstone	X	X			
488.75	Sublitharenite			X		
486	Coarse siltstone	X				
481.75	Coarse siltstone	X		X		
480.75	Shale siltstones	X		X		
479.75	Coarse siltstone	X		X		
478.75	Calcareous shale	X		X	X	
477.75	Calcareous shale			X		
476.75	Calcareous shale	X				
475.75	Calcareous shale	X		X		
474.75	Calcareous shale	X		X		X
474	Sublitharenite	X	X	X		
469	Sublitharenite	X	X	X		
448	Shale	X		X	X	
435	Sublitharenite	X	X	X		X

continued

Table 2.1 Continued

METRES ABOVE BASE	ROCK TYPE	THIN SECTION	X-RAY DIFFRACTION			SEM
			B-P ¹	<2 μ m	<0.2 μ m	
423	Sublitharenite	X	X			
387	Shale & siltstone	X		X		
330	Quartzarenite	X	X	X		X
320	Argillaceous silty limestone	X	X			
280	Sublitharenite	X	X	X	X	X
253	Argillaceous silty limestone	X		X		
228	Argillaceous silty limestone	X				
227	Argillaceous sandy limestone	X	X	X		
223	Coarse siltstone			X		
200	Sublitharenite	X	X	X		X
195	Shale & limestone	X		X		
148.8	Sublitharenite			X		
140	Argillaceous silty limestone	X				
130	Calcareous shale	X		X	X	
129	Sandy limestone	X				
119	Silty limestone	X				
118	Argillaceous silty limestone	X		X		
102.4	Argillaceous silty limestone	X		X	X	
102	Argillaceous limestone	X				
99	Argillaceous limestone	X		X		
81	Calcareous shale			X	X	

¹SEM = Scanning Electron Microscope¹B-P = Back-packed (whole rock)

Table 2.2 Section 811: Samples studied. The samples are from the Hecla Bay Formation (849.3-857m) and Weatherall Formation (0-833m).

METRES ABOVE BASE	ROCK TYPE	THIN SECTION	XRD ¹ (<2 μ m)
857	Non-calcareous sandstone	X	
849.3	Calcareous sandstone	X	
833	Calcareous sandstone	X	
822	Calcareous sandstone	X	X
818.6	Calcareous sandstone	X	X
808	Calcareous sandstone	X	
806	Calcareous sandstone	X	
751	Non-calcareous sandstone	X	X
749.75	Non-calcareous sandstone	X	X
749	Non-calcareous sandstone	X	X
747	Non-calcareous sandstone		X
736	Calcareous sandstone	X	X
735	Calcareous sandstone	X	X
690	Calcareous sandstone	X	X
647.1	Argillaceous silty limestone	X	X
644	Calcareous sandstone	X	X
592	Shale		X
591	Calcareous sandstone	X	
563.8	Argillaceous sandy limestone	X	
510	Calcareous shaly sandstone	X	
495	Shale		X
494	Argillaceous limestone	X	
334.5	Calcareous siltstone	X	X
302	Calcareous siltstone	X	X
294.5	Silty shale	X	X
257.3	Calcareous shale	X	
256.3	Calcareous sandy shale	X	
249	Calcareous sandstone	X	
243.5	Calcareous sandstone		X
238	Calcareous sandstone	X	
224.5	Calcareous sandstone	X	
216	Calcareous sandstone	X	
207	Shale		X
177.8	Calcareous sandstone	X	
171.8	Calcareous sandstone	X	
166	Shale		X
165	Argillaceous calcareous siltstone	X	
161	Silty shale	X	
145	Argillaceous siltstone	X	
144	Calcareous sandstone	X	X
143.2	Calcareous sandstone	X	
142	Non-calcareous sandstone	X	
121.8	Calcareous sandstone	X	X
119.9	Calcareous sandstone	X	
119.5	Non-calcareous sandstone	X	
114.3	Calcareous sandstone	X	
111.3	Calcareous sandstone	X	
90	Calcareous sandstone	X	

continued

Table 2.2 Continued

METRES ABOVE	ROCK TYPE	THIN SECTION	XRD ¹ (<2 μ m)
63	Non-calcareous sandstone	X	X
47.2	Calcareous sandstone	X	
31.5	Calcareous siltstone	X	
30.6	Silty shale	X	
26.4	Limestone	X	
15	Silty limestone	X	
14	Silty limestone	X	X
0	Calcareous sandstone	X	

¹XRD = X-Ray Diffraction

Table 2.3 Clay mineralogy of the <2 μ m size-fraction of shales, argillaceous limestones, siltstones and sandstones, section 80X

METRES ABOVE BASE	ROCK TYPE	RELATIVE % CLAY MINERALS					%I in I/S
		K	I	C	S	I/S	
1070	calc. ss	43	24	33			
1060	non-calc. ss	52	13	35			
1030	non-calc. ss	85	15				
935	non-calc. ss	85	15				
891	non-calc. ss	80	20				
886	calc. ss	53	23	17	6		
863.5	calc. ss	18	46	16	7	13	65
839	non-calc. ss	46	29	14	10		
734	non-calc. ss	25	18	27	31		
713	non-calc. ss	18	57	19	2	4	80
683	calc. ss	34	18	36	12		
668	non-calc. ss	40	19	27	14		
637	siltst	20	56	19		5	85
598	calc. ss	19	58	20		4	70
488.5	siltst	21	56	17		6	65
481.75	coarse siltst	29	49	16		7	80
480.75	sh/siltst	18	58	19		6	75
479.75	coarse siltst	18	57	18		7	60
478.75	calc. sh	16	63	15		7	80
477.75	calc. sh	14	63	16		6	70
475.75	calc. sh	20	61	13		6	70
474.75	calc. sh	19	61	15		5	65
474	calc. ss	21	54	16		9	65
469	calc. ss	21	58	16		5	80
448	non-calc. sh	16	62	17		5	80
435	calc. ss	34	24	36		5	60
387	sh/siltst	17	60	19		4	80
330	calc. ss	48	25	23		5	65
280	calc. ss	4	20	4		72	90
227	arg. silty ls	7	62	17		4	70
223	coarse siltst	16	64	16	4		
200	calc. ss	21	51	17	3	21	65
148.8	calc. ss	24	50	43		6	75
130	calc. sh	12	72	10		5	80
118	arg. silty ls	9	76	9		5	65
102.4	arg. ls	14	72	14		8	75
99	arg. silty ls	13	73	14			
81	calc. sh	8	74	10		8	75

K = Kaolinite
 I = Illite
 C = Chlorite
 S = Smectite
 I/S = Illite/Smectite

Table 2.4 Clay mineralogy of the $<2\mu\text{m}$ size-fraction of shales, argillaceous limestones, siltstones and sandstones, section 811

METRES ABOVE BASE	ROCK TYPE	RELATIVE % CLAY MINERALS				%I in I/S
		K	I	C	I/S	
833	calc. ss	29	35	26	10	50
822	calc. ss	21	30	44	5	75
818.6	calc. ss	45	28	22	5	50
751	non-calc. ss	52	20	23	5	70
749.75	non-calc. ss	32	44	18	6	65
749	non-calc. ss	59	20	18	4	60
747	non-calc. ss	29	46	17	8	60
736	calc. ss	40	24	30	6	65
735	calc. ss	41	26	26	6	60
690	calc. ss	48	22	25	5	65
647.1	arg. ls	25	47	18	10	60
644	calc. ss	34	38	21	7	65
592	non-calc. sh	33	40	19	9	65
495	non-calc. sh	36	35	23	6	55
334.5	calc. siltst	36	33	18	12	60
302	calc. siltst	42	28	24	6	70
294.5	non-calc. silty sh	31	44	16	10	65
243.5	calc. ss	28	45	18	10	70
207	non-calc. sh	24	49	15	12	65
166	non-calc. sh	28	44	20	9	70
144	calc. ss	48	20	26	6	70
121.8	calc. ss	35	39	17	8	75
119.5	non-calc. ss	22	52	16	10	75
63	non-calc. ss	27	43	19	12	70
14	silty ls	29	46	18	7	65

K = Kaolinite

I = Illite

C = Chlorite

I/S = Illite/Smectite

Fig. 2.1 X-ray diffractograms for representative shale and limestone samples (<2 μ m size-fraction), Section 80X. K=Kaolinite, I=Illite, I/S=Illite/Smectite, S=smectite, C=Chlorite, Q=Quartz and F=Feldspar.

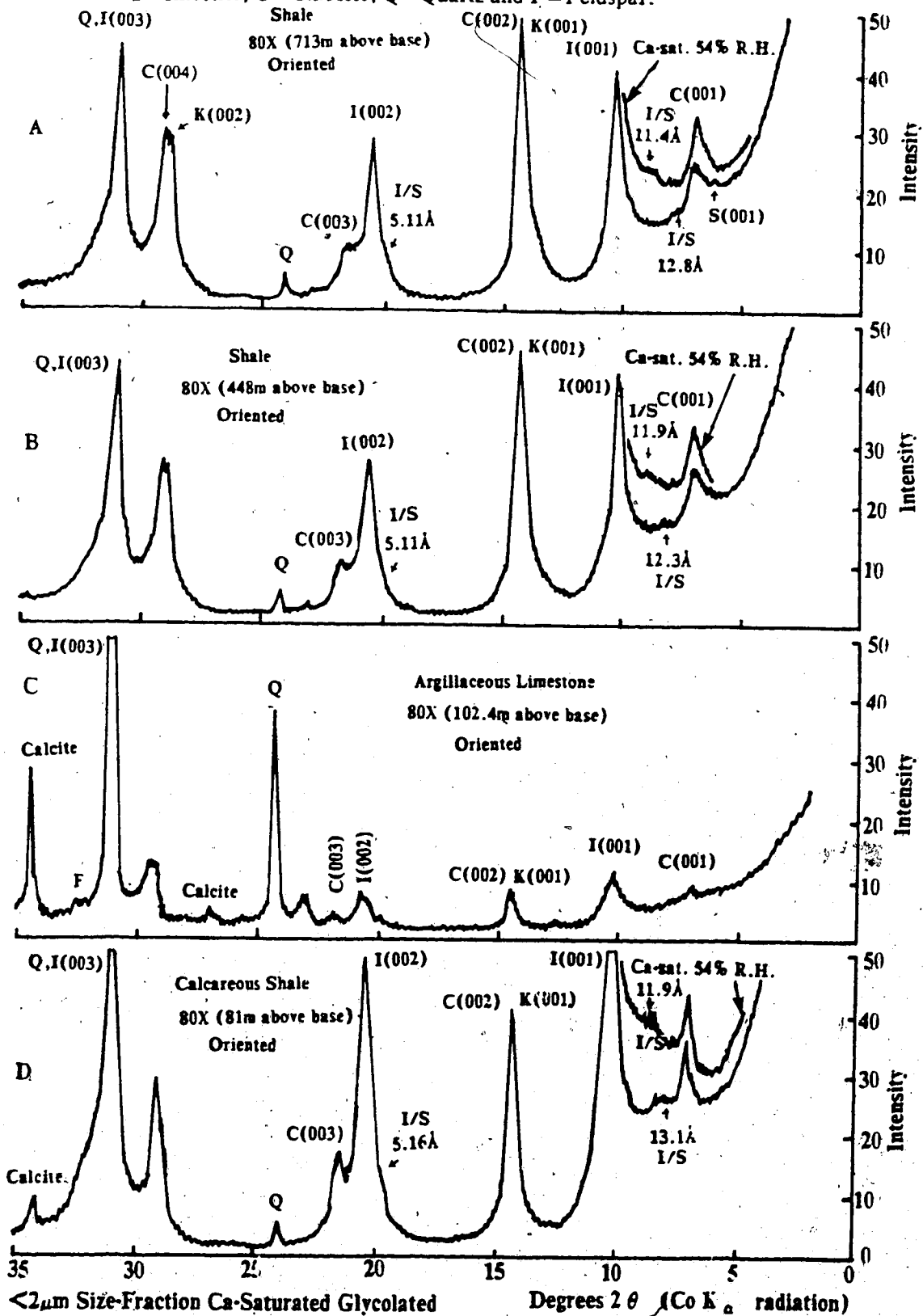


Fig. 2.2 X-ray diffractograms for representative shale and limestone samples (<0.2 μ m size-fraction), Section 80X. See Figure 2.1 for meaning of symbols.

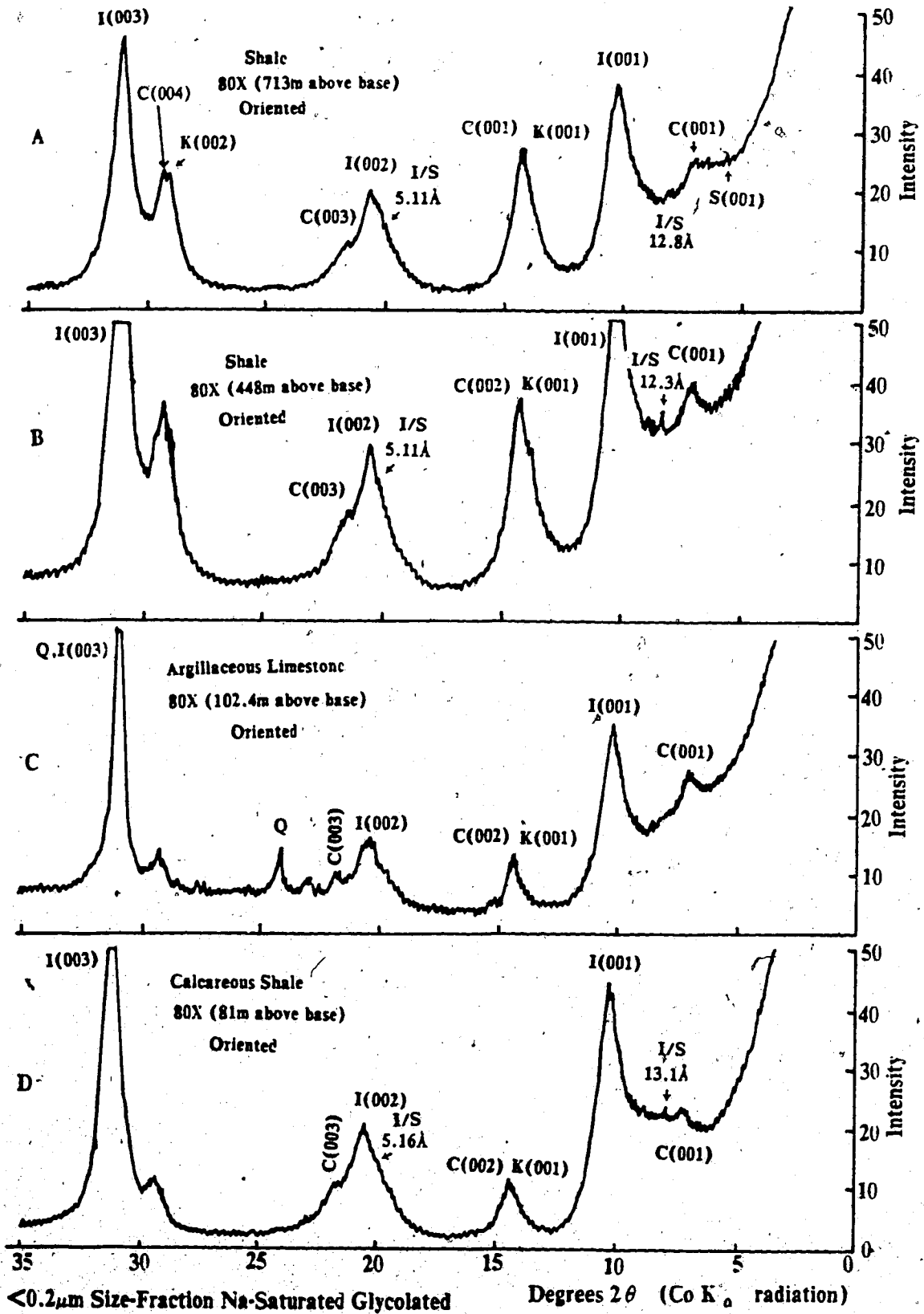


Fig. 2.3 X-ray diffractograms for representative shale and limestone samples (<2 μ m size-fraction), Section 811. See Figure 2.1 for meaning of symbols.

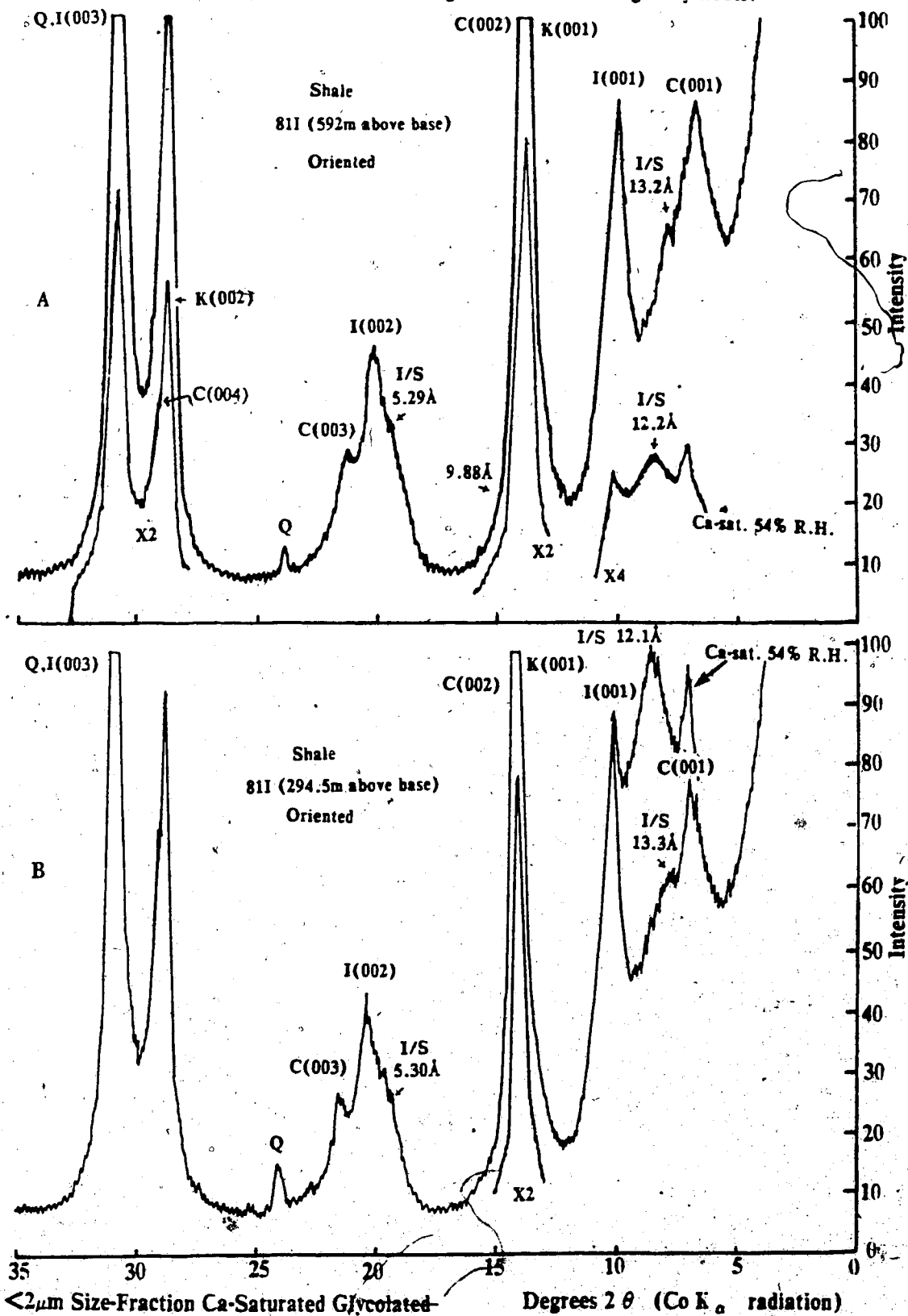
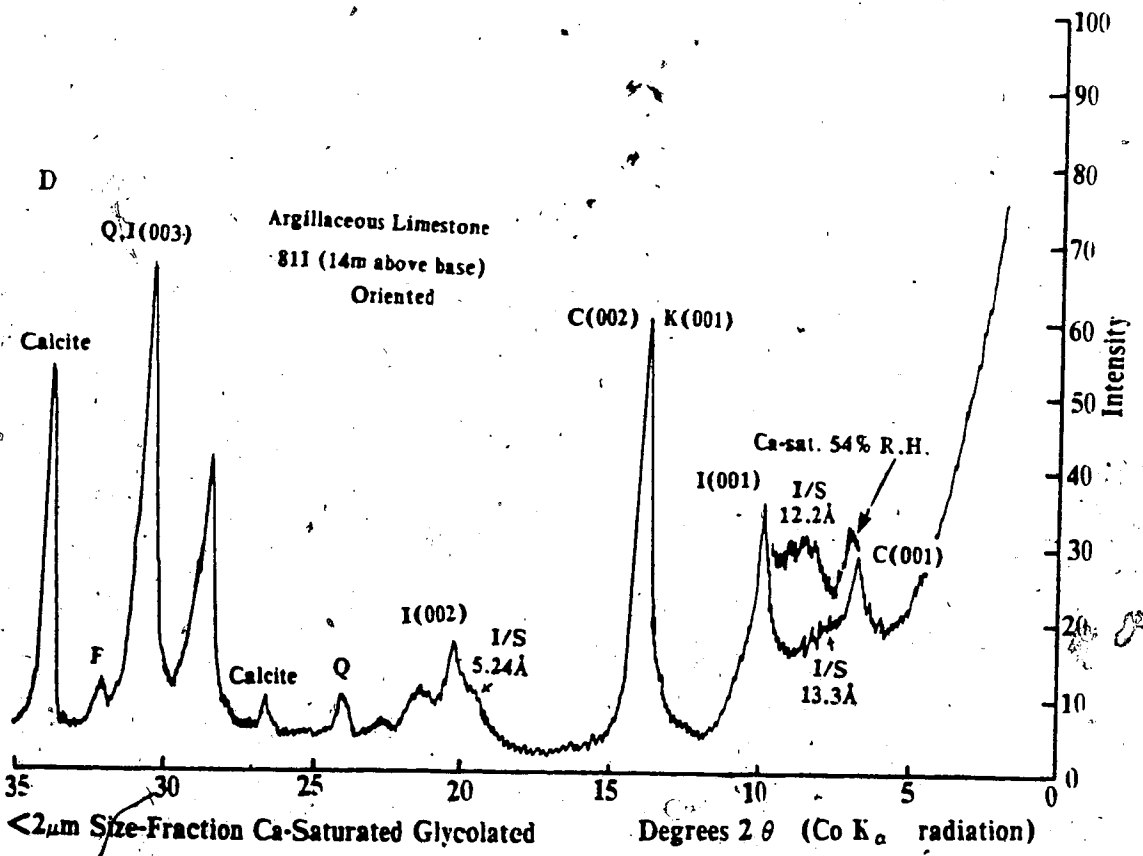
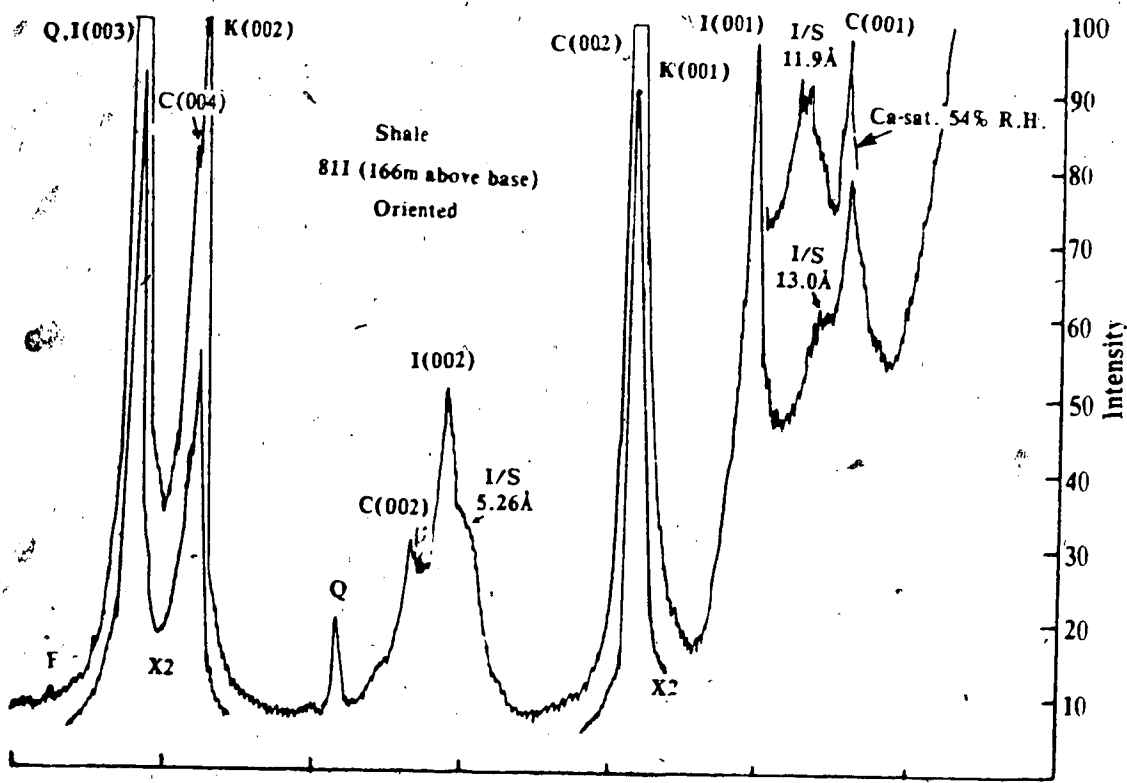


Fig. 2.3 continued



The clay mineralogy of the $<2\mu\text{m}$ size-fractions of the argillaceous limestones is similar to that of the shales. The clay minerals present in the argillaceous limestones from section 80X are illite (58-76%), kaolinite (9-19%), chlorite (9-20%) and illite/smectite (0-5%) (Fig. 2.1C; Table 2.3). Illite (46-47%), kaolinite (25-29%), chlorite (18%) and illite/smectite (7-10%) are also present in the argillaceous limestones from section 811 (Fig. 2.3D; Table 2.4). Quartz (minor to moderate amounts) and feldspars (trace to minor amounts) are also present in the $<2\mu\text{m}$ size-fraction of the argillaceous limestones from sections 80X and 811 (Figs. 2.1C, 2.3D). Minor amounts of quartz are present in the $<0.2\mu\text{m}$ size-fraction of some argillaceous limestones (Fig. 2.2C).

Nature of Illite/Smectite

The percentage of illite layers in the illite/smectite (Tables 2.3, 2.4) was determined by the methods described by Reynolds and Hower (1970), Reynolds (1980) and Hower (1981a) (Appendix I). The methods described by Srodon (1984) were not used because his methods were more suited to monomineralic samples. An attempt to get monomineralic samples of illite/smectite proved unsuccessful because other clay minerals are also present in the $<0.2\mu\text{m}$ size-fractions (see above).

Illite/smectite in the shales and argillaceous limestones in section 80X have 65-80% illite layers, compared to 55-70% in section 811. All the illite/smectite may be classified as "allevardite" ordered (with one to three illite layers between each smectite layer; i.e., IS to ISII layering) because the percentages of illite layers in the illite/smectite are mostly within the 60-85% range, and superlattice diffractions (30-35Å) are present as shoulders (Hower, 1981a). There is no apparent increase in illite layers with depth in either section (Table 2.3, 2.4).

B. DETRITAL MINERALOGY OF SANDSTONES

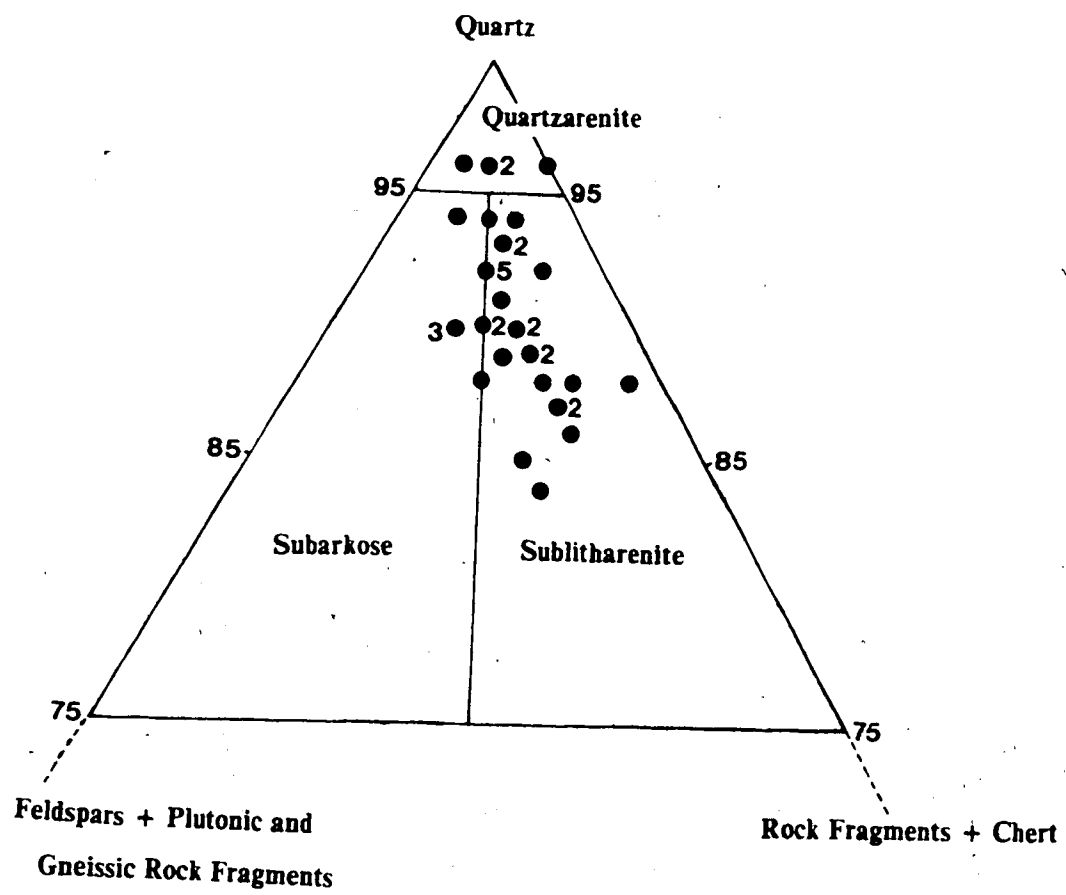
The framework material of the sandstones is predominantly quartz (45-85%), with some feldspar (1-5%), rock fragments (0-6%) and chert (0-4%) (Table 2.5). Based on the classification given by Folk (1968), most of the sandstones can be classified as sublitharenites; a few quartzarenites and subarkoses are also present (Fig. 2.4; Table 2.5). The sandstones are submature to mature with moderate to very little matrix. Most of the sandstones are very fine- to fine-grained and moderately to well sorted.

Table 2.5 Mineralogy of sandstones: Thin-section analysis, section 80X.

METRE ABOVE BASE	ROCK CLASS (Folk, 1968)	FRAMEWORK GRAINS (%)				CEMENTS (%)				MICAS P (%)	
		Q	F	CH	RF	Q	CA	K	C		
1070	S-A	70	3	0	3	5	1	7	2	8	1
1060	S-A	70	2	1	2	6	0	7	3	7	2
1030	S-A	70	2	1	2	10	0	10	0	2	3
935	S-A	70	3	0	3	6	0	15	0	1	2
891	S-A	70	3	1	2	7	0	10	0	2	5
886	S-A	60	3	3	3	3	12	5	3	5	3
881	S-A	70	3	4	2	5	1	4	3	6	2
866	S-A	70	3	3	2	10	1	4	2	1	4
863.5	S-AK	45	3	1	1	0	40	3	3	3	1
844	S-A	70	3	3	3	10	0	5	2	1	3
842	S-A	65	5	4	3	5	0	5	3	6	4
839	S-A	70	4	2	3	5	0	6	3	3	4
805	S-A	75	4	1	3	5	0	5	2	1	4
799	S-A	75	3	1	3	5	3	3	2	3	2
797	S-AK	50	2	1	0	0	35	3	2	1	1
767	S-A	45	3	2	3	1	45	0	0	1	0
766	S-A	50	1	1	1	1	40	2	1	2	1
750	S-A	75	3	1	2	10	3	1	1	2	2
742	S-A	75	3	1	2	10	3	2	1	1	2
734	S-A	80	5	2	2	5	0	2	1	2	1
725	S-A	85	3	1	1	5	0	2	1	1	1
720	S-AK	75	5	2	2	10	0	2	1	2	1
704	Q-A	75	2	0	1	7	2	2	1	7	3
683	S-A	65	3	2	5	10	4	2	2	5	2
668	S-A	70	3	2	6	10	0	3	1	2	3
600	S-A	65	3	2	2	12	5	5	2	1	3
598	S-A	45	1	2	1	0	50	0	0	1	0
501	Q-A	45	1	1	1	5	40	2	1	2	2
488.5	S-AK	45	3	0	2	0	45	1	1	2	1
474	S-A	60	2	4	2	2	25	2	1	2	0
469	S-A	50	2	2	2	2	35	2	2	2	1
435	S-A	70	1	4	5	0	10	3	3	2	2
423	S-A	45	1	2	1	1	45	2	2	1	0
330	Q-A	70	2	1	1	15	3	3	2	1	2
280	Q-A	50	1	1	0	2	45	0	0	1	0
200	S-A	55	3	1	2	4	30	1	1	2	1

S-A = sublitharenite S-AK = subarkose Q-A = quartzarenite
 Q = quartz F = feldspar CH = chert RF = rock fragments
 CA = carbonate K = kaolinite C = chlorite P = porosity

Fig. 2.4 Classification of sandstones in section 80X (after Folk, 1968).



Most quartz grains are monocrystalline (with traces of polycrystalline quartz grains) showing straight to undulatory extinction (Plate 2.1A,B). The straight to undulatory extinction is typical of a source area with high-grade metamorphic rocks and granitic intrusives (Blatt et al., 1980), suggesting that the Precambrian Shield of Greenland and Canada and the Caledonian Mountains may have been the major source areas. The low amount of chert and other rock fragments indicates that the Pearya Mountains were probably a minor supplier of clastic sediments to the study areas. However, some of the quartz grains may have been derived from the Pearya Mountains.

Sandstones with little or no carbonate cement (Plate 2.1A,B) have subrounded quartz grains with thick quartz overgrowths. Compaction has resulted in concavo-convex quartz to quartz contacts which indicate that pressure solution has probably occurred (Plate 2.1A,B; deBoer et al., 1977; Robin, 1978).

Sandstones with >40% calcite cement (Plate 2.1C,D) have angular to subangular grains with little or no quartz overgrowths. The quartz grains in these sandstones are etched into irregularly-shaped fragile grains that could not have survived transportation; partial corrosion of quartz grains and precipitation of carbonate cement has apparently occurred (Plate 2.1C) (Blatt et al, 1980). Sandstones with >40% calcite tend to have a poikilotopic texture with very few grain to grain contacts (Plate 2.1C,D).

The feldspar content of the sandstones comprises approximately equal amounts of plagioclase (mostly oligoclase) and potassium feldspar (mostly orthoclase). Partial or complete feldspar dissolution has occurred, leaving relict feldspar in large secondary pores (Plate 2.2A). Partial or complete calcite replacement of plagioclase and potassium feldspar has also taken place, leaving relict feldspar in the calcite cement (Plates 2.2B,C).

Fine-grained metamorphic rock fragments (Plates 2.1A,B, 2.2D) and shale clasts (Plate 2.2A) are usually compacted to form pseudomatrix around framework grains. These pseudomatrix are partially dissolved in most cases. Microcrystalline chert present in the sandstones is also partially dissolved (Plate 2.1A).

The most common accessory minerals (cements excluded) are micas (1-8%; Table 2.5), which comprise approximately equal amounts of muscovite and biotite. The micas are deformed about framework grains (Plate 2.2D). Some mica flakes are partially replaced by carbonate cement (Plates 2.2B,C); biotite is also altered to chlorite (Plate 2.2B).

PLATE 2.1

- A. A typical, slightly calcareous sandstone. Framework grains include quartz (Q), fine-grained metamorphic fragment (MF) compacted into pseudomatrix, chert (CHE) and feldspar (F). Quartz are mostly monocrystalline with straight to undulatory extinction and are subrounded with thick quartz overgrowths (O). PQ=polycrystalline quartz. Concavo-convex quartz to quartz contacts (CC) and muscovite (M) are also present. Scale bar=200 μ m. Cross-polarized light. Section 80X(800m)
- B. A typical, non-calcareous sandstone. Metamorphic rock fragments compacted into pseudomatrix (PM). Other symbols same as A. Scale bar=200 μ m. Cross-polarized light. Section 80X(839m)
- C. A typical sandstone with >40% carbonate cement (CAR) and a poikilotopic texture. Framework grains (mostly quartz) are angular to subangular with little or no quartz overgrowths and with little or no grain contacts. Quartz edges are highly corroded or etched by the carbonate cement. Scale bar=200 μ m. Cross-polarized light. Section 80X(767m)
- D. A typical, fossiliferous sandstone with a poikilotopic texture. Framework grains are angular to subangular with little or no quartz overgrowths. Shell fragment (SH) and calcite cement are stained red and detrital dolomite (D) is unstained. Scale bar=200 μ m. Cross-polarized light. Section 80X(280m)

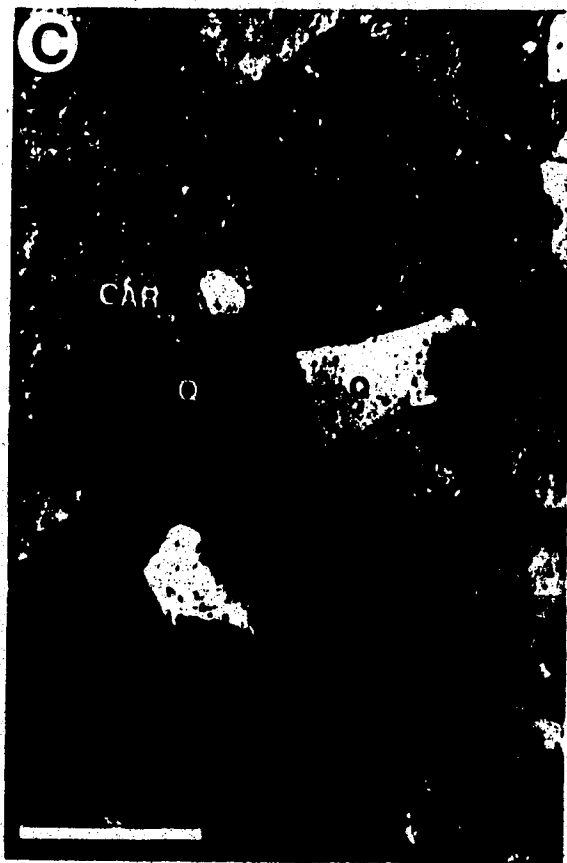


PLATE 2.2

- A. A typical sandstone with high secondary porosity (blue to purple) created by partial dissolution of feldspar (F), fine-grained metamorphic rock fragments (MF) and shale fragments (SHF). Most of the rock fragments have been compacted into pseudomatrix. Pore-filling kaolinite (K) with intercrystalline macroporosity and euhedral quartz overgrowths (O) are also present. Scale bar=200 μ m. Plane-polarized light. Section 81I(849.3m)
- B. Carbonate (CAR) replacing plagioclase (P) and muscovite (M). Biotite flake (B) is altered to chlorite. Scale bar=50 μ m. Cross-polarized light. Section 81I(510m).
- C. Feldspar (F, microcline?) and muscovite (M) replaced by calcite (Ca). Scale bar=50 μ m. Cross-polarized light. Section 80X(469m)
- D. Fine-grained metamorphic rock fragments (MF), biotite (B) and muscovite (M), are usually compacted to form pseudomatrix. Scale bar=200 μ m. Cross-polarized light. Section 80X(668m)



Shell fragments are common (traces to moderate) in calcareous samples (Table 2.6; Plates 2.1D; 2.3A). The shell fragments are partially or completely dissolved, creating secondary porosity (Plate 2.3A). Trace to moderate amounts of detrital dolomite grains are present in some samples (Table 2.6; Plate 2.1D).

Most of the porosity appears to be secondary, resulting from the dissolution of feldspar, rock fragments, carbonate cements, shell fragments and clay matrix (Plate 2.2A, 2.3A). Porosity in section 81I (up to 10%; e.g., Plate 2.2A) appears to be somewhat higher than in section 80X (0-5%; Table 2.5).

The clay mineralogy of the sandstones is shown in Tables 2.3 and 2.4; both detrital and authigenic clays are present. Detrital clays include illite, chlorite and kaolinite which may be found in the matrix and low-rank metamorphic and sedimentary rock fragments. The most common non-opaque heavy mineral is zircon, which occurs in trace amounts in some samples.

C. DIAGENETIC MINERALOGY OF SANDSTONES

Authigenic minerals in the sandstones of sections 80X and 81I include chlorite, quartz, calcite, ankerite, dolomite, kaolinite, illite, illite/smectite and smectite (Tables 2.3-2.6).

Chlorite

Authigenic chlorite, which occurs as thick grain-coatings on quartz (Plates 2.3B, 2.4A,B) and feldspar (Plate 2.4C), is an important diagenetic cement in almost all of the sandstones in sections 80X and 81I (up to 3% in section 80X, Table 2.5). It comprises 0-43% (average = 20%, Table 2.3) and 16-44% (average = 23%, Table 2.4) of the <2 μ m size-fraction of sections 80X and 81I, respectively. The euhedral, pseudo-hexagonal chlorite crystals are oriented perpendicular to the grain surface (Plate 2.4B), giving a radiating texture in thin-section (Plate 2.3B). The grain-coating chlorite appears greenish under plane-polarized light.

The EDA spectrum of chlorite indicates it is Fe-rich, with only minor Mg (Plate 2.4D). XRD analysis of the chlorite suggests that it may be chamosite. The lower intensity of the chlorite (001) peak (14.2Å) compared to the (002) (7.1Å) and (004) peaks (3.53Å) (Fig. 2.5) is characteristic of chamosite (Brindley, 1951). Furthermore, heating to 550°C greatly increases the intensity of the (001) reflection (Fig. 2.5); this behaviour is indicative of very

Table 2.6 Types of authigenic and detrital carbonates, section 80X.

METRES ABOVE BASE	AUTHIGENIC CARBONATES (% OF WHOLE ROCK)			DETRITAL CARBONATES	
	Calcite	Dolomite	Ankerite	Calcite (shell fragments)	Dolomite grains
1070	1				
1060					
1030					
935					
891					Trace ¹
886			12		
881	1				
886		1			
863.5	40			Trace	
844					
842					
839					
805					
799	2		1		Trace
797	35			Trace	Trace
767	45				Trace
766	40				
750	3				Trace
742	Trace	3			
734					
725					
720					
704	2				Trace
683	4				
668					
600	5				
598	50				Moderate ²
501	45				Moderate
488.5	50			Moderate	Moderate
474	25				Moderate
469	35			Moderate	Traces
435	10				Moderate
423	45			Trace	Moderate
330	Trace	3			Trace
280	45			Moderate	Moderate
200	15		15		

¹Trace = <1%²Moderate = 1-5%

PLATE 2.3

- A. Abundant calcareous shell fragments in an argillaceous sandstone. Shell fragments (SH) have been partially or completely dissolved. Porosity is blue. Scale bar = 1000 μ m. Plane-polarized light. Section 811(835).
- B. Complete chlorite grain-coating (C) about rounded quartz grain (Q). The chlorite grain-coating has been squashed at grain contacts (GC). Only minor quartz overgrowths (O) are present. Scale bar = 50 μ m. Cross-polarized light. Section 80X(725m).
- C. Incomplete chlorite grain-coating (C) resulting in thick, interlocking quartz overgrowths (O). The chlorite grain-coating has been squashed at grain/contact (GC). Scale bar = 50 μ m. Cross-polarized light. Section 80X(734m).
- D. Large euhedral syntaxial quartz overgrowths (O) protruding into pore. Relict feldspar (F) is present in large secondary pore (purple). Scale bar = 50 μ m. Plane-polarized light. Section 811(857m).



PLATE 2.4

- A. Thick chlorite coats (C) and quartz overgrowths (O). Section 80X(805m).
- B. Close-up of A showing characteristic euhedral, pseudo-hexagonal chlorite crystals, oriented perpendicular to the grain surface.
- C. Chlorite grain-coating (C) on feldspar grain (F) has been destroyed where feldspar dissolution has occurred. Section 80X(805m).
- D. EDA spectrum of chlorite shows that it is Fe-rich (chamosite?).
- E. Quartz overgrowths (O) engulfing chlorite coat (C). Section 80X (600m).
- F. Squashed chlorite grain-coating (C). Section 80X(683m).
- G. Interlocking large euhedral syntaxial quartz overgrowths eliminating porosity. Section 80X(330m).
- H. Small euhedral quartz overgrowths on a thick chlorite coat. Section 80X(805m).

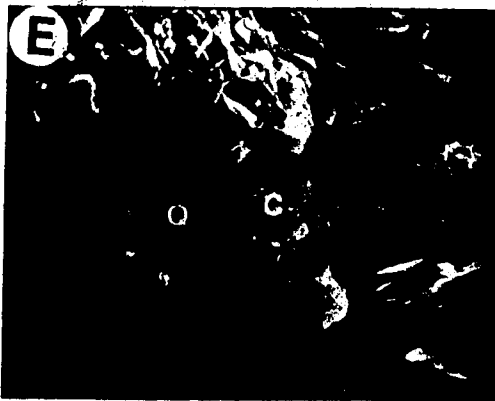
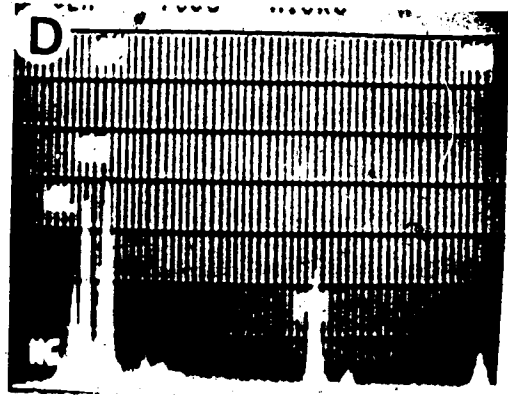
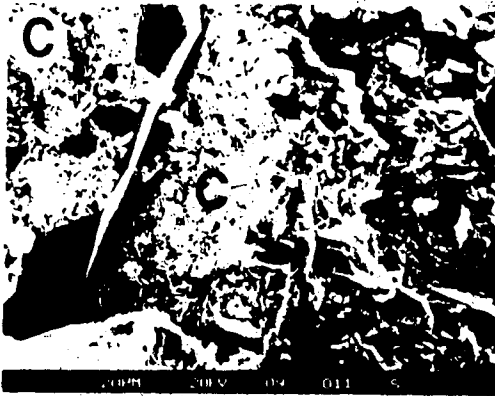
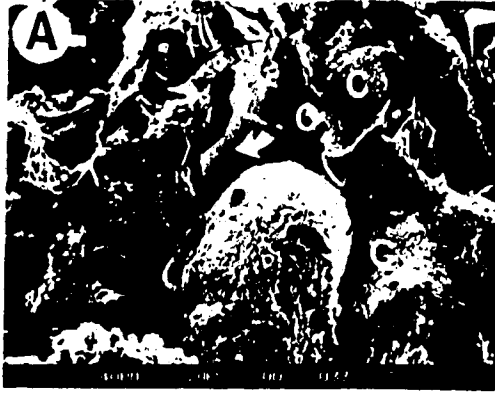
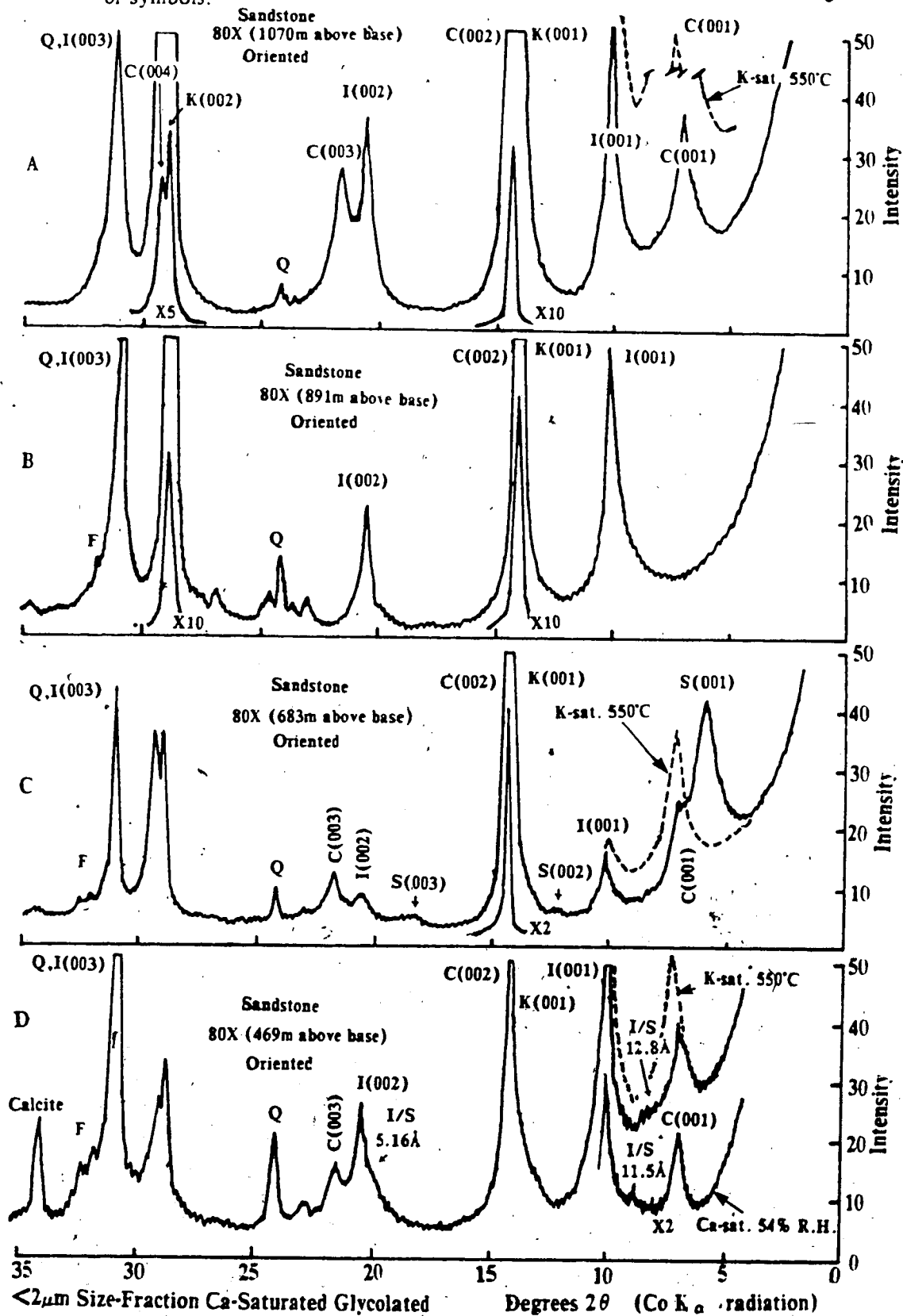


Fig. 2.5 Nature of clay minerals in sandstones, Section 80X. See Figure 2.1 for meaning of symbols.



Fe-rich chlorites (Brown and Brindley, 1980).

Early formation of the chlorite is suggested by: (i) its complete envelopment of framework grains (Plates 2.3B, 2.4A); (ii) its engulfment by quartz overgrowths (Plates 2.3B,C, 2.4E); and (iii) squashing of chlorite at grain contacts during compaction (Plates 2.3B,C, 2.4F).

Grain-coating chlorite is very abundant in samples that have little or no calcite cement and matrix (e.g., Plates 2.3B, 2.4A,B). However, samples containing over 40% calcite cement contain no chlorite (Plate 2.1C). These data suggest that the first stage of calcite precipitation was earlier than the formation of the chlorite grain-coatings, thus, inhibiting chlorite growth. Alternatively, the absence of chlorite in very calcareous sandstones may be due to a facies change.

Quartz Overgrowths and Pressure Solution

Authigenic quartz, which occurs as large euhedral syntaxial overgrowths (Plates 2.3C,D, 2.4G) and small euhedral drusy overgrowths (Plates 2.3B, 2.4A,H) on detrital quartz grains, is very abundant in sandstones with little or no carbonate cement (up to 15%, Table 2.5; Plates 2.1A,B, 2.2A). The large syntaxial quartz overgrowths may totally eliminate porosity by protruding into pore spaces and forming an interlocking texture (Plates 2.3C,D, 2.4G). However, authigenic quartz is absent or low in abundance in sandstones with >40% carbonate cement (Plate 2.5, Plate 2.1C,D).

Large syntaxial overgrowths usually engulf chlorite grain-coatings which are thin or incomplete (Plates 2.3C, 2.4E). The gaps in the incomplete chlorite coats served as preferential nucleation sites for the quartz overgrowths. If the chlorite coats are thick and continuous, the development of large syntaxial quartz overgrowths is inhibited and only small drusy quartz overgrowths have formed (Plates 2.3B, 2.4A,H). This textural relationship suggests that the formation of quartz overgrowths postdated the chlorite grain-coatings.

The presence of abundant concavo-convex quartz grain to grain contacts (Plates 2.1A,B, 2.3B, 2.5A) indicates that pressure solution has taken place due to compaction (deBoer et al, 1977; Robin, 1978). In many cases, a layer of chlorite (Plates 2.3B,C) exists at the quartz grain to grain contacts.

PLATE 2.5

- A. Concavo-convex quartz to quartz contacts (CC). Scale bar = $50\mu\text{m}$. Cross-polarized light. Section 80X(839m).
- B. Partially dissolved feldspar grain. Porosity is blue. Quartz grains (Q) have been etched or dissolved (arrows). Scale bar = $50\mu\text{m}$. Cross-polarized light. Section 811(857m).
- C & D. Calcite (Ca) is filling in large secondary pores and solution pits (black arrows) in thick quartz overgrowths (O); such behaviour probably indicates the presence of a dissolution stage prior to carbonate cementation. The host grain (HG, in C) of the quartz overgrowths may also be corroded. Scale bar for C = $200\mu\text{m}$. Scale bar for D = $50\mu\text{m}$. Cross-polarized light. C is section 80X(330m). D is section 80X(600m).



Dissolution and Alteration of Detrital Grains

This section deals with the first stage of two possible stages of dissolution and alteration of detrital grains and/or cements. The first stage is post-quartz cementation, and involves the dissolution and/or alteration of feldspar, rock and shell fragments, mica and quartz. The second stage, discussed later, occurs following carbonate cementation.

Feldspar dissolution involving both plagioclase and K-feldspar is very common (Plates 2.2A, 2.3D, 2.5B, 2.6A,B,C,D). The EDA spectrum of the plagioclase (Plate 2.6D) shows that it is Na-rich; these observations are in agreement with optical data which suggest an albitic composition for most of the plagioclase.

The dissolution of feldspar appears to postdate chlorite formation; chlorite grain-coatings have been destroyed on dissolved portions of many feldspar grains (Plate 2.4C).

Some feldspar grains have been altered to illite (Plate 2.6E); some of this alteration may also have occurred during the second dissolution stage. Feldspar has also been altered to kaolinite (Plate 2.6F).

The kaolinite formed from the feldspar appears to be corroded. This corrosion may have happened during the second dissolution stage; kaolinite precipitated following the second dissolution stage is not corroded.

The etching or corrosion of quartz overgrowths has resulted in the formation of large solution pits which are subsequently filled in by carbonates (Plate 2.5C,D). In some samples the host grain of the overgrowths has also been corroded (Plates 2.5C). The presence of carbonate cement in these solution pits suggests that quartz was corroded prior to carbonate cementation. The presence of carbonate cement in large secondary pores also suggests that there was an early stage of dissolution of feldspar and other detrital grains prior to carbonate cementation (Plates 2.1A, 2.2C, 2.5C,D).

Calcite

The type, amount and distribution of carbonate cement are shown in Table 2.5 and 2.6. Calcite, which was determined to be Fe-free by stains, EDA (Plate 2.7A) and XRD, is an important diagenetic phase (up to 50%, Table 2.6).

Some calcite cement in samples with >40% calcite formed relatively early in the diagenetic history of the sandstones in the absence of compaction and/or the crystallization of

PLATE 2.6

A. EDA spectrum of potassium feldspar in (B).

B. Partial dissolution of potassium feldspar. Section 80X(891m).

C. Partially dissolved plagioclase grain (P). See (D) for EDA. Section 80X(600m).

D. EDA spectrum of C showing that the plagioclase is Na-rich (oligoclase?).

E. Feldspar grain (F) being partially dissolved; dissolved grain has been coated by illite (I).
Section 80X(668m).

F. Potassium feldspar grain (F) being partially dissolved; dissolved grain has been coated by kaolinite (K) which is slightly corroded. Section 80X(839m).

G. EDA spectrum of kaolinite in F.

H. Calcite (Ca) completely surrounding detrital grains (D). Section 80X(280m).

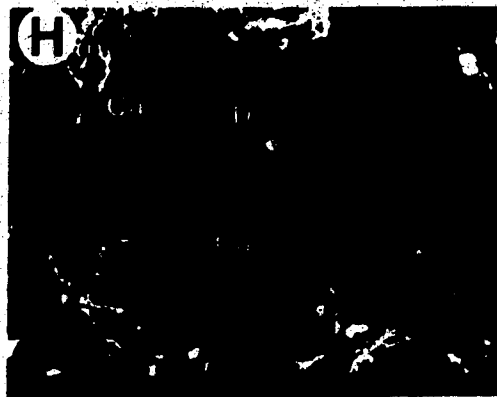
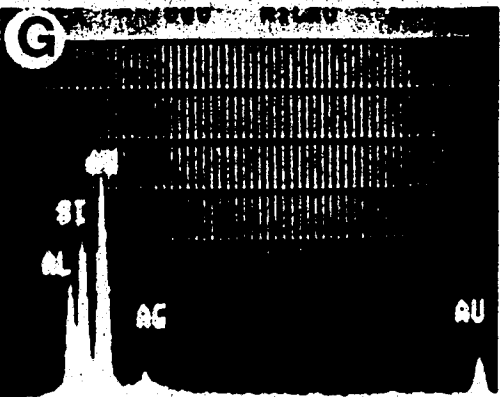
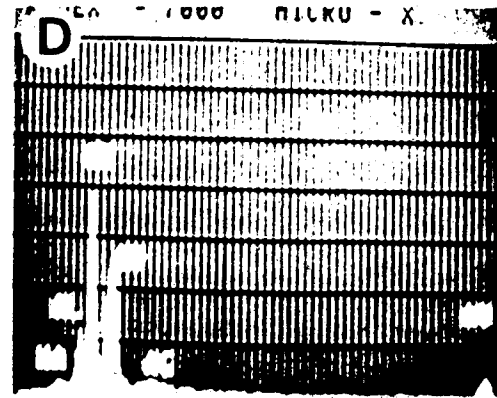
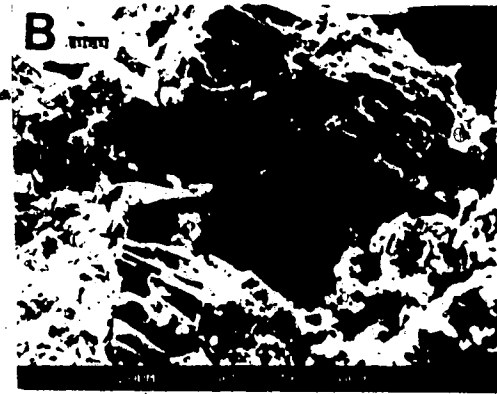
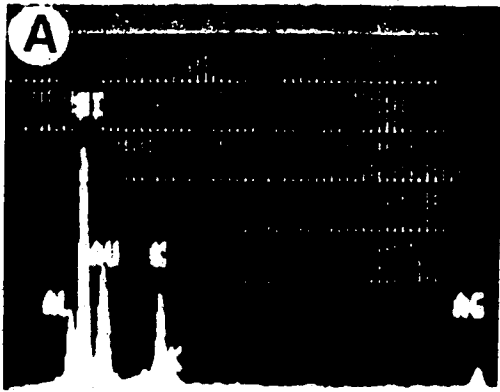
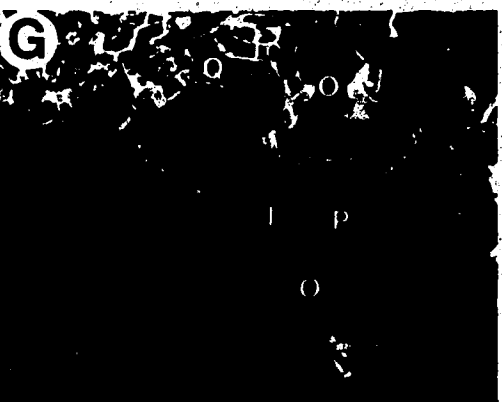
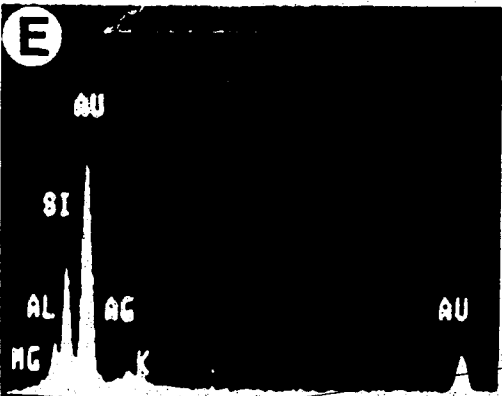
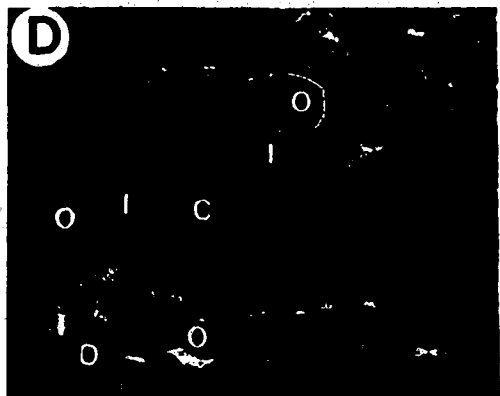
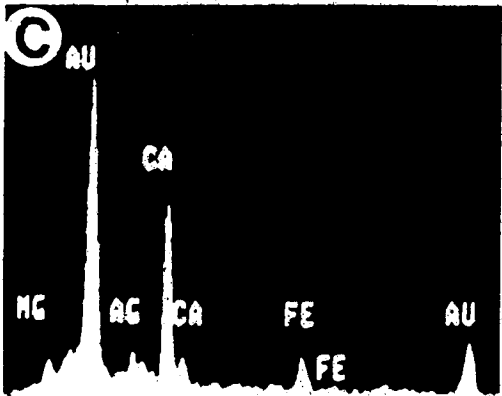
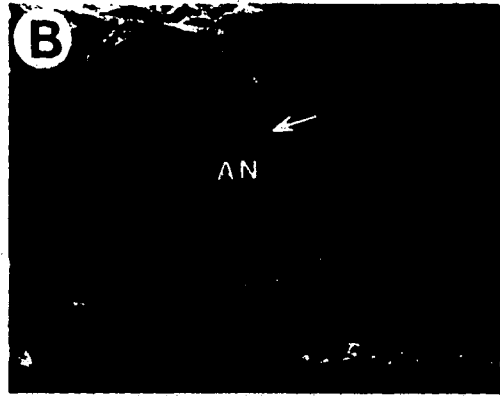
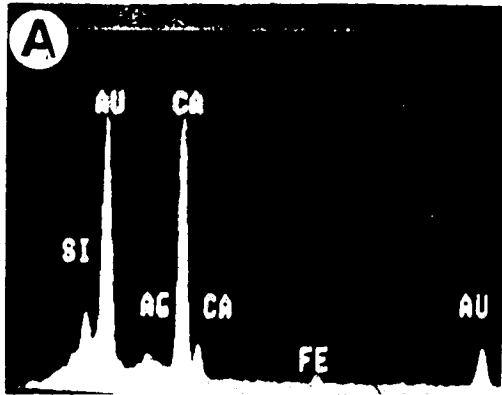


PLATE 2.7

- A.** EDA spectrum of calcite.
- B.** Pore-filling ankerite (AN) has been dissolved (arrow). Section 80X(886m).
- C.** EDA spectrum of ankerite showing about equal amounts of Fe and Mg.
- D.** Pore-lining illite (I) has grown upon and enveloped quartz overgrowths (O) and chlorite (C). Section 80X(886m).
- E.** EDA spectrum of illite.
- F.** Pore-bridging authigenic illite fibres (I). Section 80X(886m).
- G.** Net-like illite fibres (I) bridging pore (P) and coating detrital quartz (Q) and quartz overgrowths (O). Section 80X(668m).
- H.** Pore-lining authigenic illite/smectite. Section 80X(330m).



chlorite grain-coatings (Plates 2.1C,D, 2.6H). Calcite also occurs as a later phase, replacing feldspar (Plate 2.2B,C) and filling primary and secondary porosity created by the first episode of dissolution (Plates 2.1A, 2.2C, 2.5C,D).

The high percentage of calcite cement (greater than the original porosity; Plate 2.1C) suggests that carbonate has replaced some detrital grains (Blatt et al., 1980). The quartz particles are replaced, or etched into irregularly shaped fragile grains (Plate 2.1C,D).

Dolomite and Ankerite

Dolomite and ankerite cements have been identified using stains, EDA and XRD, and are present in only a few samples (Table 2.6). Calcite is present together with dolomite or ankerite, but no sample contains all three carbonates or both dolomite and ankerite together (Table 2.6).

Pore-filling dolomite (about 3%) was detected in only two samples, together with trace amounts (<1%) of calcite (Table 2.6). The diagenetic relationship between dolomite and calcite cannot be determined exactly, but calcite could have been dolomitized as diagenesis progressed. Authigenic dolomite also occurs as overgrowths on detrital dolomite grains (Plate 2.8A).

Ankerite occurs as a pore-filling cement (Plate 2.7B, 2.8B). The EDA spectrum of ankerite shows that it contains about equal amount of Fe and Mg (Plate 2.7C). When ankerite is associated with calcite, it appears that ankerite precipitation postdated the formation of calcite (Plate 2.8B). Some of the ankerite could have been formed from pre-existing calcite.

Dissolution of Carbonate Cements and Detrital Grains

Following carbonate cementation a second stage of dissolution has affected most samples. During this stage there was partial or complete dissolution of calcite (Plate 2.8C,D), dolomite (Plate 2.8A) and unstable detrital grains (e.g., feldspar, Plate 2.8C,D, 2.9A; chert, Plate 2.8A,B; fine-grained metamorphic rock fragment, Plate 2.9B). Feldspar that was partially replaced by carbonate cement earlier has been dissolved during this stage, including the carbonate replacement (Plate 2.8C,D).

— Dissolution of carbonate cement in samples with <40% carbonate cement resulted in high secondary porosity (Plate 2.2A). Secondary porosity was also created by the dissolution of

PLATE 2.8

A. Authigenic dolomite cement (AD) around detrital dolomite (DD). Both have been partially dissolved. Scale bar = $50\mu\text{m}$. Crossed-polarized light. Section 80X(330m).

P

B. Calcite (Ca) is the first carbonate cement to be formed as pore-fillings; ankerite (AN; blue) has then crystallized as pore-fillings and/or recrystallized from the calcite. Q = quartz grains, RF = rock fragment. Scale bar = $50\mu\text{m}$. Plane-polarized light. Section 80X(200m).

C & D. Partially replaced feldspar (F) has been dissolved, including the carbonate replacement (Ca). Porosity is blue. A chert fragment (Che) has also been partially dissolved along its edges. Hydrocarbon (HC) residue can also be seen in a secondary pore created in carbonate cement. Scale bar for C and D = $50\mu\text{m}$. C is cross-polarized light. D is plane-polarized light. Section 81I(144m).

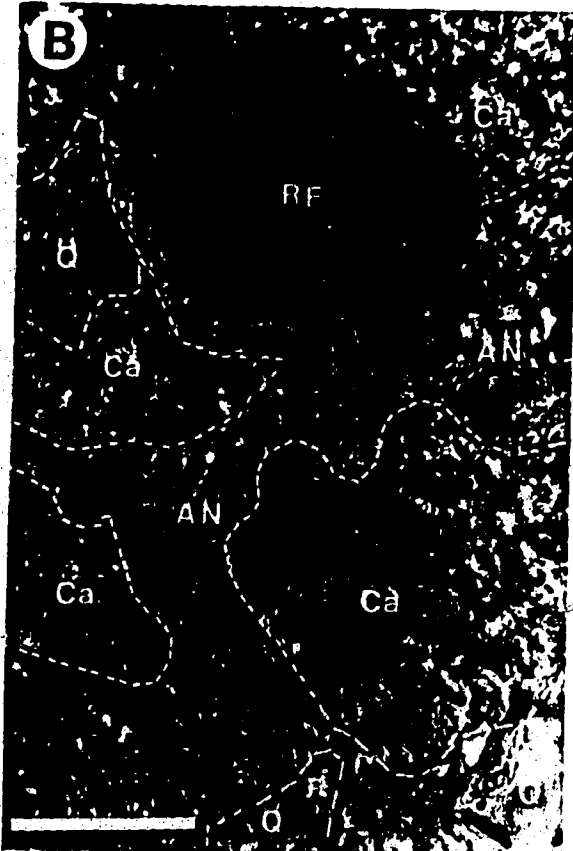
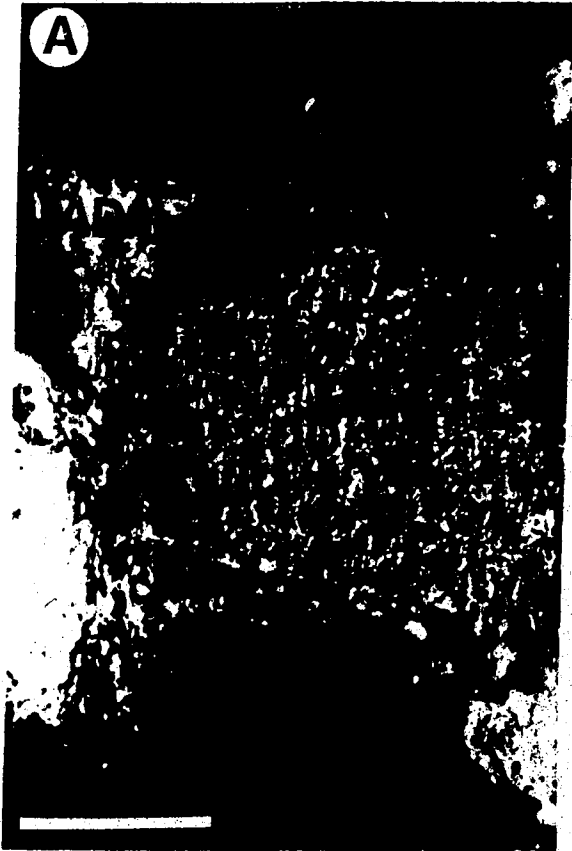
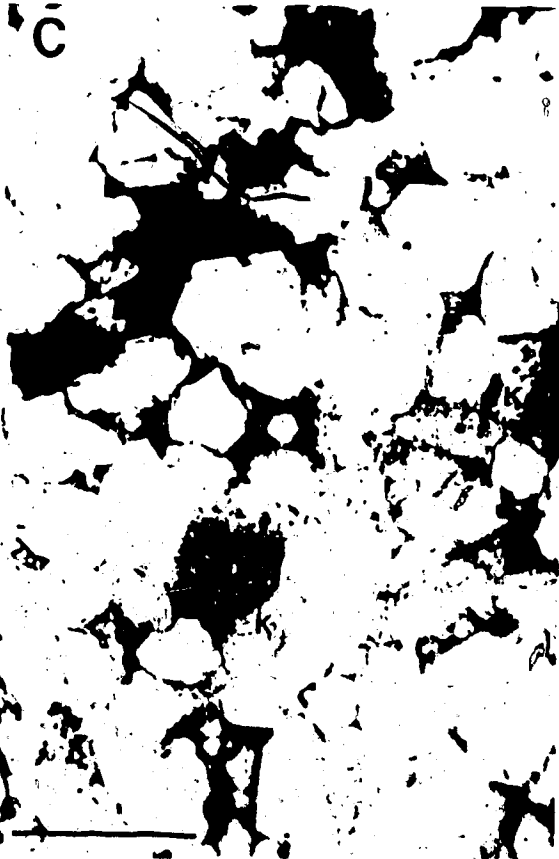


PLATE 2.9

- A.** Partially dissolved feldspar grain (F) with hydrocarbon stains (dark brown) in secondary pores. Porosity is blue. Scale bar = 50 μ m. Plane-polarized light. Section 811 (857m).
- B.** Partially dissolved fine-grained metamorphic rock fragment (MF). Porosity is blue. Scale bar = 50 μ m. Plane-polarized light. Section 811 (749m).
- C.** Hydrocarbon (black) filling in large secondary pores. Detrital grains are highly corroded as outlined by the hydrocarbon. Pores which are not filled by hydrocarbon are filled by kaolinite (K). Porosity is blue. Scale bar = 200 μ m. Plane-polarized light. Section 811 (857m).
- D.** Hydrocarbon (black) completely filling all the secondary porosity. Detrital grains are highly corroded. Scale bar = 200 μ m. Plane-polarized light. Section 80X (935m).



framework grains (Plates 2.3D, 2.9C,D). Sandstones with >40% calcite cement show little or no sign of carbonate dissolution (Plate 2.1C). This could be due to lack of porosity and permeability for pore fluid circulation.

Hydrocarbon Emplacement

Hydrocarbons (dead oil) are very common in the upper portion of sections 80X (>838m above base) and 81I (>749m above base). The hydrocarbon occurs mostly in secondary pore spaces as pore-fillings and pore-linings (Plate 2.9A,C,D). In some samples the hydrocarbon has a patchy distribution, filling secondary porosity in only some parts of the sandstone (Plate 2.9C). In other samples it completely fills all the secondary porosity (Plate 2.9D).

Hydrocarbon emplacement apparently postdated carbonate dissolution because of the presence of hydrocarbons within partially dissolved carbonate cement (Plates 2.8D, 2.10A). The presence of hydrocarbon stains in partially dissolved detrital feldspar indicates that hydrocarbon emplacement was post-feldspar dissolution (Plates 2.9A, 2.10B).

Illite

Illite is present in the <2 μ m size-fraction of all the samples in sections 80X (13-58%, Table 2.3; Figure 2.5) and 81I (20-52%, Table 2.4; Figure 2.6). The presence of illite in XRD of samples with little detrital clays suggests that most of the illite is authigenic. The presence of delicate filamentous illite, as observed by SEM, also proves that authigenic illite is present in some samples (Plate 2.7D). The EDA spectrum of authigenic illite shows that the major elements present are Si, Al and K, with minor Mg (Plate 2.7E).

The authigenic illite is observed as thin laths that bridge pores (Plate 2.7F). In some samples it also occurs as net-like fibres that (i) grow on detrital grains and syntaxial quartz overgrowths and (ii) bridge pores (Plate 2.7G). Illite also occurs as an alteration product of detrital feldspar (Plate 2.6E). This alteration may have happened during the first and/or second dissolution and alteration stages in the diagenetic history.

Authigenic illite appears to be one of the last phases to form because it occurs as pore-linings on detrital grains, quartz overgrowths and chlorite coats (Plate 2.7D,G). Its formation may be contemporaneous with illite/smectite, smectite and kaolinite.

PLATE 2.10

- A. Hydrocarbon (HC) filling in secondary pore created in calcite cement (Ca), indicating that hydrocarbon emplacement is after carbonate cement dissolution. Scale bar = 50 μ m. Cross-polarized light. Section 80X(881m).
- B. Secondary porosity created in feldspar grain (F) has been filled by hydrocarbon (dark brown to black). Note corroded edges of the quartz (Q) which is outlined by hydrocarbon. Scale bar = 50 μ m. Cross-polarized light. Section 81I(857m).
- C. Pore-filling kaolinite (K) and hydrocarbon (dark purple). Notice that pores lined by hydrocarbon (X) are not filled by kaolinite. Porosity is blue. Scale bar = 200 μ m. Plane-polarized light. Section 81I(857m).
- D. Vermicular kaolinite (K) filling in large secondary pore. The presence of residue hydrocarbon stains (HC) on detrital quartz grain (Q) and in part of the pore without the kaolinite being stained by the hydrocarbon indicates that kaolinite formation postdates hydrocarbon migration. Scale bar = 50 μ m. Plane-polarized light. Section 81I(857m).

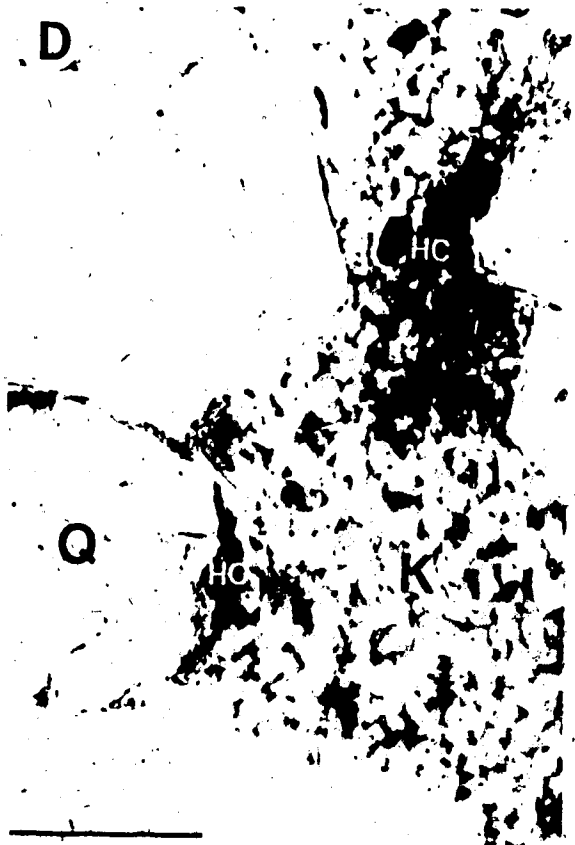
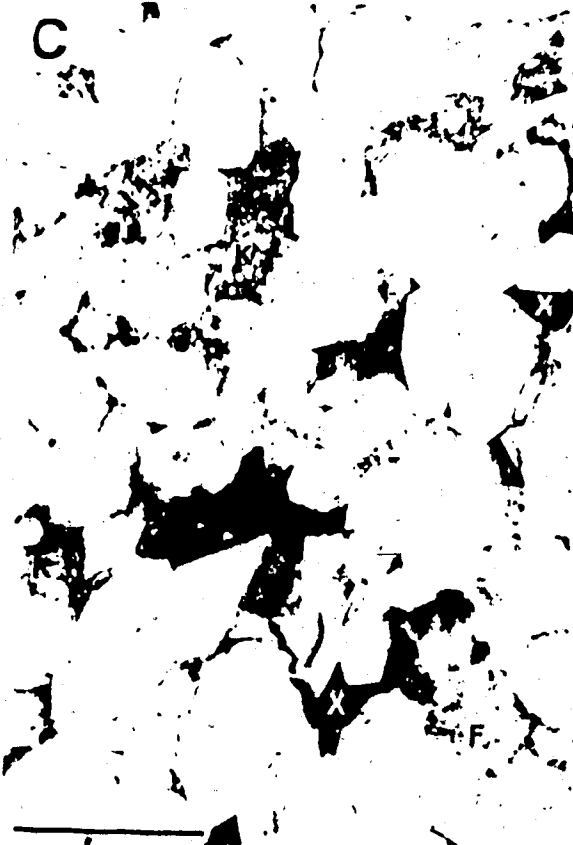


Fig. 2.6 Nature of clay minerals in sandstones, Section 811. See Figure 2.1 for meaning of symbols.

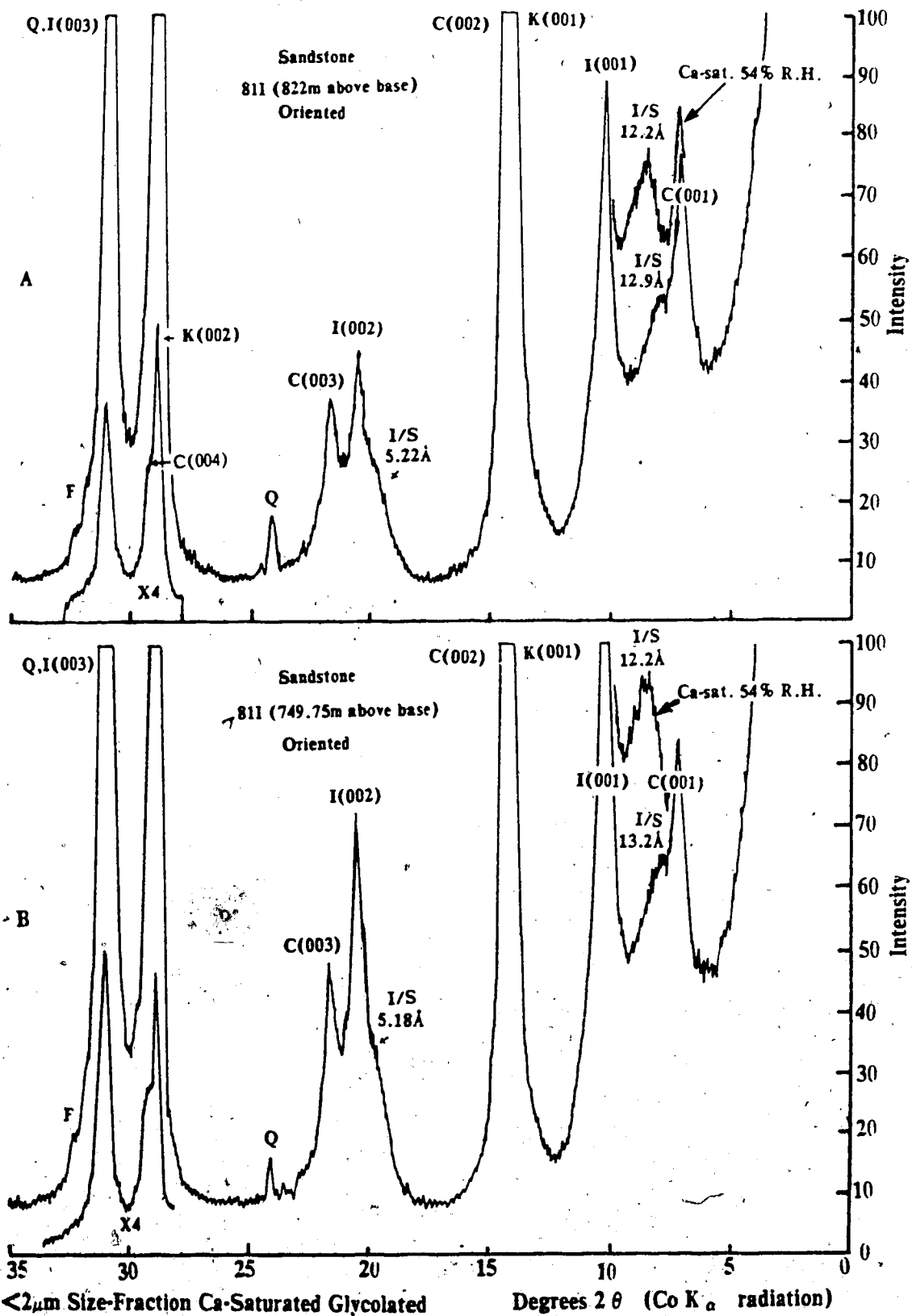
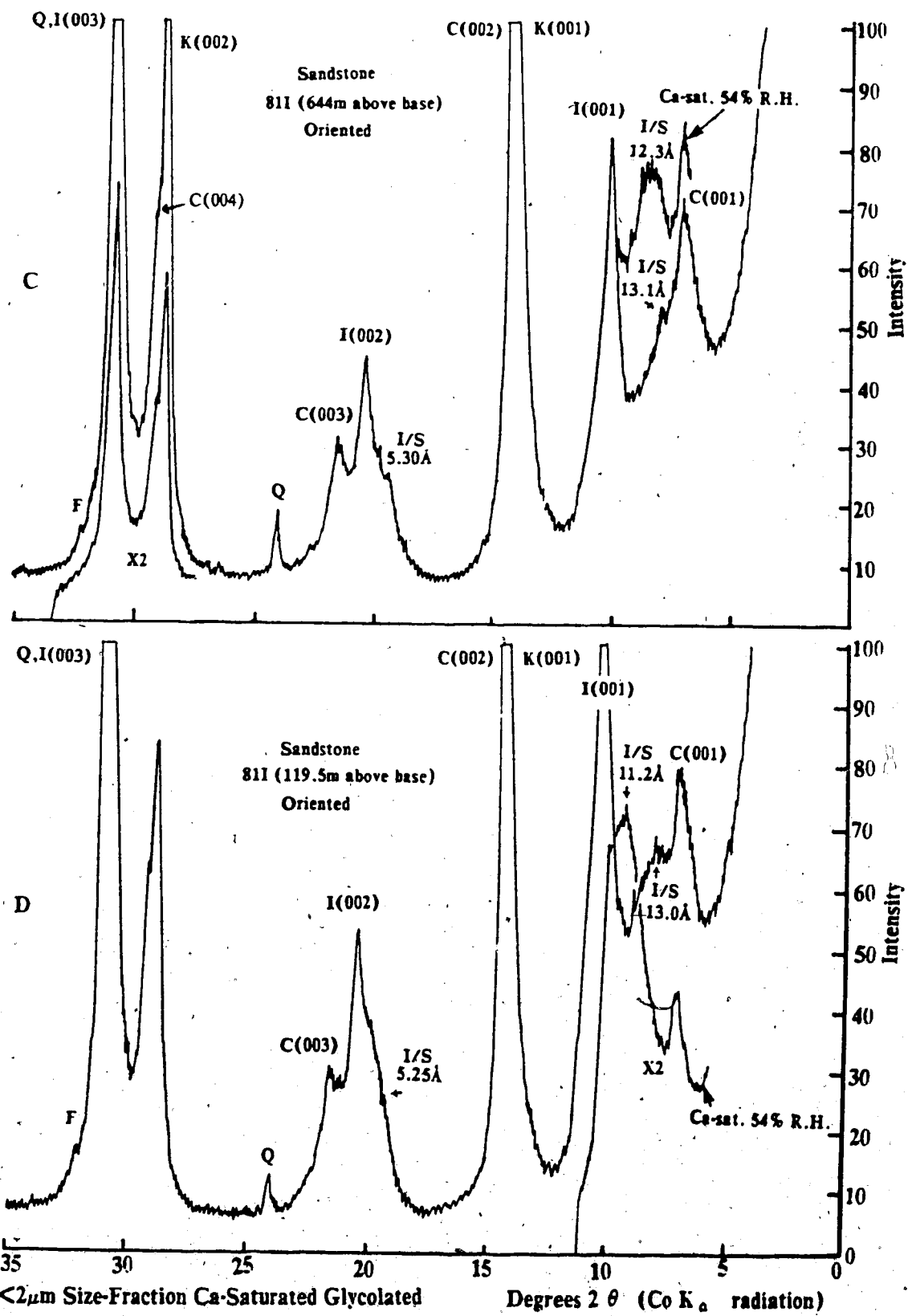


Fig. 2.6 continued



Illite/Smectite

Illite/smectite is present in the $<2\mu\text{m}$ size-fraction of many samples in section 80X (Table 2.3; Figure 2.5) and all samples in section 81I (Table 2.4; Figure 2.6). The higher intensity of the illite/smectite diffractions for section 81I samples indicates that illite/smectite is more abundant in this section (Figs. 2.5, 2.6).

In section 80X illite/smectite was not detected in most of the clean (i.e., containing little detrital clay matrix) sandstones from the delta plain, delta margin and nearshore shelf facies. (Tables 1.1 and 2.3). However, illite/smectite is present in all the shale and siltstone samples. These observations suggest that most of the illite/smectite found in section 80X is detrital. Most of the sandstones in section 81I contain moderate to high amounts of clay matrix and most of the illite/smectite may be detrital in origin.

However, at least some of the illite/smectite present in the clean sandstones from both sections may be authigenic, as indicated by the presence of honeycombed illite/smectite with lath-like projections as pore-linings (Plate 2.7H). The EDA spectrum of authigenic illite/smectite shows that it contains Mg, Al, Si, K, Ca and Fe (Plate 2.11A).

The nature of interstratification and the percentages of illite layers in the illite/smectite were determined using the methods described by Reynolds and Hower (1970), Reynolds (1980) and Hower (1981a) (Appendix I). In sections 80X and 81I the percentage of illite layers varies from 60-90% and 50-75%, respectively (Tables 2.3, 2.4). There is no apparent change in percent illite layers with depth in both sections (Tables 2.3, 2.4). The illite/smectite may be classified as "allevardite" ordered (IS to ISII layering) (Hower, 1981a). However, the superlattice diffraction (30-35Å) is very weak in most cases, and occurs as a shoulder, indicating that the ordering is probably incomplete.

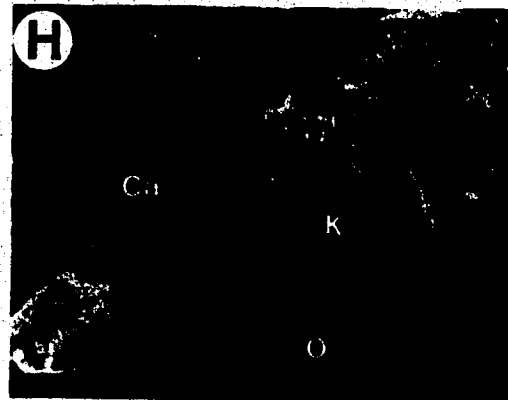
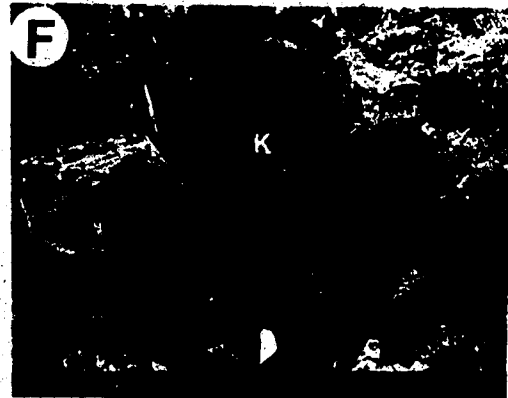
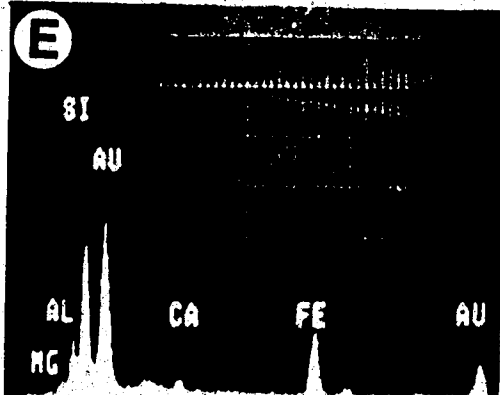
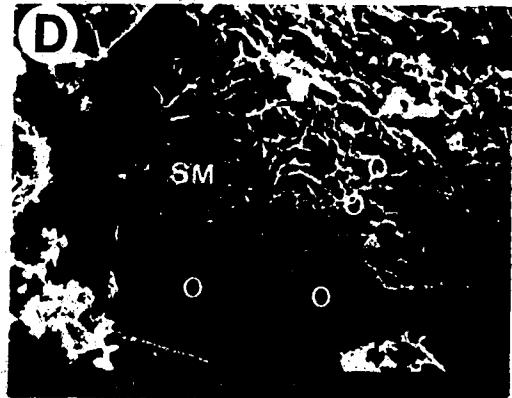
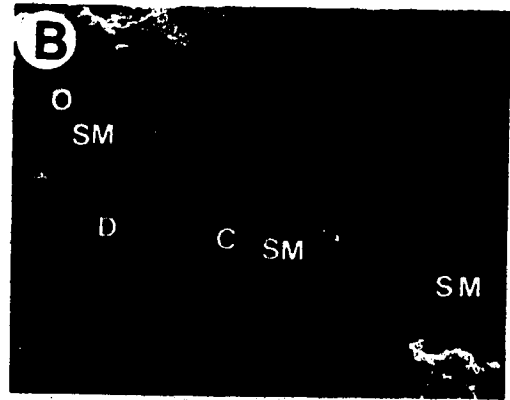
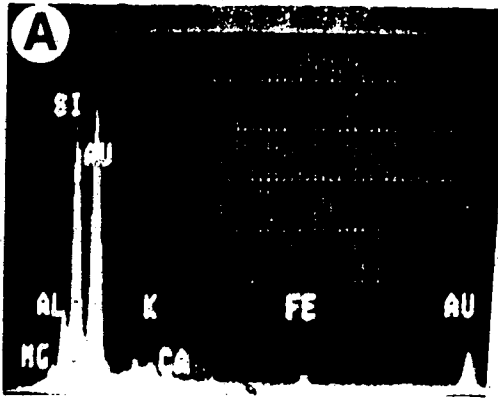
Smectite

Smectite (6-13% of the $<2\mu\text{m}$ size-fraction, Table 2.3; Fig. 2.5C) is abundant only in sandstones from the distributary channels, nearshore and proximal shelf facies in section 80X. No smectite was detected in section 81I.

Authigenic smectite, which has a honeycombed texture, is observed overlying chlorite grain-coatings (Plates 2.11C,D), thus postdating chlorite formation. Smectite also grows on the surfaces of syntaxial quartz overgrowths and engulfs smaller drusy quartz overgrowths

PLATE 2.11

- A. EDA spectrum of illite/smectite.
- B. Smectite (SM) which has grown on chlorite grain-coating (C) and quartz overgrowths (O).
D= detrital quartz, host of the chlorite and smectite. Section 80X(742m).
- C. Close-up of (B) showing the chlorite coat (C) and the smectite layer (SM) on it. Note the honey-combed texture of smectite. D= host grain.
- D. Both small and large quartz overgrowths (O) have been engulfed by authigenic smectite.
Section 80X(742m).
- E. EDA spectrum of smectite showing that it is Fe-rich.
- F. Kaolinite (K) filling large secondary pore. Section 80X(330m).
- G. Close-up of pore-filling kaolinite showing the characteristic well-crystallized booklets and vermicular stacks.
- H. A characteristic vermicular stack of kaolinite (K) on quartz overgrowth (O). Note relict calcite (Ca). Section 80X(600m).



(Plates 2.11B,D), thus postdating the quartz formation. The EDA spectrum of smectite shows that it contains major amounts of Ca and Fe with minor amounts of Mg (Plate 2.11E).

Kaolinite

Authigenic kaolinite (0-15%, Table 2.5), which occurs as well-crystallized booklets and vermicular stacks mostly in large secondary pores (Plates 2.2A, 2.9C, 2.10C,D, 2.11F,G,H, 2.12B), is very abundant in the sandstones (0-15%, Table 2.5). Kaolinite comprises 4-85% (Table 2.3) and 21-59% (Table 2.4) of the $<2\mu\text{m}$ size-fraction of sandstones from sections 80X and 81I, respectively.

In some samples authigenic kaolinite is also associated with, or altered from, detrital feldspar (Plates 2.6F, 2.12B); the relative timing of the formation of this kaolinite is uncertain. However, the pore-filling kaolinite appears to postdate quartz overgrowths because it fills the pore following quartz cementation (Plate 2.11H). In addition, authigenic kaolinite appears to postdate hydrocarbon migration and emplacement because abundant unstained kaolinite is present in secondary pores that are partially lined or filled by hydrocarbons (Plate 2.10C,D); kaolinite is lacking in secondary pores that are completely lined by hydrocarbons (Plate 2.10C). The late formation of kaolinite is also suggested by the presence of relict carbonate cement in large secondary pores filled by kaolinite; the bordering quartz grains are highly etched by the earlier-precipitated carbonate cement (Plates 2.11H, 2.12A). This texture indicates that the pore-filling kaolinite postdated carbonate precipitation and dissolution.

Fracturing, Dissolution and Tertiary Hydrocarbon Migration

The presence of extensive, large fractures filled with hydrocarbons in a few sandstone samples in both sections 80X and 81I (Plate 2.12C,D) suggests that tertiary migration of hydrocarbons occurred following fracturing, reopening of existing fractures and/or dissolution along the fractures. This stage of hydrocarbon migration postdates kaolinite because the hydrocarbon-filled fractures usually cut through authigenic pore-filling kaolinite, carbonate cement, quartz and other detrital grains (Plate 2.12D).

PLATE 2.12

- A. Relict calcite (Ca) in large secondary pore which has been filled by kaolinite (K). Quartz grains (Q) have been previously etched (arrows) by the carbonate cement. Scale bar = $50\mu\text{m}$. Cross-polarized light. Section 80X(750m).
- B. A vermicular stack of kaolinite (K), associated with, or altered from partially dissolved feldspar (F). Porosity is blue. Scale bar = $50\mu\text{m}$. Cross-polarized light. Section 811(857m).
- C. Hydrocarbon-filled fractures (dark purple). Scale bar = $1000\mu\text{m}$. Plane-polarized light. Section 80X(1060m).
- D. Hydrocarbon-filled fracture (dark purple) cutting through quartz (Q), feldspar (F), pore-filling kaolinite (K), carbonate cement (CAR) and muscovite (M). Scale bar = $50\mu\text{m}$. Cross-polarized light. Section 811(749.3m).



D. PARAGENETIC SEQUENCE - SUMMARY

The paragenetic sequence of diagenetic events in the Bird Fiord, Weatherall and basal Hecla Bay sandstones (Fig. 2.7), as determined from SEM and thin-section petrography, is as follows:

1. formation of chlorite grain-coatings on quartz and feldspar grains;
2. cementation by calcite;
3. formation of quartz overgrowths;
4. dissolution and/or alteration of feldspar, rock and shell fragments, calcite, quartz and mica;
5. precipitation of calcite in primary and secondary pore space, and/or recrystallization of early calcite to late calcite, and/or formation of late calcite as feldspar replacements;
6. precipitation of dolomite or ankerite in primary and secondary pore space, and/or recrystallization of calcite to dolomite or ankerite;
7. dissolution of carbonate cements and remaining unstable detrital grains;
8. (?) precipitation of illite, illite/smectite and smectite mostly as pore-linings in primary and secondary pore spaces (these clay minerals may have been precipitated during events 4 to 7);
9. precipitation of kaolinite as pore-fillings in mostly secondary pore spaces, and
10. tertiary migration of hydrocarbons into fissures and fractures.

E. STABLE ISOTOPE GEOCHEMISTRY

Clay Minerals

The $\delta^{18}\text{O}$ values of the $<2\mu\text{m}$ size-fraction of sandstones, shales, argillaceous limestones and siltstones in section 80X range from +12.4 to +16.7 (Table 2.7). The clay minerals present in these samples are listed in Table 2.3. Kaolinite, illite, chlorite and illite/smectite can be both authigenic and detrital; only authigenic smectite is present. Minor amounts of quartz and traces of feldspar are also present in the $<2\mu\text{m}$ size-fraction, but their effects on the $\delta^{18}\text{O}$ values are insignificant for these samples.

The $>2\mu\text{m}$ size-fraction from sandstone have lower $\delta^{18}\text{O}$ values (+12.4 to +15.1, average = +13.1; Table 2.7) than those from the shale, argillaceous limestone and siltstone

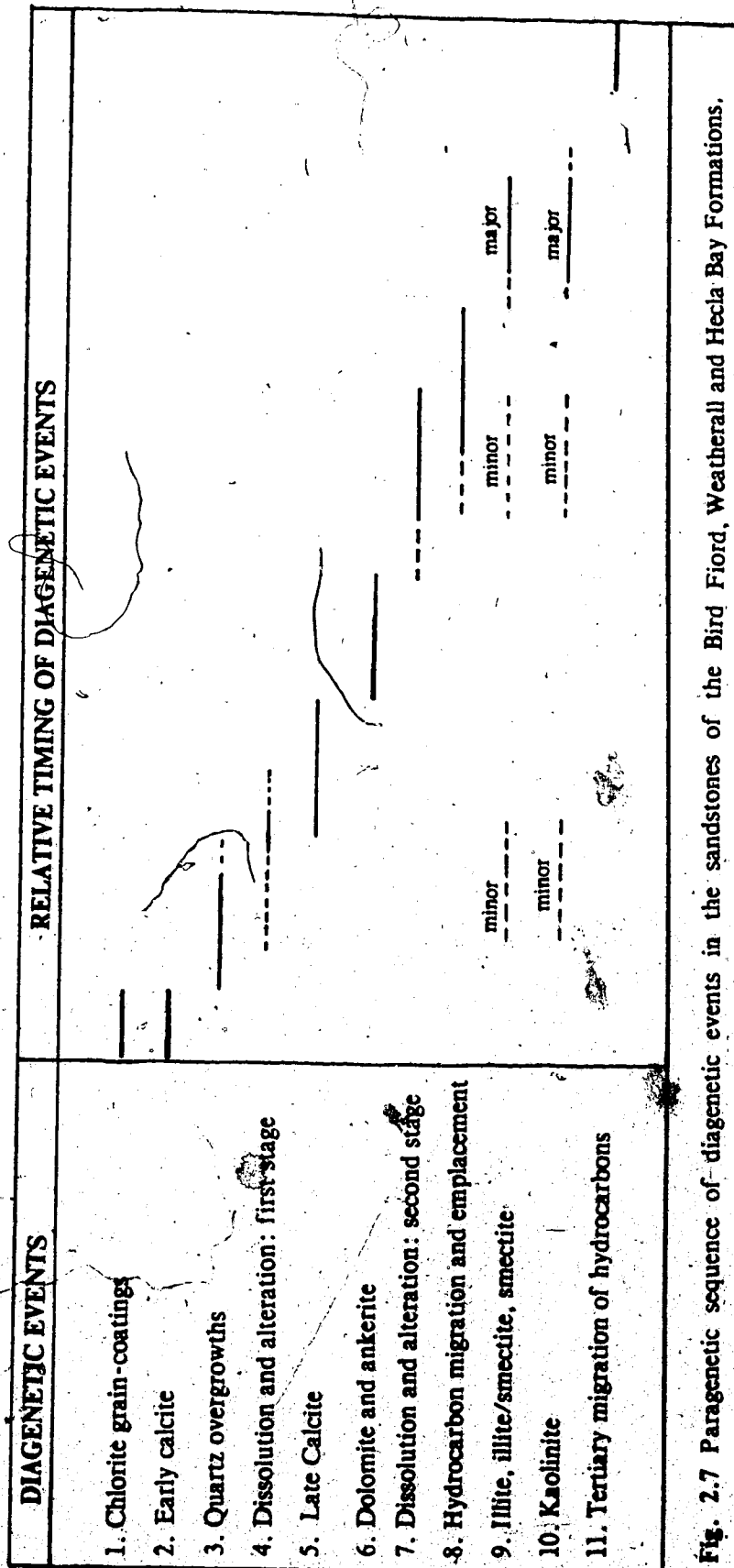


Fig. 2.7 Paragenetic sequence of diagenetic events in the sandstones of the Bird Fiord, Weatherall and Hecla Bay Formations.

Table 2.7 $\delta^{18}\text{O}$ and $\delta^{13}\text{C}$ for clay and carbonate minerals, section 80X.

METRES ABOVE BASE	ROCK TYPE	<2 μm ¹	CALCITE		DOLOMITE		ANKERITE	
			$\delta^{18}\text{O}$ SMOW	$\delta^{13}\text{C}$ PDB	$\delta^{18}\text{O}$ SMOW	$\delta^{13}\text{C}$ PDB	$\delta^{18}\text{O}$ SMOW	$\delta^{13}\text{C}$ PDB
1030	ss	+14.2						
886	ss	+13.4						
839	ss	+12.4					+19.8	-4.4
767	ss		+18.7	-3.6				
750	ss		+19.0	-4.5				
734	ss	+12.9						
683	ss	+13.1	+18.1	-3.0				
598	ss	+14.4						
501	ss		+20.0	-2.5				
488.75	sltst ¹	+15.2						
481.75	sltst	+14.7						
480.75	sh/sltst	+15.0						
479.75	sltst	+15.4						
478.75	sh	+15.9						
477.75	sh	+16.1						
474.75	sh	+15.5						
474	ss	+15.1						
469	ss	+15.1						
330	ss	+15.0			+20.0	-0.1		
280	ss	+13.3						
227	arg. ls	+16.7						

¹contain minor quartz and traces of feldspar

samples (+14.7 to +16.7, average = +15.6). Sandstones with little detrital clay matrix (>682m above base) have still lower $\delta^{18}\text{O}$ values (+12.4 to +14.2) than sandstone samples with a significant amount of detrital clay matrix (+13.3 to +15.1). The above variations are due to the higher $\delta^{18}\text{O}$ values of detrital clays from sedimentary rocks (+16 to +22; Savin and Epstein, 1970a, 1970b; Longstaffe, 1983, 1984) as compared to authigenic clays. The authigenic clays present in the samples must have $\delta^{18}\text{O}$ values much lower than typical for the detrital clays in order to give composite $\delta^{18}\text{O}$ values (authigenic + detrital clays) of +12.4 to +16.7.

The clay fraction from a sandstone sample with little detrital clay matrix (1,030m above base), which contains 85% kaolinite (mostly authigenic because pore-filling kaolinite comprises 10% of this sandstone, Table 2.5) and 15% illite, has a $\delta^{18}\text{O}$ of +14.2 (Table 2.7). Consequently, an average kaolinite $\delta^{18}\text{O}$ of +14.4, calculated by linear regression of the $\delta^{18}\text{O}$ for the clay fraction versus percent kaolinite from XRD (Tables 2.3, 2.7; Fig. 2.8), is quite reasonable. The clay fraction from another sample (280m above base) with 92% "illite" (an illite/smectite with 90% illite layers, Table 2.3) has a $\delta^{18}\text{O}$ of +13.0. Therefore, an illite $\delta^{18}\text{O}$ of +13.1, calculated from the sample with 85% kaolinite and 15% illite (1,030m above base) using a kaolinite $\delta^{18}\text{O}$ of +14.4, is also realistic.

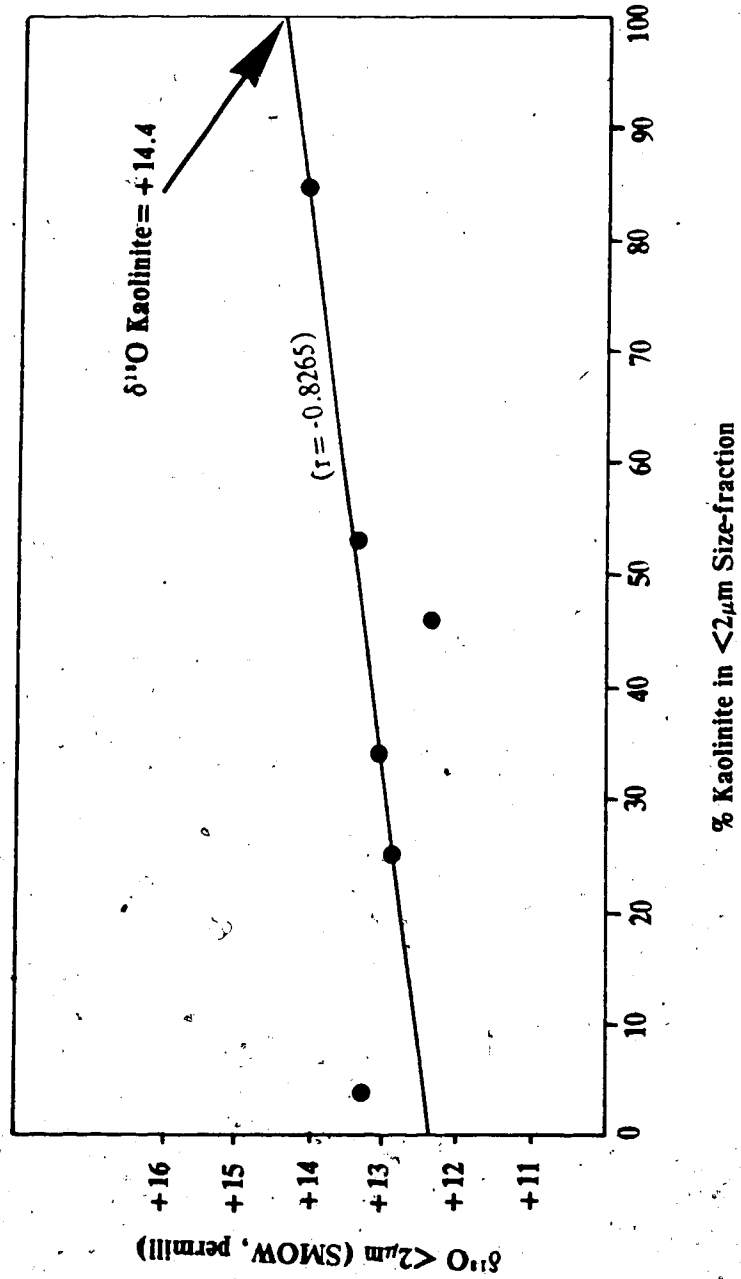
Carbonate Minerals

Oxygen- and carbon-isotope values were obtained for calcite, dolomite and ankerite cements (Table 2.7). Samples with no shell fragments (Table 2.6) were selected for analysis of the calcite cement. The ankerite sample contains no other carbonate minerals. Trace amounts of dolomite grains are present in the authigenic dolomite sample, but its influence on the isotopic values is probably insignificant.

The $\delta^{18}\text{O}$ values of the calcite cement range from +18.1 to +20.0 (Table 2.7). The range in $\delta^{18}\text{O}$ of the calcite indicates some variation in the conditions of its formation and/or recrystallization, an observation which is consistent with the petrographic data. The calcite has $\delta^{13}\text{C}$ values ranging from -2.5 to -4.5 (PDB; Table 2.7).

Authigenic dolomite and ankerite have $\delta^{18}\text{O}$ values of +20.0 and +19.8, respectively; their $\delta^{13}\text{C}$ values are -0.1 and -4.4, respectively (Table 2.7).

Fig. 2.8 $\delta^{18}\text{O}$ versus percent kaolinite in the $<2\mu\text{m}$ size-fraction. The relative abundance of kaolinite has been determined by X-ray diffraction (Fig. 2.3, see text). The composition of kaolinite ($\delta^{18}\text{O} = +14.4$) is determined by linear regression ($r = -0.8265$).



III. INTERPRETATION OF DIAGENETIC HISTORY

A. INTRODUCTION

To interpret the diagenetic history of the Bird Fiord, Weatherall and basal Hecla Bay Formations, it is important to know the burial history of these units. This history is very complex, including two episodes of uplifting, deformation and erosion, and has probably resulted in a complicated evolution of flow and fluid chemistries in the subsurface. Of particular importance are: (i) the timing of the specific episodes of burial, uplift, deformation and erosion, and (ii) the maximum burial depth attained by the unit.

Burial History - Summary

According to Embry and Klovan (1976), deposition of the Bird Fiord and Weatherall Formations commenced in Eifelian time (Fig. 3.1), and by Early Frasnian time the Hecla Bay Formation was deposited. Burial continued until Late Frasnian time; the units were uplifted and deformed in the Late Frasnian (Fig. 3.1). Deposition and burial resumed in latest Frasnian and lasted until the Famennian; the area was uplifted, deformed and eroded during Famennian to Viséan time (Ellesmerian Orogeny). Erosion of the area continued to the present day after the Ellesmerian Orogeny (Fig. 3.1).

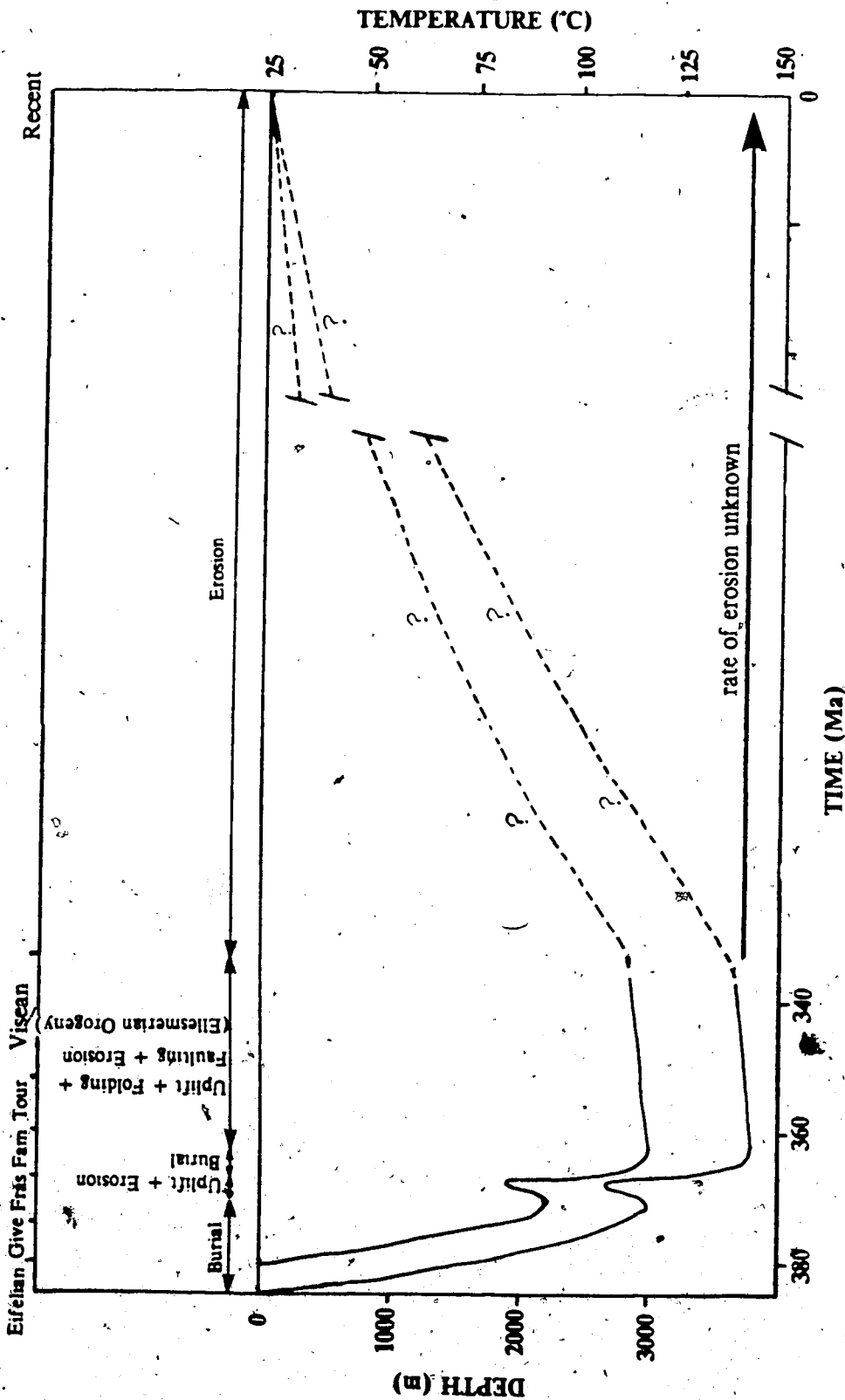
Maximum Burial Depth

The maximum burial depth achieved by the clastic rocks under investigation was determined utilizing conodont colour alteration indices and vitrinite reflectance data.

Conodont Colour Alteration Index

Conodonts from the carbonate equivalent of the Bird Fiord Formation in section 80X (Table 1.2, 118 and 123.8m above base of section; GSC locations C-136361 and C-136362) have a colour alteration index (CAI) of 1.5 (Uyeno, pers. comm.). No conodont CAI is available for section 81I. According to Epstein et al. (1977), a temperature range of 50-90°C is possible for a CAI of 1.5. The surface temperature in this area during the Devonian time was relatively high (about 25-30°C) because the area was within 10° of the equator (Smith et al., 1973); a humid equatorial to tropical climate is probable (Embry and Klovan, 1976). Thus,

Fig. 3.1 Schematic burial curves for the top (upper curve) and base (lower curve) of the Bird Fiord and Weatherall Formations. Temperature scale is based on a constant geothermal gradient of 30°C/km. Burial history assumes that 300m of strata were removed during the uplift in Late Frasnian before deposition resumed in latest Frasnian. It also assumes that after the Ellesmerian Orogeny (Famennian to Viséan) gradual erosion continued until the present day, exposing most of the Bird Fiord, Weatherall and Hecla Bay Formations.



assuming an average paleogeothermal gradient of 30°/km and a surface paleotemperature of 25°C, the temperature range of 50-90°C suggests a possible burial depth ranging from 800m to 2,200m. Even the high end of this large burial depth range does not agree with the maximum burial depth of approximately 3,300m calculated for these samples based on stratigraphic thicknesses of the units given by Embry and Klovan (1976) and Goodbody (1985). The disagreement in burial depth can be due to: (i) a low CAI for the conodonts because of a short burial time due to early uplift and erosion (Ellesmerian Orogeny; Epstein et al., 1977); and/or (ii) an overestimation of the thicknesses of the overlying formations. The first reason seems to be more likely considering the possibility that the maximum overburden may have been underestimated because some strata may have been removed from the top of the Parry Islands Formation.

Vitrinite Reflectance

Burial depths, based on vitrinite reflectance data given by Powell (1978), agree well with the estimates based on stratigraphic thicknesses of the formations. Powell (1978) gave vitrinite reflectance data from two wells (Bent Horn N-72 and Hotspur J-20; see Figure 1.5 for locations of wells) which are nearest section 80X. A vitrinite reflectance (R_o) of 0.90% at 1,667m in the Bent Horn N-72 well suggests a maximum burial temperature of about 100°C (Hunt, 1979). This generates a temperature of about 120°C for the top of the Bird Fiord Formation, assuming a geothermal gradient of 30°C/km. A vitrinite reflectance of 1.33% at 1,967m in the Hotspur J-20 well suggests a maximum burial temperature of about 130°C (Hunt, 1979), which generates a temperature of about 110°C for the top of the Bird Fiord Formation. Assuming a geothermal gradient of 30°/km and a surface temperature of 25°C, a temperature of 110-120°C suggests a maximum burial depth of 2,800-3,200m for the top of the Bird Fiord Formation in the Bathurst Island area. This depth range agrees reasonably well with the depth (2,600m) calculated from stratigraphic thicknesses of the formations. The difference of 200-600m may represent strata removed in the unconformity above the Parry Island Formation and/or may indicate a slightly higher geothermal gradient during the Devonian time (a geothermal gradient of 35°C/km would give a consistent maximum burial depth of 2,600m).

A maximum burial depth of 3,000m, which corresponds to a temperature of 115°C, is assumed for the top of the Bird Fiord and Weatherall Formations (Fig. 3.1) during the

following discussion of the diagenetic history. The Bird Fiord Formation (complete in section 80X is 800m thick; consequently the maximum burial temperature for the base of formation is about 140°C (Fig. 3.1).

Oxygen-Isotope Geochemistry

To use the oxygen-isotope data to impose constraints on diagenesis, an understanding of the possible implications of the oxygen-isotope data is required. In particular, oxygen-isotope compositions of the authigenic clays and carbonate minerals from section 80X (Bird Fiord section) can reveal much about pore-fluids and thermal history during the diagenesis of the sandstones, provided that the isotopic compositions of the minerals have remained unchanged since crystallization.

Isotopic exchange between carbonate minerals and fluid is not significant at temperatures typical of sedimentary environments except during recrystallization (Epstein et al., 1964; Anderson, 1969; Land, 1980; Longstaffe, 1983, 1984, in press). Oxygen-isotope exchange resulting from recrystallization, particularly calcite, becomes more important as temperatures increase. Silicate minerals exchange oxygen-isotopes at higher temperatures than carbonate minerals (Clayton, 1959). The exchange of oxygen-isotopes in clay minerals is normally insignificant below about 100°C (Yeh and Savin, 1977; Longstaffe, 1983, 1984, in press), except for the very finest size-fraction (<0.1 μ m; Yeh and Savin, 1976; Eslinger and Yeh, 1981).

Another factor complicating the interpretation of the $\delta^{18}\text{O}$ of the authigenic minerals is that all the samples analysed were from outcrop; no pore-fluids were available for analysis. Neither are isotopic data available for subsurface waters in this area. The original isotopic compositions of the waters buried with the sandstones depended on the environment of deposition. The Bird Fiord strata in Bathurst Island were deposited in marine or deltaic settings (Table 1.2); water buried with the Bird Fiord sediments either had an isotopic composition similar to seawater or was several permil lighter in facies where the water was brackish. During burial, formation water typically becomes enriched in ^{18}O (by +2 to +4 permil in deeply buried sandstones; Land and Dutton, 1978; Milliken et al., 1981; Dutton and Land, 1985) as a result of reaction with the enclosing sediment. (Craig, 1961; Hitchon and Friedman, 1969; Clayton et al, 1966; Kharaka et al., 1973; Land, 1980; Longstaffe, 1983). This enrichment in

^{18}O may have been partially offset by the influx of ^{18}O -poor ground waters during: (i) the deposition of the fluvial Hecla Bay and Beverley Inlet sandstones; (ii) the short period of uplift and erosion in Late Frasnian before maximum burial; (iii) the major uplift, deformation and erosion in Famennian to Viséan (Ellesmerian Orogeny), and/or (iv) the erosion of the uplifted and deformed areas to the present day after the Ellesmerian Orogeny (Fig. 3.1).

Based on the above justifications, the following assumptions of the evolving formation waters can be made:

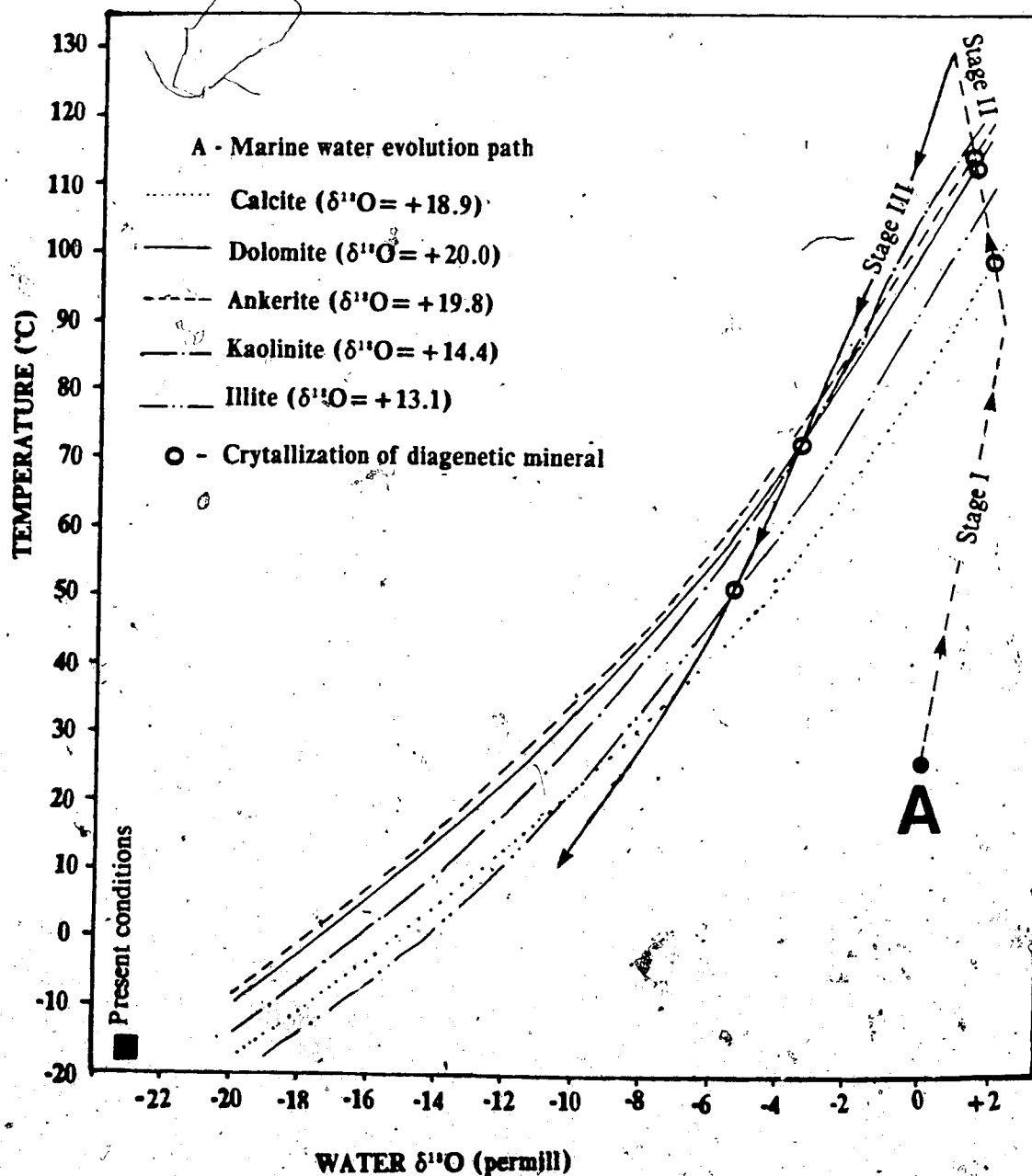
1. original connate waters were marine waters with $\delta^{18}\text{O}$ of about zero;
2. a continuous increase in $\delta^{18}\text{O}$ of the formation waters occurred during burial due to water-rock interaction until Late Frasnian when the strata were uplifted for the first time;
3. during and after the first uplift, the influx of meteoric waters caused a continuous decline in $\delta^{18}\text{O}$ of the formation waters (this decline probably diminished as the burial approached maximum), and
4. the second uplifting by the Ellesmerian Orogeny probably allowed another influx of meteoric water, causing a further decline in pore-fluid $\delta^{18}\text{O}$.

The relationships among the $\delta^{18}\text{O}$ of the diagenetic minerals (Fe-rich calcite, ankerite, dolomite, kaolinite and illite), temperature and water $\delta^{18}\text{O}$ are shown in Figure 3.2. These curves have been calculated using functions (Fig. 3.2) reported by Land and Dutton (1978), Eslinger (1971), Friedman and O'Neil (1977), and Eslinger and Savin (1973). Additional data used are (i) present mean surface temperature of about -17°C (Environment Canada, 1982), and (ii) present meteoric surface water has a $\delta^{18}\text{O}$ of about -23 (SMOW; Anderson and Arthur, 1983). Based on the above information and discussion, the most probable evolutionary path for the original formation waters of the Bird Fiord sediments is illustrated in Figure 3.2.

B. PARAGENETIC SEQUENCE

The interpretation of the diagenetic history of the sandstones from the Bird Fiord, Weatherall and basal Hecla Bay Formations is based on combined evidence from: (i) the known paragenetic sequence of diagenetic events (Fig. 2.7); (ii) the burial history which gives the relative timing of the specific episodes of burial, uplift, deformation and erosion (Fig. 3.1); and (iii) stable-isotope geochemistry which provides information about the pore-fluids and thermal history during the diagenesis (Fig. 3.2). The proposed relationship between the

Fig. 3.2 $\delta^{18}\text{O}$ of water versus temperature for authigenic carbonate and clay minerals from sandstones of the Bird Fiord Formation. The possible evolutionary path for marine formation water is also shown. See text for assumptions used in drawing the evolutionary path. The curves shown for calcite, dolomite, ankerite, kaolinite and illite have been calculated using the following equation: calcite-water [$10^3 \ln \alpha = 2.78(10^4 T^{-2}) - 2.89$] (Friedman and O'Neil, 1977); dolomite-water and ankerite-water [$10^3 \ln \alpha = 2.78(10^4 T^{-2}) + 0.32$] (Friedman and O'Neil, 1977); Kaolinite-water [$10^3 \ln \alpha = 2.5(10^4 T^{-2}) - 2.87$] (Land and Dutton, 1978; from Eslinger, 1971); illite-water [$10^3 \ln \alpha = 2.43(10^4 T^{-2}) - 4.82$] (Eslinger and Savin, 1973).



paragenetic sequence and the burial history of the rocks is shown in Figure 3.3. This relationship is used in the following discussion of the diagenetic history.

Paragenetic sequences are divided into different stages of diagenesis according to burial depths. For example, Loucks et al. (1984) divided the diagenetic sequence in the Lower Tertiary sandstones along the Texas Gulf Coast into surface-to-shallow, intermediate and deep subsurface diagenesis. In an analogous fashion, the diagenetic sequence in the Bird Fiord, Weatherall and basal Hecla Bay sandstones (Fig. 2.7) can be divided into three stages. Diagenesis in these sandstones occurred: (i) at the surface and near-surface; (ii) during intermediate to deep burial, and (iii) during and following major uplift (Ellesmerian Orogeny) (Fig. 3.3).

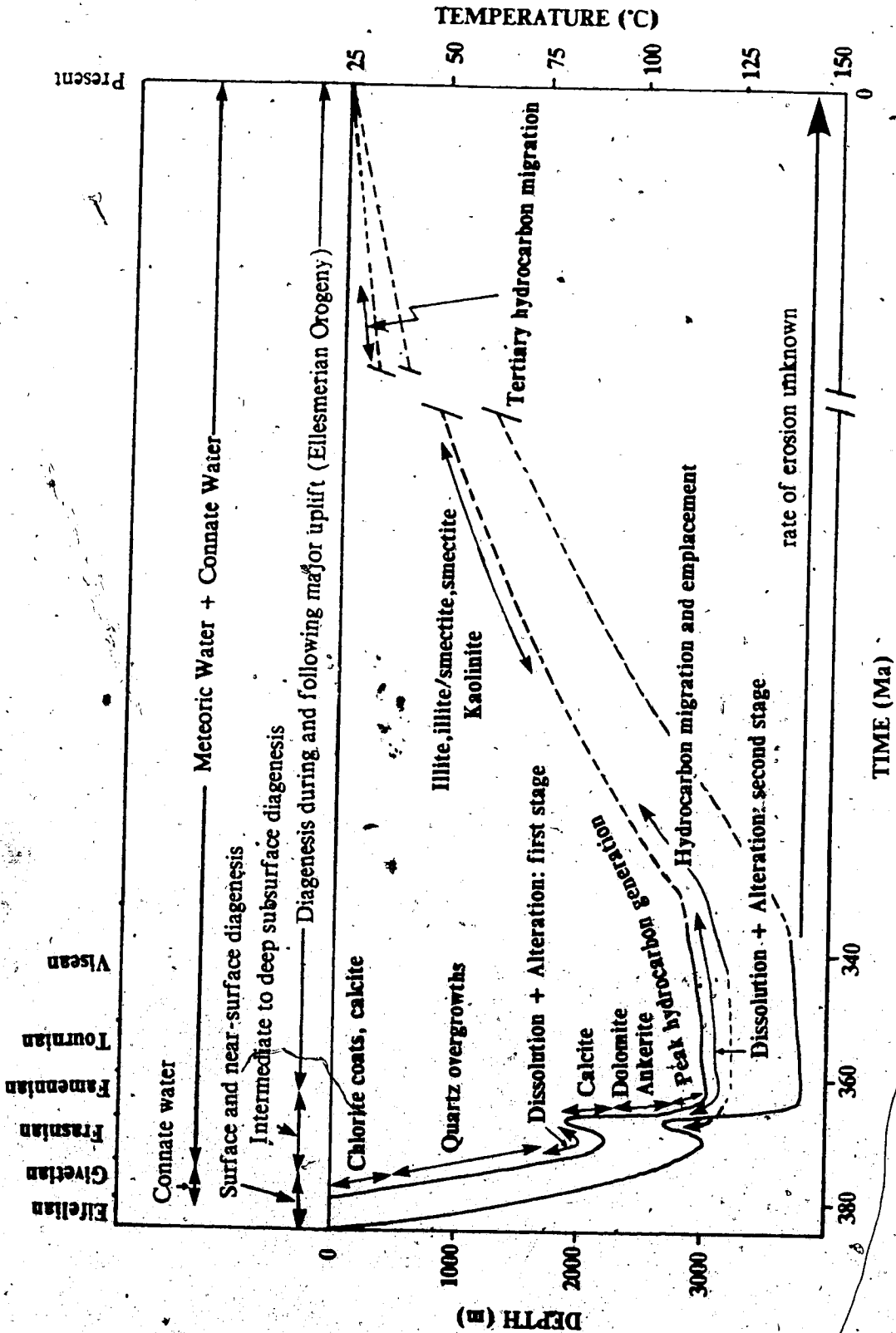
Surface and Near-Surface Diagenesis

Fe-rich, chlorite grain-coatings and the first generation calcite were the earliest-formed cements (Figs. 2.7, 3.3). Both cements were formed during or immediately following deposition, while the sediments were at or near the surface (Fig. 3.3). Textural evidence (Plate 2.1C) shows that the first generation of calcite cementation occurred in the absence of chlorite grain-coatings, and the chlorite grain-coatings were formed in the absence of calcite. The formation of these two cements is partly facies dependent; chlorite is formed mostly in deltaic sandstones, while calcite is formed mostly in marine sandstones.

Fe-rich chlorite - Radiating, Fe-rich chlorite grain-coatings around quartz and feldspar grains (Plates 2.3B, 2.4A,C) are most abundant and well-developed in sandstones deposited in a deltaic environment. This habit and facies-related distribution of the Fe-rich chlorite in the Bird Fiord, Weatherall and basal Hecla Bay sandstones are supported by the literature. Longstaffe (in press) and Storey (1982) suggested a distributary-channel environment for sandstones rich in early diagenetic, Fe-rich chlorite.

Calcite - The first stage of calcite precipitation in marine sandstones occurred in the absence of chlorite grain-coatings and before compaction. A poikilotopic or "floating" texture is produced by this early calcite cementation (Plate 2.1C).

Fig. 3-3 Relationship between the burial history and the paragenetic sequence.



The presence of early calcite cementation is consistent with the lack of later cements, such as quartz overgrowths, which are present in associated sandstones not cemented by early calcite (Franks and Forester, 1984).

Precipitation of early calcite was facies-related; most samples with >40% calcite are marine sandstones from nearshore, proximal and distal shelves (Tables 1.2, 2.5). The marine sandstones of the Bird Fiord and Weatherall Formations have abundant shell fragments (brachiopods, crinoids and pelecypods) and marine carbonate grains (dolomite). The marine environments were storm-affected; the fossils were probably broken up and incorporated into the reworked sandstones during a storm, providing an internal source of CaCO_3 .

Intermediate to Deep Subsurface Diagenesis

Intermediate to deep subsurface diagenesis comprised a complex stage of cementation, replacement and dissolution (Fig. 3.3). This stage included all the diagenetic events that happened following crystallization of Fe-rich chlorite and early calcite precipitation but before the Ellesmerian Orogeny (Figs. 3.1, 3.3).

Quartz Overgrowths - Quartz overgrowths comprised up to 15% of sandstones with little or no carbonate cement and clay matrix, thus eliminating most of the original porosity (Plate 2.1A,B; Table 2.5).

The presence of abundant concavo-convex quartz grain-to-grain contacts (Plate 2.5A) suggests that pressure solution at grain-to-grain contacts had probably provided some of the silica necessary for the quartz overgrowths at intermediate depths (500-1,800m; Fig. 3.3). The presence of a chlorite layer at the quartz grain-to-grain contacts in many samples would increase the rate of diffusion of pressure-dissolved silica away from the site of pressure solution (Weyl, 1959; deBoer, 1977; Robin, 1978). The clay layer consists of a collection of chlorite platelets with the associated water films, and the thickness of each chlorite flake with its film is in the order of 20Å. Thus, a chlorite layer 5µm thick between two quartz grains will contain about 2,500 water films instead of the one or two water films between clean grains, resulting in a considerable increase in the rate of diffusion of silica and (in the rate of pressure solution. However, this source of silica was probably minor in these quartz-rich sandstones) Sibley and Blatt (1976) demonstrated that pressure solution is minor in many quartz cemented

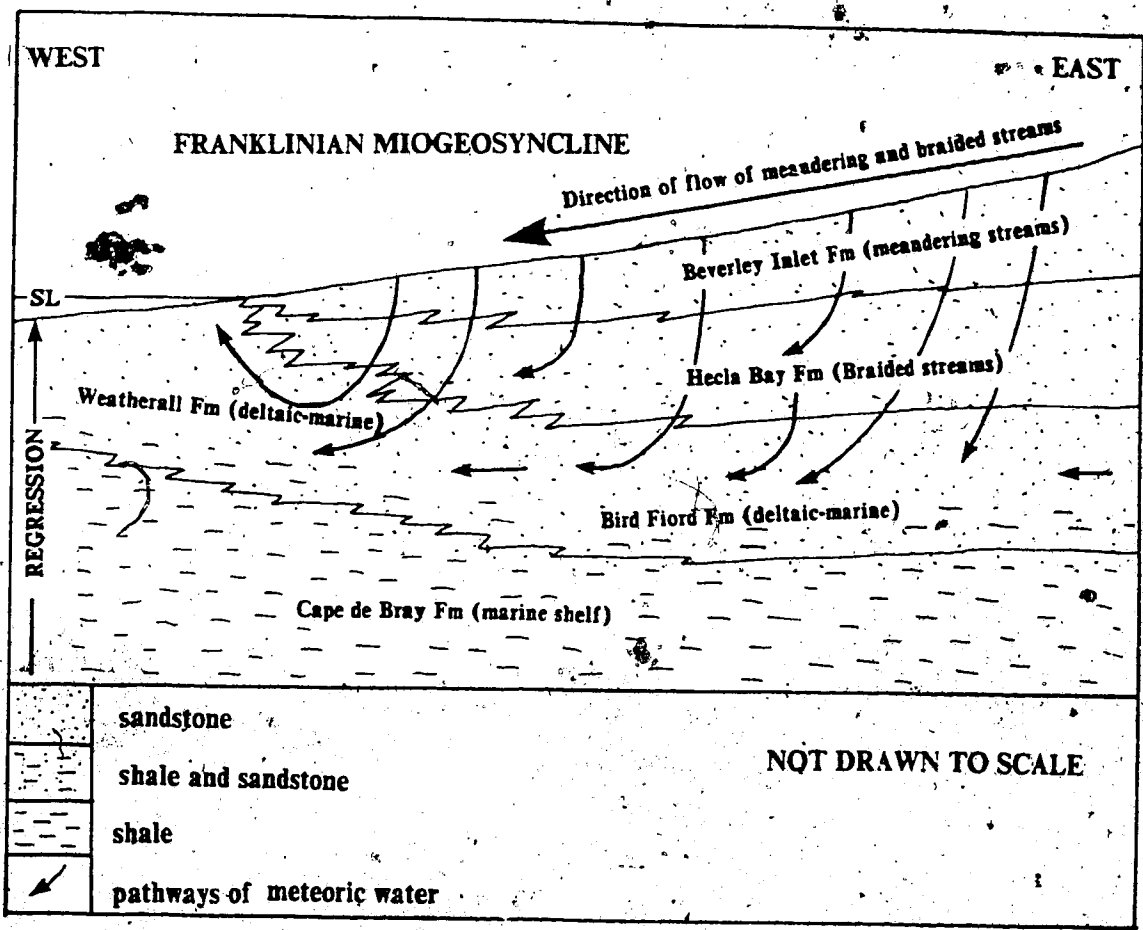
sandstones.

Many other sources of silica have been proposed for quartz cementation. Blatt et al. (1980) and Sibley and Blatt (1976) suggested that the circulation of meteoric waters aided quartz cementation in relatively shallow sandstones; meteoric waters contain about 13ppm of dissolved silica compared to modern seawaters which contain <1ppm. Vertical circulation of ground water is required in order to reach the shallow sandstones at a fast enough rate to precipitate the high amounts of quartz cement. Since quartz cementation in the Bird Fiord, Weatherall and basal Hecla Bay sandstones started relatively early during the burial history (Fig. 3.3), the circulation of silica-rich surface meteoric waters into the relatively shallow sandstones is quite likely (Fig. 3.4).

The establishment of the circulation of meteoric waters into the underlying deltaic to marine Bird Fiord and Weatherall sandstones may have resulted from the lowering of the sea level during Eifelian to Givetian time, when there was a net marine regression which resulted in the deposition of the overlying fluvial Hecla Bay sandstones (Fig. 3.4; Embry and Klovan, 1976; Goodbody, 1985). The high gravitational head on the continent resulted in a flow of ground water from the continent to the shoreline, thus flushing the Bird Fiord, Weatherall and basal Hecla Bay sandstones (Fig. 3.4; Galloway, 1984). Toth (1980) demonstrated that meteoric waters can circulate through permeable sandstone units to depths, on the order of 3,000m below ground surface, thus supporting the idea of meteoric water-derived silica for quartz cementation in these sandstones at intermediate depths (about 500-1,800m; Fig. 3.3). Other possible sources of silica, such as opaline diatoms, radiolaria, and siliceous sponges (Blatt et al., 1980), are unlikely because the sandstones from the sand bars, distributary channels, distributary mouth bars and nearshore environments are devoid of these silt-sized organisms.

Other authors have suggested that silica can be derived from the illitization of smectite layers in illite/smectite during burial of shales (e.g., Land and Dutton, 1978; Boles and Franks, 1979; Milliken et al., 1981; Perry and Hower, 1970; Hower et al., 1976). However, most silica is conserved during illitization and a very large quantity of illite/smectite would be needed before any excess silica could be transported into adjacent sandstones (Hower et al., 1976; Yeh and Savin, 1977; Hower, 1981b; Land, 1984). It is unlikely that any silica was transported into the Bird Fiord, Weatherall and Hecla Bay sandstones because illite/smectite is not abundant in the interbedded, adjacent and underlying (Cape de Bray) shales (Tables 2.3, 2.4); in addition,

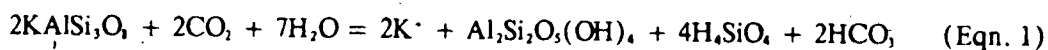
Fig. 3.4 Model for flow of surface meteoric water into the sandstones of the Bird Fiord, Weatherall and Hecla Bay Formations during deposition of the Beverley Inlet sandstone as a result of a net marine regression or progradation of shoreline.



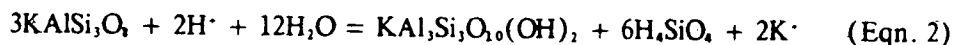
progressive illitization with depth has not been observed (see chapter II).

Dissolution and alteration: first stage - Following quartz cementation, changes in pore fluid chemistry resulted in the first stage of dissolution and alteration (Fig. 3.3) of feldspar (Plate 2.5B), rock and shell fragment (Plates 2.2A, 2.3A), quartz (Plate 2.5D), micas (Plate 2.2B) and probably early calcite. Minor amounts of illite (Plate 2.6E) and kaolinite (Plate 2.6F) were formed as alteration products of feldspar (Fig. 2.7).

Feldspar decomposition has long been associated with a process of acidic dissolution which produces authigenic kaolinite as follows (Hurst and Irwin, 1982; Land, 1984):

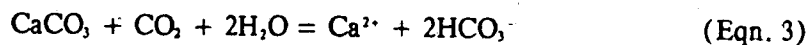


Other detrital silicates, particularly micas, also produce kaolinite by the process of acidic dissolution (Hurst and Irwin, 1982). Under pore-fluid conditions of higher K^+/H^+ ratios than are typical for kaolinite formation, illite may have been produced from feldspar dissolution according to the following reaction (Bjørlykke et al., 1979):



Potassium from the mica or feldspar may contribute to the formation of illite.

The dissolution of the early calcite may follow the reaction:



A source of acidic fluids is necessary for the above reactions (equations 1-3) to proceed. Possible sources of acidic fluids are influxing meteoric waters and fluids released during hydrocarbon maturation. During this dissolution and alteration stage (at <2,500m burial depth) the relatively shallow Weatherall and Bird Fiord sandstones were overlain by the porous fluvial sandstones of the Hecla Bay and Beverley Inlet Formations. Therefore, it is likely that most of the acidic fluids necessary for dissolving the silicates and carbonate cements were derived from acidic meteoric waters that circulated through the unexposed sandstones

during the deposition of the upper section of the Beverley Inlet Formation (Fig. 3.4). The ground waters probably contained mostly carbonic acids; some organic acids formed from the decay of organic matter in the soil zone may also have been present. The circulation of acidic waters into the subsurface was probably enhanced by the first uplift, deformation and erosion in the Late Frasnian, when at least 300m of strata was removed from the top of Beverley Inlet Formation (Fig. 3.1; Embry and Klovan, 1976).

This diagenetic stage occurred relatively early during the burial history of the sandstones (at <2,500m burial depth, i.e., <100°C; Fig. 3.3). Therefore, it is likely that only a small fraction of the acidic fluids were derived from the release of CO₂ and carboxylic acids during hydrocarbon maturation at or near maximum burial (Loucks et al., 1977; McBride, 1977; Carothers and Kharaka, 1978; Momper, 1978; Schmidt and McDonald, 1979; Porter and Weimer, 1982; Surdam et al., 1984; Land, 1984; Franks, 1984). Franks and Forester (1984) suggested that peak maturation of organic matter in sediments occurs at approximately 100°C.

It can be concluded that the dissolution and alteration of feldspars, quartz, rock and shell fragments, mica and perhaps calcite were the result of an influx of acidic fluids which were derived from the mixing of surface-derived meteoric water, and lesser amounts of acidic fluids released from shales.

Calcite - Poikilotopic sandstones (with >40% calcite; Plate 2.1C) may have a more or less continuous carbonate cementation process from early calcite to late calcite without the intervening quartz cementation. However, sandstones with <10% calcite or other carbonate cements show no evidence of an early stage of calcite cementation (Plate 2.5C); the calcite was precipitated in secondary pores created by the first dissolution and alteration stage.

The relationship among the $\delta^{18}\text{O}$ (average = +18.9) of the calcite, temperature and water $\delta^{18}\text{O}$ is shown in Figure 3.2. To calculate an isotopic temperature for the crystallization of a diagenetic mineral requires that the $\delta^{18}\text{O}$ of both solid and liquid be known. The calcite was probably formed in equilibrium with modified seawaters. The seawaters ($\delta^{18}\text{O}$ of about zero) trapped during sedimentation was probably enriched in ^{18}O by exchange with the host sedimentary rocks during diagenesis (Stage I of evolutionary path; Fig. 3.2). Low- ^{18}O meteoric waters, which flushed the sandstones during and after the uplift and deformation in Late Frasnian, were probably sufficient to cause a decline in the $\delta^{18}\text{O}$ of the formation waters (Stage

II of evolutionary path, Fig. 3.2; also see Fig. 3.3). Following this evolutionary path, a crystallization temperature of about 100°C can be calculated for calcite precipitation if the formation water has a $\delta^{18}\text{O}$ of about +2 permill (Fig. 3.2).

The possibility that more ^{18}O -poor fluids were responsible for the crystallization of the calcite cannot be ruled out entirely. If brackish water ($\delta^{18}\text{O} < 0$) was trapped during sedimentation, a more ^{18}O -poor fluid was possible. However, due to the warm paleoclimatic conditions (25-30°C; Smith et al., 1973), the brackish water would only be slightly depleted in ^{18}O . This is because freshwater resulting from atmospheric precipitation at higher temperatures would be less depleted in ^{18}O (Anderson and Arthur, 1983). Lower crystallization temperatures for calcite would result if the $\delta^{18}\text{O}$ of the formation waters was lower than +2 permill.

The range in $\delta^{18}\text{O}$ of the calcite (+18.1 to +20.0) reflects a mixture of isotopic signatures that resulted from precipitation and recrystallization throughout diagenesis, an observation which is consistent with the petrographic data for very calcareous sandstones (Longstaffe, in press). The isotopic signature reflecting the temperatures and fluids involved in the formation of early calcite was probably not retained completely. Instead, the early calcite cement probably underwent isotopic exchange with pore fluids during hotter periods of diagenesis.

The estimated overburden above the top of the Bird Fiord and Weatherall Formations just before the first uplift (Late Frasnian) is 2,200m; this would give a burial temperature of about 90°C, assuming a geothermal gradient of 30°C/km and a surface temperature of 25°C (Fig. 3.1). Since the Bird Fiord Formation is about 800m thick in this section, a burial temperature of about 115°C (3,000m) can be calculated for the bottom of the Bird Fiord Formation prior to the first uplift. These estimated temperatures based on amount of overburden are in close agreement with the temperatures calculated from the isotopic data. This suggests that isotopic exchange of the calcite with pore fluids during later periods of diagenesis (i.e., after the Ellesmerian Orogeny) was insignificant.

The calcite is slightly depleted in ^{13}C ($\delta^{13}\text{C} = -2.5$ to -4.5 , PDB; Table 2.7). Such values probably resulted from mixing carbon derived from marine carbonate and shell fragments ($\delta^{13}\text{C} = 0 \pm 4$; e.g., Gross, 1964), with ^{13}C -depleted organic carbon from the maturation of organic matter (oxidation, decarboxylation, CO_2 from methane generation, etc.; Hudson, 1977; Carothers and Kharaka, 1980; Kharaka et al., 1983). Longstaffe (in press) suggested that

without knowing the specific nature of the reactions involving organic carbon, the relative contributions of organic and inorganic reservoirs cannot be resolved accurately. For most calcite samples the inorganic carbon reservoir appears to have been the most important; abundant shell fragments and carbonate grains are present in the sandstones. However, the isotopic temperature of about 100°C for calcite crystallization suggests that at least some ¹³C-depleted organic carbon from the maturation of organic matter was also probably involved in the crystallization of the calcite because at this temperature the hydrocarbon maturation process is approximately at its peak. Schmidt and McDonald (1979) suggested that the zone of active carbonate dissolution, which is the source of carbonate, generally underlies the zone of maximum active carbonate cementation. Upward movement of carbonate is only possible when CO₂ from organic maturation mobilizes the CaCO₃ present in the shales, and the carbonate-charged pore waters have been expelled into the overlying and adjacent sandstones (Land, 1984). The upward moving acidic fluids from the shales may have also resulted in the dissolution and reprecipitation of the shell fragments and marine carbonate grains in the sandstones as calcite. Some of the CaCO₃ was probably derived from a slow compaction process (stylolitization) of marine limestones deeper in the section.

Petrographic evidence shows that calcite also replaced both K-feldspar and plagioclase (Plates 2.2B,C). Both feldspar and calcite have increased stability at high pH and become more soluble as pH decreases. The replacement effect probably resulted from the increased solubility of feldspar with increased temperature, and the decrease in solubility of carbonate under the same conditions (Blatt et al., 1980). Surdam et al. (1984) indicated that the pore fluid must contain a high P CO₂ and an acid buffer reaction, such as decarboxylation, in order that feldspar would dissolve and calcite would precipitate.

Dolomite and Ankerite - Dolomite is not an important cement compared to calcite and ankerite. The minor amounts of dolomite cement associated with calcite (Table 2.6) may represent minor dolomitization of the calcite cement. Authigenic dolomite also occurs as overgrowths on detrital dolomite grains (Plate 2.8A). The relationship between dolomite and ankerite cements cannot be documented by petrographic data because these two cements do not occur together. Dolomite and ankerite precipitation and/or recrystallization (dolomitization and ankeritization, respectively) from calcite may be contemporaneous (Fig. 2.7), and their occurrence may be

controlled by the local variation in Mg and Fe content in the pore fluid.

The $\delta^{13}\text{C}$ of ankerite (-4.4) and dolomite (-0.1) are similar to the $\delta^{13}\text{C}$ of the calcite, suggesting that the earlier calcite cement may have been dolomitized and ankeritized. However, if the dolomite and ankerite were precipitated directly from the pore-fluids, the slightly depleted $\delta^{13}\text{C}$ values may have resulted from the mixing of carbon derived from marine carbonates and shell fragments in the sandstones, and ^{13}C -depleted organic carbon from the maturation of organic matter. Again, without knowing the specific nature of the reactions involved in organic carbon, the relative contributions of organic and inorganic reservoirs cannot be resolved accurately. Both the organic and inorganic carbon reservoirs appeared to be involved in the formation of ankerite and dolomite.

The relationships among the $\delta^{18}\text{O}$ of dolomite (+20.0) and ankerite (+19.8), temperature and water $\delta^{18}\text{O}$ are shown in Figure 3.2. The dolomite (330m above base) and ankerite (886m above base) were sampled from the proximal shelf and deltaic environments, respectively; they were probably formed in equilibrium with modified seawaters similar to that for calcite formation, but at higher temperatures. After the formation of calcite the $\delta^{18}\text{O}$ of the formation water probably continued to decline due to mixing with meteoric waters (Stage II, Fig. 3.2). If the $\delta^{18}\text{O}$ of the formation waters declined to about +1 permil, a crystallization temperature of 110-115°C can be calculated for the precipitation of the dolomite and ankerite (Fig. 3.2).

An isotopic temperature of 110-115°C would be quite compatible with the burial history of the sandstones from the Bird Fiord and Weatherall Formations (Fig. 3.1). These temperatures correspond to depths near or at the maximum burial (Fig. 3.3), indicating that isotopic exchange after uplift was insignificant. At these burial depths the hydrocarbon maturation process was probably at or near its peak (Fig. 3.3). The Fe and Mg necessary for the formation of dolomite and ankerite were probably derived from the breakdown of organic matter (Curtis, 1978; Irwin, 1980), or from the breakdown of Fe- and Mg-rich minerals (e.g., detrital biotite and authigenic chlorite) by the acidic fluids derived from the hydrocarbon maturation process. The Fe- and Mg-charged acidic fluids would probably result in the dissolution and recrystallization of the calcite and remaining shell fragments and marine carbonate grains to dolomite or ankerite depending on the local variation of Fe content in the pore fluids.

Other sources of Fe and Mg have been suggested by other authors. Boles (1978), Boles and Franks (1979) and Franks and Forester (1984) suggested that ankeritization of calcite is related to the late stage release of Fe and Mg from smectite diagenesis which is associated with the organic maturation process in the shales. This source of Fe and Mg is unlikely here because of the relatively low illite/smectite content in the shales interbedded with, adjacent to, and immediately underlying the Bird Fiord and Weatherall sandstones.

The possibility that more ^{18}O -poor fluids were involved in the crystallization of the ankerite cannot be ruled out entirely because the ankerite sample was from a deltaic sandstone, and the starting pore fluid was probably brackish. A lower temperature for the crystallization of ankerite would result in this case.

Hydrocarbon maturation - Maximum generation of liquid hydrocarbons in interbedded, adjacent and underlying shales probably occurred at or near maximum burial at temperatures greater than 110°C (Fig. 3.3). Hunt (1979) stated that the largest quantity of petroleum hydrocarbons is formed from organic matter heated to temperatures between 60 and 150°C .

The transition from mature to overmature strata occurs in the lower part of or below the Cape de Bray and Blue Fiord Formations (Powell, 1978), thus placing the overlying Bird Fiord, Weatherall and Cape de Bray Formations in the mature zone. This suggests that peak hydrocarbon generation in the shales of these formations occurred at or near maximum burial before the Ellesmerian Orogeny (Fig. 3.3). Maximum hydrocarbon generation in the underlying high potential source rocks, namely Cape Phillips, Blackley, Eids Formations, probably occurred slightly earlier than the overlying units. Earlier-formed hydrocarbons from deeper shales may be trapped within stratigraphic traps (e.g., carbonate build-ups of the Blue Fiord Formation); subsequent epeirogenic movements may have caused tertiary migration of these hydrocarbons into structural traps formed by the orogeny.

Diagenesis During and Following Major Uplift (Ellesmerian Orogeny)

The Ellesmerian Orogeny, a period of uplifting, folding, faulting and erosion from Famennian to Viséan time, ended hydrocarbon generation in the basin (Fig. 3.3). In addition it produced a new recharge area in the uplifted and deformed areas for another stage of meteoric water influx. From this period onwards there was a progressive mixing of meteoric waters with

formation waters (Fig. 3.3). This progressive mixing effect was reflected by the dissolution of detrital feldspars and carbonate cements, and the subsequent precipitation of late diagenetic clays (Figs. 2.7, 3.3).

Dissolution and alteration: second stage - Following carbonate cementation, changes in pore fluid chemistry resulted in the second stage of dissolution of feldspar (Plate 2.9A), calcite (Plate 2.8C,D), dolomite (Plate 2.8A) and ankerite, and alteration of feldspar to illite and kaolinite (Plate 2.12B) (Fig. 2.7). The initial stage of this diagenetic event was probably contemporaneous with peak hydrocarbon maturation at or near maximum burial, and the later stage was probably contemporaneous with the Ellesmerian Orogeny (Fig. 3.3). The initial acidic fluids necessary for dissolving the silicates and carbonate cements were probably derived from the release of CO₂ and carboxylic acids during peak hydrocarbon maturation in the interbedded, adjacent and underlying shales at or near maximum burial (Loucks et al., 1977; McBride, 1977; Carothers and Kharaka, 1979; Momper, 1978; Schmidt and McDonald, 1979; Porter and Weimer, 1982; Surdam et al., 1984; Land, 1984; Franks, 1984). Additional acidic fluids necessary for dissolution during the major uplift were probably derived from surface-derived meteoric waters which mixed with the formation waters.

The decomposition of feldspar, according to equation 1 and 2, would produce the authigenic kaolinite and illite associated with the partially altered feldspar. The dissolution reaction for the Fe-rich calcite may follow equation 3.

Hydrocarbon migration and emplacement - The beginning of hydrocarbon migration was probably contemporaneous with peak hydrocarbon maturation and the second dissolution stage (Fig. 3.3). Secondary porosity created in the carbonate cements (Plate 2.10A) and feldspar (Plate 2.10B) were filled by hydrocarbons. The acidic fluids associated with the organic maturation process may have reached the sandstones by the process of pressure-drive transport of dissolved CO₂, resulting from increased pore pressures associated with the hydrocarbon maturation process at depth (Porter and Weimer, 1982). The increase in pore pressure is due to the higher volume occupied by the products which were derived from the original organic material. Initially, dissolved CO₂ lowered the pH of pore fluids, thus providing an acidic solvent for carbonates and aluminosilicates dissolution. But during a later stage of organic

matter maturation, the CO₂ gas created a gas-drive mechanism for the migration of hydrocarbons into the secondary porosity in the sandstones which was created by the dissolution process (Porter and Weimer, 1982; Mompér, 1978).

However, the Ellesmerian Orogeny probably changed the style of hydrocarbon migration. Fissuring and fracturing associated with the deformation probably induced secondary permeability and porosity, which favoured vertical migration (Hunt, 1979). Folding and faulting created structural traps for the accumulation of the hydrocarbons. The tilting of the strata by the faulting and folding may have caused updip secondary migration of the hydrocarbons along the permeable sandstone units.

A drive-mechanism for the hydrocarbon migration may be created by the circulating meteoric water that penetrated the permeable sandstones during and after the Ellesmerian Orogeny. Primary migration of hydrocarbons into the sandstone units from interbedded, adjacent and underlying shales may have resulted from the gas-drive mechanism created by the CO₂ gas, but secondary migration along the sandstone units may have resulted from fluid pressures and the water-drive mechanism created by the circulating meteoric water. Secondary migration of the hydrocarbons into structural traps probably continued after the tectonic activities (Fig. 3.3).

Late authigenic clays. - The relative timing of the formation of authigenic illite, illite/smectite, smectite and kaolinite cannot be determined from thin-section and SEM petrography. These clays can be contemporaneous with each other (Figs. 2.7, 3.3). Kaolinite is pore-filling after hydrocarbon migration and emplacement (Plate 2.10C,D).

The authigenic clay minerals from the sandstones of the Bird Fiord and Hecla Bay Formations have much lower $\delta^{18}\text{O}$ values than the detrital clay minerals from the argillaceous rocks (Chapter II; Table 2.7). The $\delta^{18}\text{O}$ for kaolinite and illite are +14.4 and +13.1, respectively. Typical $\delta^{18}\text{O}$ values for detrital clay minerals from fine-grained sediments throughout the world range from +16 to +22 permil (Savin and Epstein, 1970a,b,c; Longstaffe et al., 1982; Longstaffe, 1983, 1984). The $\delta^{18}\text{O}$ values of clay minerals from the shales, argillaceous limestones and siltstones from the Bird Fiord Formation (+14.7 to +16.7; Table 2.7) show that the detrital clays in these rocks attained their isotopic signatures at the source through weathering (Longstaffe, 1984). A logical explanation for the difference in $\delta^{18}\text{O}$

values between the authigenic and detrital clays is that the authigenic clay minerals have formed in equilibrium with low- ^{18}O ground water.

The relationship between kaolinite and illite $\delta^{18}\text{O}$ (+14.4 and +13.1, respectively), fluid $\delta^{18}\text{O}$ and temperature (Fig. 3.2) make possible more detailed speculation concerning the formation of the authigenic clay minerals in the Bird Fiord Formation. These authigenic clays were formed after the Ellesmerian Orogeny and hydrocarbon emplacement (Plate 2.10C,D; Fig. 2.7). The $\delta^{18}\text{O}$ of the formation water was continuously depleted in ^{18}O after the Ellesmerian Orogeny since meteoric waters continued to flush the pre-existing formation water from the sandstones (Stage III, Fig. 3.2). Assuming this evolutionary path, the kaolinite and illite would have precipitated at approximately 75 and 50°C, respectively, from formation water of $\delta^{18}\text{O} = -3$ to -6 (Fig. 3.2). These temperatures correspond to a burial depth of about 1,200m (Fig. 3.3).

The kaolinite and illite could have formed at lower temperatures from more ^{18}O -depleted formation waters. Longstaffe (1983, 1984) reported kaolinite forming at low temperatures (+3 to +5°C) from ^{18}O -depleted ground waters ($\delta^{18}\text{O} = -19.2$ to -18.2) in the Milk River Formation, Alberta. The positions of the kaolinite and illite curves and the position of the present day conditions show that kaolinite and illite could have been formed continuously as the formation waters evolved to the present day conditions. In that case, the evolutionary path would not be as shown in Fig. 3.2, but would more or less coincide with the kaolinite and illite curves. At these temperatures, oxygen-isotope exchange between the water and the clay minerals was probably insignificant.

According to Grim (1953), Garrels and Christ (1965) and Biscaye (1965), kaolinite is precipitated under generally acidic conditions. The occurrence of authigenic kaolinite in the Bird Fiord, Weatherall and basal Hecla Bay sandstones may be related to the low pH of meteoric water which contains dissolved CO_2 from the atmosphere and soil horizon. One possible source for dissolved Al and Si was the dissolution of remaining feldspar by the acidic meteoric water. Authigenic kaolinite is usually associated with relict feldspar in large secondary pores (Plates 2.6F, 2.12B), indicating some kind of replacement has occurred. These kaolinite replacements may have acted as nuclei for precipitation of the extensive pore-filling kaolinite (Loucks et al., 1984). Grim (1953) pointed out that kaolinite is the most common alteration product of weathered feldspars.

The formation of authigenic illite means that the formation water contained a much higher K/H ratio than is typical of meteoric water (Montoya and Hemley, 1975; Longstaffe, 1984). This may suggest that the authigenic illite was formed at relatively low temperature from formation fluids that resulted from the mixing of evolved connate waters rich in K with evolved meteoric waters (Longstaffe, 1984). The release of K by the dissolution and/or replacement of feldspar by kaolinite (equation 1) may have increased the K in the pore fluid too. The kaolinite and illite could have co-precipitated in the pore system, with the illite using up the K released from the breakdown or kaolinite replacement of K-feldspar. All the K needed for the minor amount of authigenic illite present in the sandstones can probably be accounted for by this reaction. In fact, illite was seen directly replacing K-feldspar (Plate 2.6E); in this case the necessary Al, K and Si were derived from the K-feldspar directly (equation 2).

The smectite and illite/smectite may have been formed under similar conditions as the kaolinite and illite. Longstaffe (1984) reported the formation of smectite at low temperatures from ^{18}O -depleted formation waters. The formation of Fe-rich smectite suggests that it was formed where the meteoric water-affected pore fluids were locally enriched in Fe, Mg and Ca, but were poor in K. Illite/smectite was probably formed locally where the pore fluid was enriched in K.

Tertiary Migration of Hydrocarbons - Tertiary migration of hydrocarbons into fractures or fissures postdated the precipitation of authigenic kaolinite (Plate 2.12D; Fig. 2.7, 3.3). The formation and/or reopening of the fractures or fissures probably also postdated kaolinite precipitation. The Late Cretaceous and Tertiary deformation of Middle Pennsylvanian to Early Tertiary strata in the Sverdrup Basin, which superimposed the Franklinian Geosyncline (Thorsteinsson, 1960, 1970), probably induced the formation and/or reopening of these fractures and fissures in the underlying Middle-Upper Devonian strata.

Hunt (1979) pointed out that fracturing and fissuring, as a result of natural tension, is a common process at all burial depths in brittle rocks such as carbonates, calcareous shales and silicified sands. Radchenko et al. (1951) cited many examples of smears and seeps of liquid hydrocarbons and impregnations of solid asphalts along bedding planes of fissures and faults in carbonate rocks, silicified sands, and some metamorphosed rocks. Goldberg (1973) found several types of bitumens in a dense network of nearly vertical fractures occurring through the

argillaceous carbonate Ordovician cover of a Cambrian oil reservoir in the Baltic region. Fluid pressure may also play an important role in the tension fracturing process and reopening of previously formed fractures at depth equivalent to current drilling ranges (Secor, 1965).

Fractures or fissures in the silicified or calcareous sandstones of the Bird Fiord, Weatherall and Hecla Bay Formations may have developed as a result of such processes. The influx of meteoric water, as a result of continual erosion since uplift, may have caused dissolution along the fractures, thus widening them. The extension of the fractures or fissures into diagenetic or structural hydrocarbon traps may have caused tertiary migration of the hydrocarbons out of the reservoirs into the fractures or fissures, thus some of the previous hydrocarbon accumulations were lost.

IV. CONCLUSIONS

Clastic diagenesis in the Bird Fiord, Weatherall and basal Hecla Bay sandstones was controlled by their burial history. The burial history influenced the hydrogeologic evolution of the sedimentary basin. The relationship between the diagenetic and burial histories of the sandstones is summarised in Figure 3.3. Diagenesis occurred in three main stages: (i) early diagenesis, at or near surface conditions; (ii) burial diagenesis under intermediate to deep subsurface conditions, and (iii) late diagenesis, which occurred during and following a major episode of uplift (Ellesmerian Orogeny) (Figs. 3.1, 3.2).

Surface and Near-Surface Diagenesis - This diagenetic stage is characterized by grain-coating, Fe-rich chlorite and early calcite cement. Both cements were formed during or immediately following deposition, probably from the original connate water. Calcite cementation occurred where chlorite grain-coatings were absent. Chlorite was formed mostly in deltaic sandstones, while calcite was formed mostly in marine sandstones.

Intermediate to Deep Subsurface Diagenesis - Quartz cementation occurred at intermediate burial depths (500-1,800m). Most of the silica necessary for quartz cementation was probably derived from meteoric waters which circulated in the relatively shallow sandstones. Pressure solution probably supplied some of the silica.

The first stage of dissolution and/or alteration of feldspar, rock and shell fragments, quartz, micas and early calcite occurred following quartz cementation. The acidity of the formation fluids was probably enhanced by the addition of fluids derived from the release of CO₂ and carboxylic acids produced in interbedded and underlying fine-grained units by hydrocarbon maturation. In addition, the circulation of surface-derived, meteoric waters into these rocks was probably enhanced during the first, minor uplift in Late Frasnian time.

As burial resumed in Latest Frasnian time, calcite, dolomite and ankerite cements were formed. The $\delta^{18}\text{O}$ values of these cements (+18.1 to +20.0, SMOW) probably reflect crystallization at temperatures of 100-115°C from formation waters with $\delta^{18}\text{O}$ of about +1 to +2 permill. The slightly depleted $\delta^{13}\text{C}$ values of the authigenic calcite (-2.5 to -4.5, PDB), dolomite (-0.1) and ankerite (-4.4) probably resulted from mixing of carbon derived from marine carbonate and shell fragments, and lesser amounts of ^{13}C -depleted organic carbon from the maturation of organic matter. The calcite may also have been dolomitized and ankeritized.

Maximum generation of liquid hydrocarbons in interbedded and surrounding shales probably occurred at or near maximum burial at temperatures greater than 110°C.

Diagenesis During and Following Major Uplift (Ellesmerian Orogeny) - Hydrocarbon generation in the basin was terminated by the Ellesmerian Orogeny, which was a period of uplifting, deformation and erosion from Famennian to Viséan time. The progressive mixing of meteoric waters with formation fluids during and following this orogeny resulted in a second stage of dissolution and/or alteration, and the subsequent precipitation of late diagenetic clays.

Some of the acidic fluids necessary for the dissolution of silicate and carbonate minerals were probably provided by hydrocarbon maturation in the interbedded and underlying fine-grained units; the initiation of the second stage of dissolution was probably contemporaneous with peak hydrocarbon maturation. Hydrocarbon migration probably began contemporaneously with the onset of this dissolution, and filled newly created secondary porosity. Additional fluids for dissolution during the uplift were also provided by downward circulating meteoric waters which also mixed with the formation fluids. Hydrocarbons continued to fill secondary porosity and fractures during and after uplifting.

Following hydrocarbon emplacement, diagenetic kaolinite, illite, illite/smectite and smectite were precipitated. The low $\delta^{18}\text{O}$ values of these diagenetic clays (kaolinite $\delta^{18}\text{O} = +14.4$; illite $\delta^{18}\text{O} = +13.1$) are best explained by crystallization at low temperatures (<75°C) from fluids containing a sizeable fraction of meteoric water. Meteoric waters continued to flush the pre-existing formation waters from the sandstones as the rocks were slowly exposed by erosion.

The tertiary migration of hydrocarbons into fractures and fissures occurred after the precipitation of late diagenetic clays. These fractures and fissures were formed and/or reopened by tectonic activity in the overlying Sverdrup Basin during Late Cretaceous and Tertiary time.

BIBLIOGRAPHY

- AAPG and U.S. Geological Survey, 1976, Geothermal gradient map of North America: United States Geological Survey. Scale 1:5,000,000. Two sheets.
- Anderson, T.F., 1969, Self-diffusion of carbon and oxygen in calcite by isotope exchange with carbon dioxide: *Journal of Geophysical Research*, v. 74, p. 3918-3932.
- Anderson, T.F., and Arthur, M.A., 1983, Stable isotopes of oxygen and carbon and their application to sedimentologic and paleoenvironmental problems: *Stable Isotope In Sedimentary Geology*, Society of Economic Paleontologists and Mineralogists Short Course No. 19, chapter 1.
- Biscaye, P.E., 1964, Distinction between kaolinite and chlorite in Recent sediments by X-ray diffraction: *The American Mineralogist*, v. 49, p. 1281-1289.
- 1965, Mineralogy and sedimentation of Recent deep-sea clay in the Atlantic Ocean and adjacent seas and oceans: *Geological Society of America Bulletin*, v. 76, p. 803-832.
- Bjørlykke, K., Elverhøi, A., and Malm, A.O., 1979, Diagenesis in Mesozoic sandstones from Spitsbergen and North Sea - a comparison: *Geologische Rundschau*, v. 68, p. 1152-1171.
- Blatt, H., Middleton, G., and Murray, R., 1980, *Origin of sedimentary rocks*, second edition: Prentice-Hall, Incorporated, Englewood Cliffs, New Jersey, 782p.
- Boles, J.R., 1978, Active ankerite cementation in the subsurface Eocene of southwest Texas: *Contributions to Mineralogy and Petrology*, v. 68, p. 13-22.
- Boles, J.R., and Franks, S.G., 1979, Clay diagenesis in Wilcox sandstones of southwest Texas: implications of smectite diagenesis on sandstone cementation: *Journal of Sedimentary Petrology*, v. 49, p. 55-70.
- Bradley, W.F., 1954, X-ray diffraction criteria for the characterization of chlorite material in sediments: *Clays and Clay Minerals*, Second National Conference, 1953.
- Brindley, G.W., 1951, The crystal structure of some chamosite minerals: *Mineral Magazine*, v. 30, p. 57-70.
- Brown, G., and Brindley, G.W., 1980, X-ray diffraction procedures for clay mineral identification, in Brindley, G.W., and Brown, G., (eds.), *Crystal structures of clay minerals and their x-ray identification*: Mineralogical Society of London Monograph 5, p. 305-359.
- Carothers, W.W., and Kharaka, Y.K., 1980, Stable carbon isotopes of HCO_3^- in oil field waters - implications for the origin of CO_2 : *Geochimica et Cosmochimica Acta*, v. 44, p. 323-332.
- Cauffman, L.B., 1974, A study of the mineralogy and geochemistry of the Melville Island Group (Middle-Upper Devonian) and Imperial Formation (Upper Devonian), N.W.T.: Unpublished M.Sc. thesis, University of Calgary, 63p.
- Clayton, R.N., 1959, Oxygen isotope fractionation in the system calcium carbonate-water: *Journal of Chemical Physics*, v. 30, p. 1246-1250.
- Clayton, R.N., Friedman, I., Graf, D.L., Mayeda, K., Meents, W.F., and Shimp, N.F., 1966, The origin of saline formation waters - 1. Isotopic composition: *Journal of Geophysical Research*, v. 71, p. 3869-3882.
- Clayton, R.N., and Mayeda, T.K., 1963, The use of bromine pentafluoride in the extraction of

- oxygen from oxides and silicates for isotopic analysis: *Geochimica et Cosmochimica Acta*, v. 27, p. 43-52.
- Craig, H., 1957, Isotopic standards for carbon and oxygen and correction factors for mass-spectrometric analysis of carbon dioxide: *Geochimica et Cosmochimica Acta*, v. 12, p. 133-149.
- 1961, Standards for reporting concentrations of deuterium and oxygen-18 in natural waters: *Science*, v. 133, p. 1833-1834.
- Curtis, C.D., 1978, Possible links between sandstone diagenesis and depth-related geochemical reactions occurring in enclosed mudstones: *Journal of Geological Society of London*, v. 135, p.107-117.
- deBoer, R.B., 1977, On the thermodynamics of pressure solution-interaction between chemical and mechanical forces: *Geochimica et Cosmochimica Acta*, v. 41, p. 249-256.
- Dineley, D.L., 1975, North Atlantic Old Red Sandstone - some implications for Devonian paleogeography, in Yorath, C.J., Parker, G.R. and Glass, D.J. (eds.), *Canada's Continental Margins and Offshore Petroleum Exploration*: Canadian Society of Petroleum Geologists, Memoir 4, p. 773-790.
- Dutton, S.P., and Land, L.S., 1985, Meteoric burial diagenesis of Pennsylvanian arkosic sandstones, southwestern Anadarko Basin, Texas: *Bulletin of the American Association of Petroleum Geologists*, v. 69, p. 22-38.
- Embry, A., and Klovan, J.E., 1976, The Middle-Upper Devonian clastic wedge of the Franklinian Geosyncline: *Bulletin of Canadian Petroleum Geology*, v. 24(4), p.485-639.
- Environment Canada, 1982, Canadian climate normals, Temperature 1957-1980: A publication of the Canadian Climate Program, v. 2, 306p.
- Epstein, A.G., Epstein, J.B., and Harris, L.D., 1977, Conodont color alteration - an index to organic metamorphism: U.S. Geological Survey Professional Paper 995, 27p.
- Epstein, S., Graf, D.L., and Degens, E.T., 1964, Oxygen isotope studies on the origin of dolomite, in Craig, H., et al (eds.), *Isotopic and Cosmic Chemistry*: Amsterdam, North Holland Publishing Company, p. 169-180.
- Eslinger, E.V., 1971, Mineralogy and oxygen isotope ratios of hydrothermal and low-grade metamorphic argillaceous rocks: Ph.D. dissertation, Case Western Reserve University, 205p.
- Eslinger, E.V., and Savin, S.M., 1973, Mineralogy and oxygen isotope geochemistry of the hydrothermally altered rocks of the Ohaki-Broadlands, New Zealand geothermal area: *American Journal of Science*, v. 273, p. 240-267.
- Eslinger, E.V., and Yeh, H., 1981, Mineralogy, O^{18}/O^{16} , and D/H ratios of clay-rich sediments from Deep Sea Drilling Project Site 180, Aleutian Trench: *Clays and Clay Minerals*, v. 29, p. 309-315.
- Folk, R.L., 1968, *Petrology of sedimentary rocks*: Austin, Texas, Hemphill's Book Store.
- Friedman, I., and O'Neil, J.R., 1977, Compilation of stable isotope fractionation factors of geochemical interest, in Fleisher, M. (ed.), *Data of Geochemistry*, sixth edition: United States Geological Survey Professional Paper 440-KK, 12p. + figures.
- Franks, S.G., and Forestor, R.W., 1984, Relationship among secondary porosity, pore-fluid chemistry and carbon dioxide, Texas Gulf Coast, in McDonald, D.A., and Surdam, R.C. (eds.), *Clastic Diagenesis*: American Association of Petroleum Geologists, Memoir 37, p. 63-79.

- Galloway, W.E., 1984, Hydrogeologic regimes of sandstones diagenesis, in McDonald, D.A., and Surdam, R.C., (eds.), *Clastic Diagenesis: American Association of Petroleum Geologists, Memoir 37*, p. 3-13.
- Garrels, R.M., and Christ, C.L., 1965, *Solution, mineral and equilibria*: Freeman, Cooper and Company, San Francisco, 450p.
- Gautier, D.L., 1983, Diagenesis, in Rice, D.D. and Gautier, D.L. (authors), *Pattern of sedimentation, diagenesis and hydrocarbon accumulation in Cretaceous rocks of the Rocky Mountains: Society of Economic Paleontologists and Mineralogists, Special Publication 11*, p. 4.1-4.14.
- Goldberg, I.S., 1973, Solid bitumens in petroleum deposits of the Baltic region as indicators of stages in the migration of petroleum: *Dokl. Akad. Nauk USSR*, v. 209 No. 2, p. 462-465.
- Goodbody, Q.H., 1985, Stratigraphy, sedimentology, and paleontology of the Bird Fiord Formation, Canadian Arctic Archipelago, Ph.D. thesis, University of Alberta, 205p.
- Grim, R.E., 1953, *Clay mineralogy*: New York McGraw-Hill Book Company, Incorporated, 384p.
- Gross, M.G., 1964, Variations in the O^{18}/O^{16} and C^{13}/C^{12} ratios of diagenetically altered limestones in the Bermuda Islands: *Journal of Geology*, v. 72, p. 170-194.
- Hitchon, B., and Friedman, I., 1969, Geochemistry and origin of formation waters in the western Canada sedimentary basin - 1. Stable isotopes of hydrogen and oxygen: *Geochimica et Cosmochimica Acta*, v. 33, p. 1321-1349.
- Hower, J., 1981a, X-ray diffraction identification of mixed-layer clay minerals, in Longstaffe, F.J., (ed.), *Mineralogical Association of Canada, Short Course in Clays and the Resource Geologist*, v. 7, p. 39-59.
- 1981b, Shale Diagenesis, in Longstaffe, F.J., (ed.), *Mineralogical Association of Canada, Short Course in Clays and the Resource Geologist*, v. 7, p. 60-80.
- Hower, J., Eslinger, E.V., Hower, M.E., and Perry, E.A., 1976, Mechanisms of burial metamorphism of argillaceous sediments - 1. Mineralogical and chemical evidence: *Bulletin of the Geological Association of America*, v. 87, p. 725-737.
- Hudson, J.D., 1977, Stable isotopes and limestone lithification: *Journal of the Geological Society of London*, v. 133, p.637-660.
- Hunt, J.M., 1979, *Petroleum geochemistry and geology*: San Francisco, W.H. Freeman and Company, 617p.
- Hurst, A., and Irwin, H., 1982, Geological modelling of clay diagenesis in sandstones: *Clay Minerals*, v. 17, p. 5-22.
- Hutcheon, I., 1983, Diagenesis 3. Aspects of the diagenesis of coarse-grained siliciclastic rocks: *Geoscience Canada*, v. 10, No. 1, p. 3-14.
- Ignasiak, T.M., Kotlyar, L., Longstaffe, F.J., Strausz, O.P., and Montgomery, D.S., 1983, Separation and characterization of clay from Athabasca asphaltene, *Fuel*, v. 10, p. 43-58.
- Irwin, H., 1980, Early diagenetic carbonate precipitation and pore-fluid migration in the Kimmeridge Clay of Dorset, England: *Sedimentology*, v. 27, p. 577-591.
- Kharaka, Y.K., Berry, A.F., and Friedman, I., 1973, Isotopic compositions of oil-field brines from Kettleman North Dome, California, and their geological implications: *Geochimica et Cosmochimica Acta*, v. 37, p.1899-1908.
- Kharaka, Y.K., Carothers, W.W., and Rosenbauer, R.J., 1983, Thermal decarboxylation of

- acetic acid: implications for origin of natural gas: *Geochimica et Cosmochimica Acta*, v. 47, p. 397-402.
- Land, L.S., 1980, The isotopic and trace element geochemistry of dolomite: the state of the art, *in* Zenger, D.H., Dunham, J.B., and Ethington, R.A., (eds.), *Concepts and Models of Dolomitization*: Society of Paleontologists and Mineralogists, Special Paper 28, p.87-110.
- 1984, Frio sandstones diagenesis, Texas Gulf Coast: a regional isotopic study, *in* McDonald, D.A., and Surdam, R.C., (eds.), *Clastic Diagenesis*: American Association of Petroleum Geologists, Memoir 37, p. 47-62.
- Land, L.S., and Dutton, S.P., 1978, Cementation of a Pennsylvanian deltaic sandstone: isotopic data: *Journal of Sedimentary Petrology*, v. 48, p. 1167-1176.
- Longstaffe, F.J., 1983, Diagenesis 4. Stable isotope studies of diagenesis in clastic rocks: *Geoscience Canada*, v. 10, p. 43-58.
- 1984, The role of meteoric water in diagenesis of shallow sandstones: stable isotope studies of the Milk River aquifer and gas pool, *in* Surdam, R., and MacDonald, D., (eds.), *Clastic Diagenesis*: American Association of Petroleum Geologists, Memoir 37, p. 81-98.
- in press, Oxygen-isotope studies of diagenesis in the Basal Belly River sandstone, Pembina 1-pool, Alberta: *Journal of Sedimentary Petrology*.
- Longstaffe, F.J., Nesbitt, B.E., Muehlenbachs, K., 1982, Oxygen-isotope geochemistry of shales hosting the Pb-Zn-Ba mineralization at the Jason prospect, Selwyn Basin, Yukon: *in* Current Research, Part C, Geological Survey of Canada, Paper 82-1C, p. 45-49.
- Loucks, R.G., D.G., Bebout, and W.E., Galloway, 1977, Relationships of porosity formation and preservation to sandstone consolidation history - Gulf Coast Lower Tertiary Frio Formation: *Transactions of the Gulf Coast Association of Geological Societies*, v. 27, p. 109-120.
- Loucks, R.G., Dodge, M.M., and Galloway, W.B., 1984, Regional controls on diagenesis and reservoir quality in Lower Tertiary sandstones along the Texas Gulf Coast, *in* McDonald, D.A., and Surdam, R.C., (eds.), *Clastic Diagenesis*: American Association of Petroleum Geologists, Memoir 37, p. 217-224.
- McBride, E.F., 1977, Secondary porosity - Importance in sandstone reservoirs in Texas: *Transactions of the Gulf Coast Association Geological Societies*, v. 27, p.121-122.
- McCrea, J.M., 1950, On the isotopic chemistry of carbonate and a paleotemperature scale: *Journal of Chemical Physics*, v. 18, p.849-857.
- McLaren, D.J., 1963, Goose Fiord to Bjorne Peninsula, *in* Fortier, Y.O., (ed.), *Geology of the North Central part of the Arctic Archipelago, Northwest Territories (operation Franklin)*: Geological Survey of Canada Memoir 320, p.310-338.
- Meyerhoff, A.A., 1982, Hydrocarbon resources in Arctic and Subarctic regions, *in* Embry, A.F., and Balkwill, H.R., (eds.), *Arctic Geology and Geophysics, Proceedings of the Third International Symposium on Arctic Geology*: Canadian Society of Petroleum Geologists, Memoir 8, p. 451-552.
- Milliken, K.L., Land, L.S., and Loucks, R.G., 1981, History of burial diagenesis determined from isotopic geochemistry, Frio Formation, Brazoria County, Texas: *Bulletin of the American Association of Petroleum Geologists*, v. 65, p. 1397-1413.
- Momper, J.A., 1978, Oil migration limitations suggested by geological and geochemical considerations, *in* Physical and chemical constraints on petroleum migration: American Association of Petroleum Geologists, Short Course 8, p. B.1-B.60.

- Montoya, J.W., and Hemley, J.J., 1975, Activity relations and stabilities in alkali feldspar and mica alteration reactions: *Economic Geology*, v. 70, p.577-583.
- Perry, E., and Hower, J., 1970, Burial diagenesis in Gulf Coast pelitic sediments: *Clays and Clay Minerals*, v. 18, p.165-177.
- Porter, K.W., and Weimer, R.J., 1982, Diagenetic sequence related to structural history and petroleum accumulation: Spindle Field, Colorado: *Bulletin of the American Association of Petroleum Geologists*, v.66, p.2543-2560.
- Powell, T.G., 1978, An assessment of the hydrocarbon source rock potential of the Canadian Arctic Islands: *Geological Survey of Canada, Paper 78-12*, 82p.
- Radchenko, O.A., Karpova, I.P., and Chernysheva, A.S., 1951, A geochemical investigation of weathered and highly altered mineral fuels from South Fergana: *Trudy VNIGRI, new series No. 5, Contributions to Geochemistry, No. 2-3*, p. 180-202. Translated by Isreal Program for Scientific Translations, Jerusalem, 1965.
- Reynolds, R.C., Jr., 1980, Interstratified clay minerals, *in* Brindley, G.W., and Brown, G., (eds.), *Crystal structures of clay minerals and their X-ray identification: Mineralogical Society of London*, p. 249-303.
- Reynolds, Jr., R.C., and Hower, J., 1970, The nature of interlayering in mixed-layer illite-montmorillonites: *Clays and Clay Minerals*, v. 18, p. 25-36.
- Robin, P.-Y. F., 1978, Pressure solution at grain-to-grain contacts: *Geochimica Cosmochimica Acta*, v. 42, p.1383-1389.
- Savin, S.M., and Epstein, S., 1970a, The oxygen and hydrogen isotope geochemistry of clay minerals: *Geochimica et Cosmochimica Acta*, v. 34, p. 25-42.
- 1970b, The oxygen and hydrogen isotope geochemistry of ocean sediments and shales: *Geochimica et Cosmochimica Acta*, v. 34, p. 43-63.
- 1970c, The oxygen isotope chemistry of coarse grained sedimentary rocks and minerals: *Geochimica et Cosmochimica Acta*, v. 34, p. 323-329.
- Schmidt, V. and McDonald, D.A., 1979, The role of secondary porosity in the course of sandstone diagenesis, *in* P.A. Scholch and P.R. Schluger, eds., *Aspects of diagenesis: SEPM Special Publication*, v. 26, p.175-207.
- Secor, D.T., Jr., 1965, Role of fluid pressure in jointing: *American Journal of Science*, v. 263, p.633-646.
- Sibley, D.F., and H. Blatt, 1976, Intergranular pressure solution and cementation of the Tuscarora orthoquartzite: *Journal of Sediment Petrology*, v. 46, p.881-896.
- Smith, A.G., Briden, J.C. and Drewry, G.E., 1973, Phanerozoic world maps, *in* Hughes, N. F. (ed.), *Organisms and continents through time: Paleontological Association of London, Special Papers in Palaeontology* 12, p. 1-42.
- Srodon, J., 1984, X-ray powder diffraction of illitic materials: *Clays and Clay Minerals*, v. 32, p. 337-349.
- Storey, S.R., 1982, Optimum reservoir facies in an immature, shallow-lobate delta system: basal Belly River Formation, Keystone-Pembina area, *in* Hopkins, J.C., ed., *Depositional Environments and Reservoir Facies in some western Canadian oil and gas fields: University of Calgary Core Conference*, p. 3-13.
- Surdam, R.C., Bosse, S.W., and Crossey, L.J., 1984, The chemistry of secondary porosity, *in* McDonald, D.A., and Surdam, R.C. (eds.), *Clastic Diagenesis: American Association of Petroleum Geologists, Memoir 37*, p. 127-149.

- Taylor, H.P., Jr., 1974, The application of oxygen and hydrogen isotope studies to problems of hydrothermal alteration and ore deposition: *Economic Geology*, v. 69, p. 843-883.
- Thorez, J., 1976, Practical identification of clay minerals, 90p.
- Thorsteinsson, R., and Tozer, E.T., 1960, Summary account of structural history of the Canadian Arctic Archipelago since Precambrian time: *Canada Geological Survey Paper* 60-7, 25p.
- 1970, Chapter VII, The Arctic Archipelago, *in* Douglas, R.J.W., (ed.), *Geology and Economic Minerals of Canada Report No. 1*, Fifth edition, p. 548-590.
- Toth, J., 1980, Cross-formational gravity-flow of groundwater: a mechanism of the transport and accumulation of petroleum (the generalized hydraulic theory of petroleum migration): *American Association of Petroleum Geologists, Studies in Geology*, v. 10, p. 121-167.
- Tozer, E.T., and Thorsteinsson, R., 1964, Western Queen Elizabeth Islands, Arctic Archipelago: *Geological Survey of Canada Memoir* 332, 242p.
- Walters, Jr., L.J., Claypool, G.E., and Choquette, P.W., 1972, Reaction rates and O^{18} variation for the carbonate-phosphoric acid preparation method: *Geochimica et Cosmochimica Acta*, v. 36, p. 129-140.
- Weyl, P.K., 1959, Pressure solution and the force of crystallization - a phenomenological theory: *Journal of Geophysical Research*, v. 64, p. 2001-2005.
- Wilson, M.D., 1982, Origins of clays controlling permeability in tight gas sands: *Journal of Petroleum Technology*, v. 7, p. 2871-2876.
- Wolf, K.H., Easton, A.J., and Warne, S., 1967, Techniques of examining and analyzing carbonate skeletons, minerals, and rocks, *in* Chilingar, Bissell, and Fairbridge, (eds.), *Carbonate Rocks*, v. B, Elsevier Publishing Company.
- Yeh, H., and Savin, S.M., 1976, The extent of oxygen isotope exchange between clay minerals and sea water: *Geochimica et Cosmochimica Acta*, v. 40, p. 743-748.
- 1977, Mechanism of burial metamorphism of argillaceous sediments - 3. Oxygen isotope evidence: *Geological Society of America Bulletin*, v. 88, p. 1321-1330.

APPENDIX I

A. ANALYTICAL METHODS

Thin Section Petrography

The abundance and textural relationships of the detrital and authigenic minerals were determined in thin section. Sixty-three thin sections from section 80X (Table 2.1) were stained with a multi-purpose stain (potassium ferricyanide and alizarin red) to determine the type of carbonate cements. The characteristic colours obtained from the staining are: Fe-free calcite - red; Fe-poor calcite - mauve; Fe-rich calcite - purple; Fe-free dolomite - not stained; Fe-rich dolomite - light blue; and ankerite - dark blue (Wolf et al., 1967). For sandstones, the percentages of original framework grains, cements, other minerals and porosity were obtained by point-counting.

Fifty thin sections from section 81I (Table 2.2) were impregnated with blue epoxy to ensure easy identification of porosity and to show the morphology of the pore-filling authigenic minerals.

X-Ray Diffraction Analysis

The $<2\mu\text{m}$ size-fraction of 37 and 25 rock samples from sections 80X and 81I (Tables 2.1, 2.2), respectively, were analysed by X-ray diffraction (XRD) to determine the clay mineralogy. The $<0.2\mu\text{m}$ size-fraction of nine rock samples from section 80X (Table 2.1) were also analysed by XRD to help determine the percentage of illite in the mixed layer illite/smectite clay.

The procedure for preparing the samples for X-ray diffraction analysis roughly follows that of Ignasiak et al. (1983). The rock samples were disaggregated in a mortar and pestle, care being taken to preserve the original grain size distribution. A minimum of 20g of material from each sample was soaked in 125ml of a 4% sodium hexametaphosphate solution for 8 hours to further disperse the particles. Finally, an ultrasonic probe was used to ensure thorough dispersion of clay-sized particles. Each sample was then dispersed in distilled water and the $<2\mu\text{m}$ size-fraction removed by standard sedimentation techniques. The clay-sized material was treated with a 3% sodium hypochlorite solution for 48 hours at $+65^\circ\text{C}$ to destroy residual

organic matter. Each clay sized sample was then thoroughly washed with distilled water using a high speed centrifuge.

The $<2\mu\text{m}$ size-fraction was split into three portions; the first and second portions were saturated with two molar solutions of Ca^{2+} and K^+ , respectively, for use in identification of clay minerals by XRD. The third portion was set aside for isotopic analysis or separation of $<0.2\mu\text{m}$ size-fraction. All the samples were freeze-dried following thorough washing of the residual Ca^{2+} and K^+ solutions. About 50mg of the Ca and K saturated samples were dispersed in distilled water and deposited by suction upon a ceramic disc to produce a preferred basal orientation of platy minerals.

The Ca- and K-saturated samples were analysed using a Philips X-ray diffractometer. Analytical conditions (Ignasiak et al., 1983) were: Co K-alpha radiation (50KV 20mA), 1° slit, time constant = 2, and scan rate = $1^\circ 2\theta/\text{min}$. X-ray diffraction patterns were obtained for the Ca-saturated samples at 54% relative humidity and following saturation with ethylene glycol. To confirm the identification of the clay minerals, additional diffractograms were obtained for the K-saturated sample at 0% and 54% relative humidity, and upon heating to 300 and 550°C.

The $<0.2\mu\text{m}$ size-fraction was separated from the unsaturated $<2\mu\text{m}$ size fraction by centrifuge. The $<0.2\mu\text{m}$ samples were then deposited on glass slides by a pipette after being dispersed in ethanol. Diffractograms were obtained for the samples at 54% relative humidity, after glycolation and upon heating to 550°C.

The relative percentages of individual clay minerals in the $<2\mu\text{m}$ size-fraction were estimated following the procedures of Biscaye (1964, 1965). This approach is particularly useful for Fe-rich chlorites; when Fe-rich chlorite is heated to 550°C, the intensity of the 14Å (001) peak is enhanced too much to allow the use of this peak for semi-quantitative analysis. However, the (002) reflection at 3.58Å of kaolinite may become resolved from the corresponding (004) of chlorite at 3.53Å (Thorez, 1976, summarising other workers; Biscaye, 1964, 1965; Bradley, 1954). The resolution and intensities of this doublet equally depends on the relative proportion of both minerals in the clay mixture and also on their crystallinity. All the diffractograms in this study have a doublet at 3.5Å; hence the semi-quantitative method described by Biscaye (1964, 1965) could be used here.

The assumption that clay minerals constitute 100% of the mineralogy in the $<2\mu\text{m}$ size-fraction is generally reasonable. In this study peak heights were used instead of peak areas. The peaks (from the Ca-saturated glycolated diffractogram) and weighting factors for all the clay minerals followed Biscaye (1964, 1965), except for illite/smectite which followed Longstaffe (pers. comm.). The peaks and weighting factors are as follows:

1. Smectite = height of 17\AA peak
2. Illite = $4 \times$ height of 10\AA peak
3. Kaolinite + chlorite = $2 \times$ height of 7\AA peak
4. Illite/smectite = $2 \times$ height of 13\AA peak

The 7\AA peak, common to both kaolinite and chlorite, was divided between the two in proportion to the fraction of each mineral (according to their peak heights) in the resolved 3.5\AA kaolinite-chlorite doublet. The five weighted peak heights were summed, and the weighted peak height of each mineral multiplied 100 and divided by the sum of the heights gave the percentage of each mineral. The percentages obtained are only semi-quantitative.

The amount of illite layers in the mixed layer illite/smectite of sections 80X and 811 were determined from the <0.2 and/or $<2\mu\text{m}$ size-fraction following the procedures of Reynolds and Hower (1970), Reynolds (1980) and Hower (1981a). The diffractions of illite/smectite used for the calculations are $(002)_{27}/(001)_{17}$ or $(002)_{27}/(001)_{10}$, $(003)_{27}/(001)_{10}$ or $(003)_{27}/(002)_{17}$ and $(005)_{27}/(003)_{17}$ or $(005)_{27}/(002)_{10}$ of the glycolated diffractogram (Fig. 2.1-2.3, 2.5, 2.6). Using the d-spacings of these diffractions, the percentages of illite layers in the ordered illite/smectite were determined graphically using the data calculated by Reynold and Hower (1970). Unfortunately, the d-spacings of the second and third reflections mentioned above cannot be determined accurately because of the polymineralic assemblages present in the samples; the second diffraction is usually not detected because it is under the $10\text{\AA}(001)$ of illite, while the third diffraction is sometimes obscured by the (002) of the illite. The $(002)_{27}/(001)_{17}$ or $(002)_{27}/(001)_{10}$ can be more accurately determined but sometimes it is obscured by the chlorite (001) .

To increase the accuracy of the calculated percent illite in the illite/smectite, another diffraction from the 54% relative humidity (Ca-saturated) diffractogram was considered. Assuming the air-dried condition described by Hower (1981a) is equivalent to the 54% relative humidity condition, the water-smectite layer spacing will be 15\AA . This assumption is valid

because samples which contained discrete smectite have a layer spacing of about 15Å on the 54% relative humidity diffractogram. The data presented by Hower (1981a) were calculated assuming two moles of interlayer water per formula weight of smectite ($2H_2O$ -smectite) and a layer spacing of 15Å. The diffraction used for the illite/ $2H_2O$ -layer smectite is the $(002)_{25}/(001)_{15}$ or $(002)_{25}/(001)_{10}$. Determination of percent illite layers in the ordered illite/smectite were done graphically using the data calculated by Hower (1981a). The final percentages of illite layers calculated for the samples (Tables 2.3, 2.4) are based on the four diffractions mentioned above; not all four diffractions are always well defined.

Thirty-nine backpacked bulk rock samples from 80X (Table 2.1) were analysed by XRD to help and confirm identification of non-clay minerals. For example, the types of carbonate cements identified by the staining technique and the types of feldspars identified by petrographic methods were confirmed by the X-ray diffractograms from the backpacked samples. Bulk rock samples were powdered by a tungsten carbide swing mill and then placed in an aluminium holder for X-ray diffraction at room humidity from 2-60° 2θ.

Scanning Electron Microscope

The habit, distribution, mode of aggregation and other textures of authigenic and detrital minerals were studied using the scanning electron microscope (SEM). An energy dispersive analyser (EDA) attached to the SEM was used for semi-quantitative chemical analysis and confirmation of mineral identification.

The 20 rock samples from section 80X that were studied by SEM were listed on Table 2.1. A small chip from the centre of each sample was mounted on SEM stubs using conductive silver paint. The stubs were sputter-coated with 20nm of gold to ensure proper grounding during the analysis by a Cambridge Stereoscan S250 scanning electron microscope. Its accelerating voltage was fixed at 25KV. The SEM's associated energy dispersive analyser was a Kevex System 7000. Analysis was done using a beam diameter of 1µm (spot analysis). Accelerating voltage was kept at 20KEV for all analyses and samples were properly oriented to minimize beam scatter.

It is important to note that elements with low atomic numbers (e.g., Na and Mg) are suppressed on the energy dispersive analysis (EDA) spectrum, while elements with high atomic numbers (e.g., Fe) are enhanced.

Stable Isotope Analysis

Oxygen isotope analysis were performed on 18 $<2\mu\text{m}$ size-fraction samples, from section 80X. All the $<2\mu\text{m}$ size-fraction samples consisted of a mixture of clay minerals, minor amounts of quartz ($<10\%$) and trace amounts of feldspar ($<1\%$). Carbonates were removed from the samples using HCl prior to analysis.

Oxygen isotope analyses of the $<2\mu\text{m}$ size-fraction samples were performed using the BrF_3 method of Clayton and Mayeda (1963). The samples were dried at $+105^\circ\text{C}$ for two hours and maintained at near zero humidity for 24 hours prior to treatment with BrF_3 . Replicate analyses of clay samples were better than ± 0.3 permill.

Authigenic Fe-rich calcite, dolomite and ankerite were analysed for their oxygen- and carbon-isotope composition. Petrographic and XRD studies were used to select rock samples with authigenic carbonate minerals for isotope analysis.

The carbonate minerals were prepared for isotopic analysis by reacting powdered rock samples (crushed by swing mill) in phosphoric acid using the procedure described by Walther et al. (1972), modified after McCrea (1950) and Epstein et al. (1964). Replicate analyses of carbonate minerals were better than ± 0.2 permill (Longstaffe, in press).

The isotope data are presented in the usual δ notation with respect to Standard Mean Ocean Water (SMOW) for oxygen (Craig, 1961) and the *Belemnitella americana* from the Peedee Formation (PDB) for carbon (Craig, 1957). The partitioning of ^{18}O between two phases, 1 and 2, is given by

$$\Delta_{1-2} = 10^3 \ln \alpha_{1-2} (\alpha - 1) 10^3 \approx \delta_1 - \delta_2$$

where α is the oxygen isotope fractionation factor between phases 1 and 2.